Technical Report Documentation Page

1. Report No.	2. Government Accession No.	3. Recipient's Catalog No.
SWUTC/12/476660-00017-1		

4. Title and Subtitle	5. Report Date
Nanotechnology-Based System for Damage-Resistant Concrete Pavements	August 2012
	6. Performing Organization Code

7. Author(s)	8. Performing Organization Report No.
Rashid K. Abu Al-Rub	476660-00017-1

9. Performing Organization Name and Address	10. Work Unit No. (TRAIS)
Texas Transportation Institute Zachry Department of Civil Engineering Texas A&M University College Station, Texas 77843-3136	11. Contract or Grant No. DTRT07-G-0006

12. Sponsoring Organization Name and Address	13. Type of Report and Period Covered
Southwest Region University Transportation Center Texas Transportation Institute Texas A&M University System College Station, Texas 77843-3135	Technical Report 14. Sponsoring Agency Code

15. Supplementary Notes
Supported by a grant from the U.S. Department of Transportation, University Transportation Centers Program

16. Abstract
The focus of this study was to explore the use of nanotechnology-based nanofilaments, such as carbon nanotubes (CNTs) and nanofibers (CNFs), as reinforcement for improving the mechanical properties of Portland cement paste and creating multifunctional and sensing concrete. Due to their ultra-high strength and very high aspect ratios, CNTs and CNFs have been excellent reinforcements for enhancing the physical and mechanical properties of polymer, metallic, and ceramic composites. Very little attention has been devoted to exploring the use of nanofilaments in the transportation industry, however. Therefore, this study aimed to bridge the gap between nanofilaments and transportation materials. This was achieved by testing the integration of CNTs and CNFs in ordinary Portland cement paste through state-of-the-art techniques. Different mixes in fixed proportions (e.g., water-to-cement ratio, air content, admixtures) along with varying concentrations of CNTs or CNFs were prepared. Different techniques commonly used for other materials (like polymers) were used in achieving uniform dispersion of nanofilaments in the cement paste matrix and strong nanofilament/cement bonding. Small-scale specimens were prepared for mechanical testing in order to measure the modified mechanical properties as a function of nanofilament concentration, type, and distribution. With 0.1% CNFs, the ultimate strain capacity increased by 142%, the flexural strength increased by 79%, and the fracture toughness increased by 242%. A scanning electron microscope was used to discern the difference between crack bridging and fiber pullout. Test results showed that the strength, ductility, and fracture toughness can be improved with the addition of low concentrations of either CNTs or CNFs.

17. Key Words	18. Distribution Statement
Carbon Nanotubes, Carbon Nanofibers, Cement, Dispersion, Fracture, Nano Reinforcements	No restrictions. This document is available to the public through NTIS: National Technical Information Service Springfield, Virginia 22161 http://www.ntis.gov

19. Security Classification (of this report)	20. Security Classification (of this page)	21. No. of Pages	22. Price
Unclassified	Unclassified	124	

Nanotechnology-Based System for Damage-Resistant Concrete Pavements

by

Rashid K. Abu Al-Rub
Zachry Department of Civil Engineering
Texas A&M University

Performing Agency:
Texas A&M University

Report No. SWUTC/12/476660-00017-1

Sponsored by the
Southwest Region University Transportation Center
Texas Transportation Institute
Texas A&M University System
College Station, Texas 77843-3135

August 2012

DISCLAIMER

The contents of this report reflect the views of the authors, who are responsible for the facts and the accuracy of the information presented herein. This document is disseminated under the sponsorship of the U.S. Department of Transportation, University Transportation Centers Program, in the interest of information exchange. The U.S. Government assumes no liability for the contents or use thereof.

SPECIAL NOTE

The acronyms MWCNT and MWNT are used interchangeably throughout this document.

ACKNOWLEDGMENTS

The author recognizes that support for this project was provided by a grant from the U.S. Department of Transportation, University Transportation Centers Program, to the Southwest Region University Transportation Center. Moreover, the author acknowledges the extensive help from—and fruitful discussions with—Professor Zachry Grasley and Mr. Ardavan Yazdanbakhsh, from the Zachry Department of Civil Engineering at Texas A&M University, on carbon nanofiber and carbon nanotube integration in cementitious materials. The helpful remarks made by Professor Jaime Grunlan, from the Department of Mechanical Engineering at Texas A&M University, about the effective dispersions of carbon nanotubes in aqueous solutions are greatly appreciated. The author also wishes to thank David Burton from Applied Science, Inc. for providing the pyrograph carbon nanofibers used in this project. Thanks to Ara Jeknavorian from W.R. Grace for providing the superplasticizers and related technical information. Finally, the author wishes to thank Tom Stephens, Stanislav Vitha, Christos Savva, Yordanos Bisrat, and Amanda Young in the Microscopy and Imaging Center and the Material Characterization Facility of Texas A&M University for their support throughout the imaging phase of the experiment.

ABSTRACT

The focus of this research was to investigate the use of functionalized/non-functionalized multi-walled carbon nanotubes (MWCNTs) as reinforcements for Portland cement paste and for creating multifunctional and sensing concrete. The unique geometrical characteristics of the carbon nanotubes (CNTs), as well as their unique mechanical properties such as high strength, ductility, and stiffness, were the vital motivation for this study. The researchers combined the CNTs with concrete, which is the most used manmade material. When compared to other composite materials, a limited amount of research has been conducted on CNTs/cement composites.

In order to investigate how the aspect ratio of functionalized/non-functionalized MWCNTs affects the mechanical properties of cementitious composites, 10 different mixes of MWCNTs/cement composites were prepared and tested. The different batches had a fixed water/cement ratio of 0.4, and variations of MWCNT length, concentration, and surface treatment. The cement nanocomposites were cast in small-scale specimens (beams) for the three-point flexural testing. Four major mechanical properties were evaluated at the ages of 7, 14, and 28 days from the casting day: maximum flexural strength, ultimate strain capacity (ductility), modulus of elasticity, and modulus of toughness. The results for the different nanocomposite batches were compared with the plain cement (reference) batch.

The mechanical testing results showed that at 28 days, almost all of the MWCNT composites increased the flexural strength of the cement nanocomposites. At 28 days, the long MWCNTs increased the flexural strength more than the short MWCNTs. In general, the ultimate strain (ductility) of the short MWCNT nanocomposites was higher than the ultimate strain of the long MWCNT nanocomposites. The flexural strength of short 0.2% MWCNT and long 0.04% MWCNT (OH) increased by 269% and 83%, respectively, compared to the plain cement sample at 28 days. The highest ductility at 28 days for the short 0.1% MWCNT and the short 0.2% MWCNT was 86% and 81%, respectively.

Clear evidence was obtained from the scanning electron microscope images for micro-crack bridging; many of the MWCNTs were stretching across the micro-cracks.

In conclusion, CNTs as nano reinforcements can effectively improve certain mechanical properties of cement paste composites.

TABLE OF CONTENTS

Page

LIST OF FIGURES x

LIST OF TABLES xiv

EXECUTIVE SUMMARY xv

1. INTRODUCTION 1

1.1 Problem Statement 1
1.2 Carbon Nanotubes 5

1.2.1 Nature of CNTs 5
1.2.2 Manufacturing of CNTs 9
1.2.3 Properties of CNTs 10

1.3 Literature Review 10

1.3.1 CNTs in Polymers, Metals, and Ceramics 10
1.3.2 CNTs in Cementitious Materials 11

1.4 Research Objectives 15

2. FUNCTIONALIZATION AND DISPERSION OF CARBON NANOTUBES 17

2.1 Introduction 17
2.2 Mechanical Dispersion of CNTs 17
2.3 Chemical Treatment of CNTs 18

2.3.1 Non-Covalent Functionalization 19
2.3.2 Covalent Functionalization 20

2.4 Dispersion and Acid Treatment of MWCNTs (Experimental Work) 22

2.4.1 Dispersion 22
2.4.2 Acid Treatment and Defect Site Functionalization 23
2.4.3 Functionalized MWCNT Characterization 24

3. MIXING CARBON NANOTUBES IN AN AQUEOUS SOLUTION WITH CEMENT TO MAKE THE NANOCOMPOSITE 27

3.1 MWCNT Materials 27

3.1.1 Long MWCNTs 27
3.1.2 Short MWCNTs 27

3.1.3 Portland Cement and Superplasticizer....28
3.1.4 Mixing Water....28

3.2 Methodology....28

3.2.1 Carbon Nanotube Solution Preparation....28
3.2.2 Mixing Carbon Nanotube Solutions with Portland Cement....30
3.2.3 Casting the Nanocomposite into the Molds....31

3.3 Cement Composite Batches....35

4. EXPERIMENTAL RESULTS AND MICROSTRUCTURAL CHARACTERIZATION....37

4.1 Testing Fixture....37
4.2 Data Analysis....40
4.3 Mechanical Properties....40

4.3.1 Long vs. Short Non-Functionalized MWCNT Nanocomposites....45
4.3.2 Long vs. Short Functionalized MWCNT Nanocomposites....52

4.4 Results and Discussion....56

4.4.1 Long vs. Short MWCNTs....57
4.4.2 MWCNT Pullout and Result Variability....62
4.4.3 Weakening Due to Functionalization....63
4.4.4 Effect of the Cement Paste Curing Method and the Superplasticizer....64

4.5 SEM and TEM Microstructural Imaging....70

4.5.1 CNT Pullout and Crack Bridging....70
4.5.2 Dispersion and Agglomeration....72

5. CONCLUSIONS AND FUTURE WORK....77

5.1 Conclusion....77
5.2 Limitations....79
5.3 Future Work....80

REFERENCES....81

APPENDIX....91

LIST OF FIGURES

Page

Fig. 1. The aspect ratio effect on the surface area/volume ratio for different lengths of SWCNTs, MWCNTs, CNFs, and CMFs. 4

Fig. 2. The aspect ratio effect on the surface area/volume ratio for different lengths of SWCNTs and MWCNTs, and the relations between surface area/volume ratio with mass fraction of CNTs by cement weight and their number per 1 g of cement. 6

Fig. 3. First images of carbon nanotubes published in 1952 by Russian scientists [14]. 7

Fig. 4. Comparison between an (a) graphite structure [16], (b) graphene sheet [17], and (c) fullerenes (buckyball) structure [18]. 8

Fig. 5. Schematic of an (a) SWCNT [19] and (b) MWCNT [20]. 8

Fig. 6. CNT structural orientations: (a) armchair structure, (b) zigzag structure, (c) chiral structure [21]. 9

Fig. 7. Ultrasonic wave mixer from Sonics & Materials, Inc. used to mechanically disperse CNTs within aqueous solutions [66]..... 18

Fig. 8. Cryo-TEM image for the MWCNTs dispersed in a water/surfactant solution. No obvious agglomerations of the MWCNTs were noticed after ultrasonication (picture courtesy of Bryan M. Tyson) [100]. 23

Fig. 9. SEM images for comparison of (a) an untreated MWCNT, (b) an acid-treated short MWCNT (COOH), and (c) a treated long MWCNT (OH). All the MWCNT surfaces look similar, indicating no severe damage (defects) for the functionalized MWCNTs (pictures a and b courtesy of Bryan M. Tyson) [100]. 26

Fig. 10. Accurate scale used to weigh the CNTs. 29

Fig. 11. Water-jacketed beaker (250 ml) used to sonicate the CNTs within the water using the ultrasonic mixer. Constant flow of the water jacket reduced the temperature of the solution and helped prevent excessive evaporation. 30

Fig. 12. Ultrasonic wave mixer from Sonics & Materials, Inc. used for CNT dispersion [66]. ... 30

Fig. 13. Variable-speed planetary mixing blender (Oster Fusion™). 31

Fig. 14. Vacuuming chamber and the air pump. 32

Fig. 15. Vibration table used for casting the composite cement paste. 33

Fig. 16. View of the square acrylic mold. 34

Fig. 17. Soldering iron of 200 W power used for demolding the specimens from the acrylic molds. 34

Fig. 18. Three-point bending testing frame dimensions (picture courtesy of Bryan M. Tyson). 37

Fig. 19. Testing frame setup, showing the aluminum frame, the specimen, the LVDT, the load cell, and the actuator. 38

Fig. 20. The 2.5 kg capacity load cell with a small loading bar welded at top of adjustable screw (left) and the Newport NSA12 actuator (right). 39

Fig. 21. Example of stress-strain curves for the plain cement and the non-functionalized short and long MWCNT specimens at 7 days. 42

Fig. 22. Example of stress-strain curves for the plain cement and the non-functionalized short and long MWCNT specimens at 14 days. 43

Fig. 23. Example of stress-strain curves for the plain cement and the non-functionalized short and long MWCNT specimens at 28 days. 43

Fig. 24. Example of stress-strain curves for the plain cement and the functionalized short and long MWCNT specimens at 7 days. 44

Fig. 25. Example of stress-strain curves for the plain cement and the functionalized short and long MWCNT specimens at 14 days. 44

Fig. 26. Example of stress-strain curves for the plain cement and the functionalized short and long MWCNT specimens at 28 days. 45

Fig. 27. Average flexural strength results for the plain cement and the non-functionalized short and long MWCNT composite specimens with the standard error of the mean. 49

Fig. 28. Average ultimate strain results for the plain cement and the non-functionalized short and long MWCNT composite specimens with the standard error of the mean. 49

Fig. 29. Average modulus of elasticity results for the plain cement and the non-functionalized short and long MWCNT composite specimens with the standard error of the mean. 50

Fig. 30. Average modulus of toughness results for the plain cement and the non-functionalized short and long MWCNT composite specimens with the standard error of the mean. 50

Fig. 31. Average flexural strength results for the plain cement and the functionalized short and long MWCNT composite specimens with the standard error of the mean. 53

Fig. 32. Average ultimate strain results for the plain cement and the functionalized short and long MWCNT composite specimens with the standard error of the mean. 53

Fig. 33. Average modulus of elasticity results for the plain cement and the functionalized short and long MWCNT composite specimens with the standard error of the mean. 54

Fig. 34. Average modulus of toughness results for the plain cement and the functionalized short and long MWCNT composite specimens with the standard error of the mean. 54

Fig. 35. Average flexural strength results for the plain cement and the long MWCNT composite specimens with the standard error of the mean. 58

Fig. 36. Average flexural strength results for the plain cement and the short MWCNT composite specimens with the standard error of the mean. 59

Fig. 37. Average ultimate strain results for the plain cement and the long MWCNT composite specimens with the standard error of the mean. 59

Fig. 38. Average ultimate strain results for the plain cement and the short MWCNT composite specimens with the standard error of the mean. 60

Fig. 39. Average modulus of elasticity results for the plain cement and the long MWCNT composite specimens with the standard error of the mean. 60

Fig. 40. Average modulus of elasticity results for the plain cement and the short MWCNT composite specimens with the standard error of the mean. 61

Fig. 41. Average modulus of toughness results for the plain cement and the long MWCNT composite specimens with the standard error of the mean. 61

Fig. 42. Average modulus of toughness results for the plain cement and the short MWCNT composite specimens with the standard error of the mean. 62

Fig. 43. SEM image showing the C-S-H and the crystalized CH of the cement paste. 65

Fig. 44. Average flexural strength results for different plain cement specimens with the standard error of the mean. 68

Fig. 45. Average ultimate strain results for different plain cement specimens with the standard error of the mean. 68

Fig. 46. Average modulus of elasticity results for different plain cement specimens with the standard error of the mean. 69

Fig. 47. Average modulus of toughness results for different plain cement specimens with the standard error of the mean. 69

Fig. 48. SEM image showing the micro-crack bridging and breakage of the MWCNTs within the cement paste. 71

Fig. 49. SEM image showing a micro-crack bridging by a few MWCNTs within the cement paste. 71

Fig. 50. SEM image of MWCNT agglomerations within a small area of cement paste. 73

Fig. 51. A cryo-TEM image of MWCNTs within cement paste (picture courtesy of Bryan M. Tyson). 74

Fig. 52. SEM image showing a huge formation of ettringite needles within the C-S-H of the cement paste (notice the air void [space] within and surrounding the ettringite formation). 75

LIST OF TABLES

Page

Table 1 The atomic mass percentages of carbon and oxygen for the MWCNTs. 25

Table 2 Physical properties for the long treated MWCNTs (OH) and long untreated MWCNTs. 27

Table 3 Physical properties for the short MWCNTs (COOH) and short untreated MWCNTs. 28

Table 4 Mix design of the functionalized and non-functionalized MWCNT test specimens..... 36

Table 5 Newport NSA12 actuator specifications..... 39

Table 6 Average ultimate flexural strength for the functionalized and the non-functionalized MWCNT test specimens (MPa). 46

Table 7 Average ultimate strain capacity for the functionalized and the non-functionalized MWCNT test specimens (%)..... 46

Table 8 Average modulus of elasticity for the functionalized and the non-functionalized MWCNT test specimens (GPa). 47

Table 9 Average modulus of toughness for the functionalized and the non-functionalized MWCNT test specimens (kPa). 47

EXECUTIVE SUMMARY

Nanotechnology, through the use of carbon nanofilaments, offers many possibilities for creating self-sensing materials. These multifunctional materials can recognize the state of distress (e.g., thermal cracking, damage, moisture-induced damage) in a structural system. Moreover, these nano inclusions can act as reinforcements for enhancing the thermo-mechanical properties and fracture/damage-resistance of various types of materials. Imagine a concrete material that has comparable compressive and tensile strengths without the need for steel reinforcements to make the material stronger. Imagine what potential benefits these comparable compressive and tensile strengths may offer to the concrete structures for making them stronger, lighter, safer, more durable, and even more economical. Many construction industries use Portland cement in the construction of many concrete structures. In fact, each year, more than 5 billion cubic yards of concrete are used worldwide in constructing many structures.

Health monitoring of concrete and asphalt pavements holds promise as a way to provide information for near real-time condition assessment of pavement distresses and for development of damage-resistant pavements. This information can be used to assess the integrity, durability, and incipient damage of pavement due to various traffic and environmental loading conditions and for early scheduling of repair and maintenance. However, one of the major obstacles preventing sensor-based monitoring is the lack of reliable, easy-to-install, cost-effective, and harsh-environment-resistant sensors that can be densely embedded into large-scale civil infrastructure systems. Furthermore, the current integrated sensors are still unable to have many of the properties monitored, are only capable of providing surface measuring, and are too large to be used in pavements. Nanotechnology and micro/nano electromechanical systems (MEMS/NEMS) that have matured in recent years represent an innovative solution to monitor appropriate physical properties of asphalt and concrete pavements that could indicate the onset of pavement distresses (e.g., stress and strain, cracking, temperature, and moisture), leading to wireless, inexpensive, durable, compact, and high-density information collection. However, until now, these MEMS/NEMS-based systems have been developed and used with great success in electronic, computer, automobile, aerospace, defense, and medical industries but have had very limited development in pavements and transportation infrastructures. Therefore, the main goal of this research effort was to develop an inexpensive and reliable self-sensing concrete material that

could be easily used for real-time monitoring of pavement health. This was achieved by first exploring the potential use of carbon nanofilaments for increasing the mechanical properties of concrete and their potential as a self-sensing material.

The main focus of this study was to explore the use of nanotechnology-based nanofilaments, such as carbon nanotubes (CNTs) and nanofibers (CNFs), as reinforcements for improving the mechanical properties of Portland cement paste and creating multifunctional and sensing concrete. Due to their ultra-high strength and very high aspect ratios, CNTs and CNFs have been excellent reinforcements for enhancing the physical and mechanical properties of polymer, metallic, and ceramic composites. Very little attention has been devoted to exploring the use of nanofilaments in the transportation industry, however. Therefore, this study aimed to bridge the gap between nanofilaments and transportation materials. This was achieved by testing the integration of CNTs and CNFs in ordinary Portland cement paste through state-of-the-art techniques. Different mixes in fixed proportions (e.g., water-to-cement ratio, air content, admixtures) along with varying concentrations of CNTs or CNFs were prepared. Different techniques commonly used for other materials (like polymers) were used in achieving uniform dispersion of nanofilaments in the cement paste matrix and strong nanofilament/cement bonding. Small-scale specimens were prepared for mechanical testing in order to measure the modified mechanical properties as a function of nanofilament concentration, type, and distribution. With 0.1% CNFs, the ultimate strain capacity increased by 142%, the flexural strength increased by 79%, and the fracture toughness increased by 242%. A scanning electron microscope was used to discern the difference between crack bridging and fiber pullout. Test results showed that the strength, ductility, and fracture toughness can be improved with the addition of low concentrations of either CNTs or CNFs.

1. INTRODUCTION

1.1 Problem Statement

It is well known that concrete is the most used and produced manmade material. The importance of this fundamental material motivates scientists and engineers to investigate and study the properties and behavior of cementitious materials in order to have a better understanding and to improve their mechanical properties, such as strength, ductility, and toughness. Concrete is a brittle material that has low tensile strength, low ductility, and early development and propagation of micro-cracks due to shrinkage. Beginning as early as the 1980s, fiber-reinforced concrete (FRC), using macro fibers as reinforcements, was used to improve the tensile strength, ductility, and toughness of concrete. However, the gain in ductility was obtained for the fiber-reinforced concrete as a composite, not for the concrete itself as a cementitious material. Recently, a wide range of reinforcements, at macro, meso, and micro scales, has been used to control the early stages of crack propagations within cementitious materials [1-7]. Reinforcing cementitious materials has varied from using macro fibers, like steel reinforcement rebar that is continuously aligned along the tensile material fibers of the cementitious element, to discrete micro and nanofibers, like microfibers, carbon nanofibers (CNFs), and carbon nanotubes (CNTs).

The motivation of using these nanofilaments is based on their unique characteristics. The nano scale of the CNTs and CNFs reduces the defects in their molecular structure as well as increases their surface-to-volume ratio. This unique structure allows carbon nanotubes to have extraordinary mechanical, electrical, thermal, and chemical properties that make them promising filaments for many engineering materials and applications [8, 9]. CNTs and CNFs have shown great potential as reinforcements for polymer-based materials [10-12].

In the last few years, scientists and researchers have started to investigate and implement the use of these nanofilaments—CNTs and CNFs—in reinforcing concrete. The idea behind using the CNTs and CNFs is their potential to control and prevent the nucleation of cracks at the nano scale by the crack-bridging mechanism, hence preventing the growth and propagation of the cracks to a larger scale. This would result in high-performance cementitious materials, with higher stiffness and durability.

However, to date, many challenges and requirements have not been met to allow for effective utilization of CNTs and CNFs in cementitious materials. The extraordinary aspect ratio of nanofilaments (especially single-walled carbon nanotubes [SWCNTs] [13]) and the graphitic nature of their surfaces have created major challenges for implementation in cementitious materials. These challenges include acceptable dispersion with optimum concentration of the nanofilaments within the cementitious matrix, uniform alignment of the nanofilaments, and solid bonding between the nanofilaments and the surrounding cement matrix. These challenges associated with the implementation of nanofilaments as reinforcements for cementitious materials are discussed in this report. For example, it has been shown that dispersion is a very important element for effectively utilizing CNTs in cementitious composites. CNTs form agglomerations and bundles (clumps) with each other in their normal state due to the high van der Waals forces at the nano scale. These agglomerations are difficult to separate (disperse) within any media. Poor dispersion of these CNTs within any media will not only prevent the CNTs from effectively reinforcing the material but will also cause inclusions and voids that will degrade the properties of the matrix and weaken it. Effective dispersion of the CNTs within the matrix will guarantee uniform distribution and bonding of the CNTs within the matrix with evenly distributed stresses, and hence will uniformly transfer the tensile stresses from the matrix to the CNTs.

Uniform alignment of nanofilaments within cementitious composites is very challenging in practice. However, theoretically, due to their needle-like shape (long tubes), CNTs and CNFs can transfer stresses mainly in one direction—the axial direction—parallel to their length. Hence, if they are aligned perpendicular to the direction of the stresses, they will not be able to transfer the stresses. The optimum scenario occurs when these nanofilaments are aligned within the matrix parallel to the direction of the stresses. However, in practice, three-dimensional random distribution of the nanofilaments within different materials has been shown to still be effective to some aspect because the material hardens under the intersection of the cracks propagated randomly in the three dimensions.

Bonding between nanofilaments and cement paste matrix is very important to effectively transfer stresses at the interface between the nanofilaments and the matrix. The adhesive and friction forces at the interface play a major role in determining the mechanical behavior of the

nanocomposite. Unfortunately, these bonds between cement paste and CNTs are naturally very weak because of the smooth surface of the CNTs, and due to the non-covalent bonds. Enhancing these bonds through chemical treatment of the CNTs' surfaces will result in increasing the forces needed to pull out the nanofilaments from the cement paste matrix. This study found that the pullout action of the CNTs significantly increases the flexural strength, ductility, and toughness of the CNTs/cement paste composites.

In this study, the aspect ratio effects of short and long multi-walled carbon nanotubes (MWCNTs) implemented into cement paste were investigated in order to improve the cement paste's mechanical properties. The hypothesis adopted was that due to the large contact area between the long MWCNT surfaces and the surrounding cement matrix—compared to the short MWCNTs—the larger adhesive surface energy and friction forces would develop at the interface, which should increase the pullout action energy and hence improve the nanocomposite mechanical properties, like strength, ductility, and toughness. However, this hypothesis required acceptable dispersion of the long MWCNTs within the cement composite, which was very challenging due to the high aspect ratio.

In order to physically visualize the effects of the aspect ratio of the nanofilaments, a chart was developed to show the aspect ratio effect on the surface area/volume ratio for different lengths of SWCNTs, MWCNTs, CNFs, and carbon microfibers (CMFs; as shown in Fig. 1). It is clear from the chart that only CNTs can provide an extremely high aspect ratio, as well as a very high surface area/volume ratio. The high surface area/volume ratio is a crucial and desired factor in order to provide the most efficient fiber-reinforced composite system. The higher the surface area means the higher the contact area with the matrix, and hence the higher the bonding strength and reinforcement.

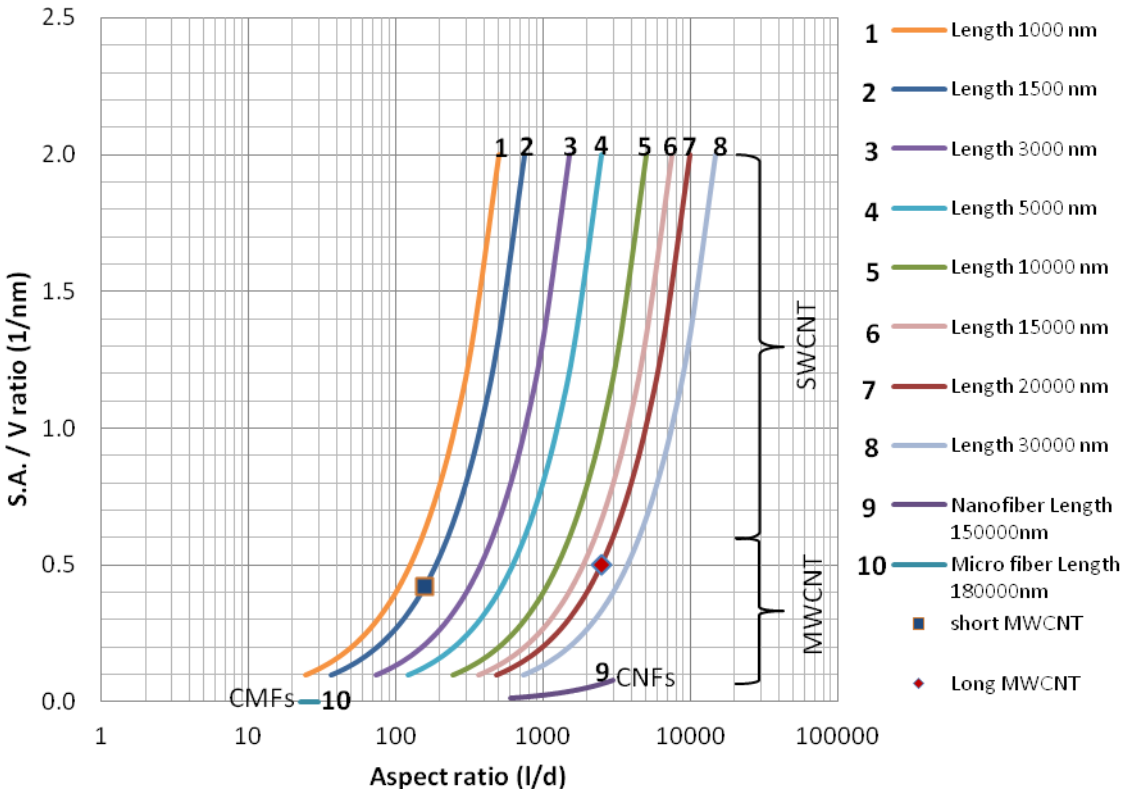

Fig. 1. The aspect ratio effect on the surface area/volume ratio for different lengths of SWCNTs, MWCNTs, CNFs, and CMFs.

Fig. 1 shows that SWCNTs can provide a surface area/volume ratio that exceeds 1.0/nm. This is unique and cannot be achieved in any material on earth except SWCNTs, especially when considering ultra-long CNTs, which have an aspect ratio of several million. On the other hand, CMFs and CNFs show very limited ranges of aspect ratio and a relatively low surface area/volume ratio. These unique geometrical characteristics of CNTs, as well as the unique mechanical properties, like high strength, ductility, and stiffness, were the vital motivation for this study, which sought to combine CNTs with concrete.

After adopting CNTs as the focus of this study, additional physical/geometrical relationships between the different geometrical properties were studied. Factors such as length, aspect ratio, and surface area/volume ratio of the CNTs, along with cement paste/CNT composite parameters such as mass fraction of CNTs by weight of dry cement, and the approximate number of the CNTs obtained for that specific mass fraction were examined. Fig. 2 includes a chart

showing the relationships for CNTs and cement composites and the aspect ratio effect on the surface area/volume ratio for different lengths of SWCNTs and MWCNTs.

1.2 Carbon Nanotubes

1.2.1 Nature of CNTs

Carbon nanotubes have always existed in nature; however, they were first discovered in 1952 by Russian scientists L. V. Radushkevich and V. M. Lukyanovich [14]. Fig. 3 shows the first images of CNTs. Still, CNTs were not scientifically recognized and used until the last two decades. In 1991, Sumio Iijima [15] published the first article that systematically describes the formation of helical microtubes made of pure carbon atoms linked together by carbon-carbon (C-C) bonds.

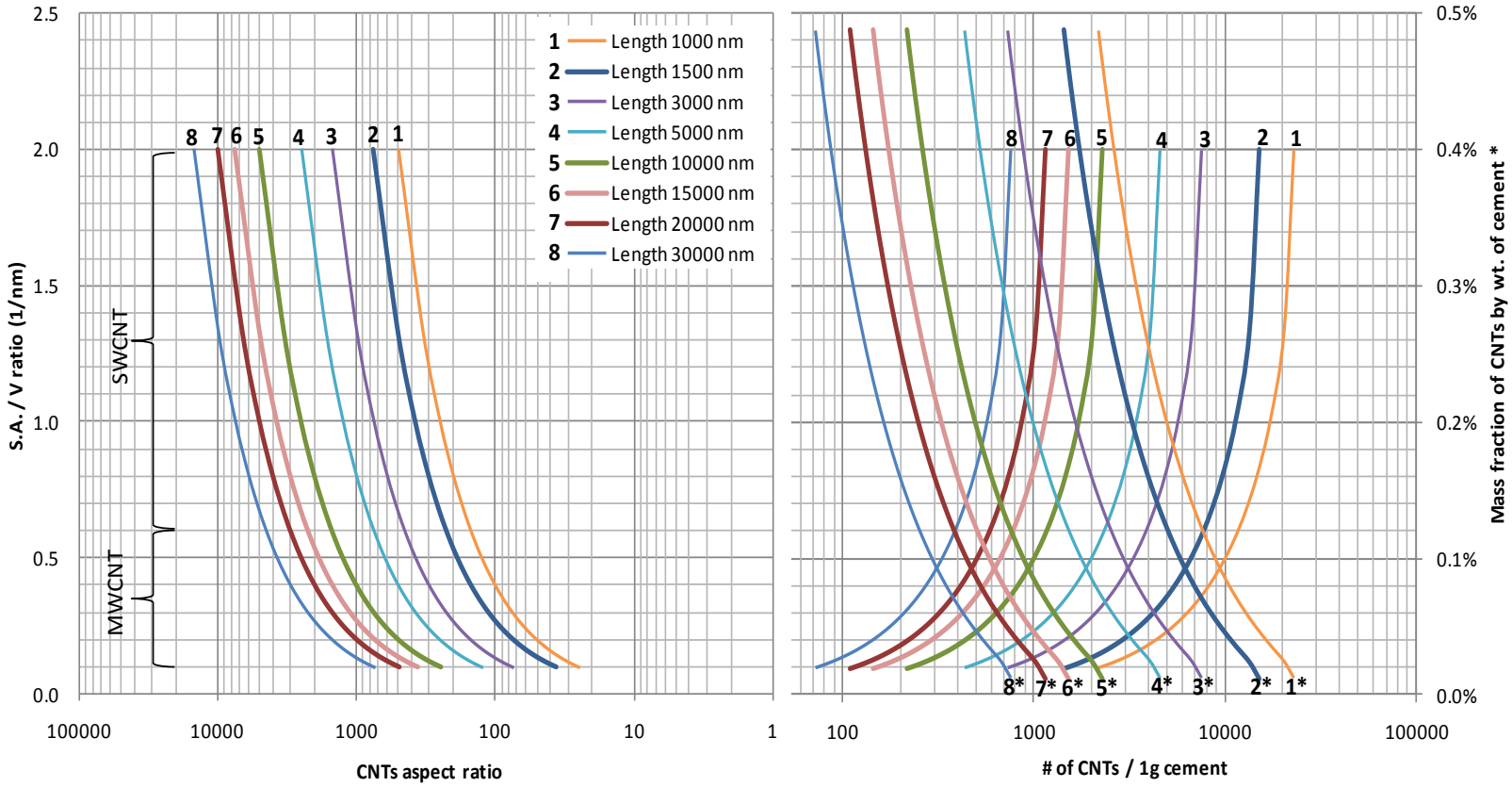

Reading the mass fraction values should be done through the curves with "" numbers.

Fig. 2. The aspect ratio effect on the surface area/volume ratio for different lengths of SWCNTs and MWCNTs, and the relations between surface area/volume ratio with mass fraction of CNTs by cement weight and their number per 1 g of cement.

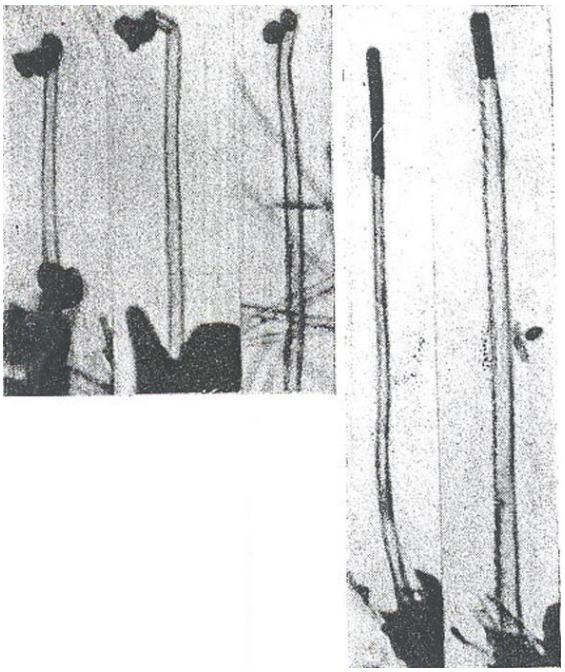

Fig. 3. First images of carbon nanotubes published in 1952 by Russian scientists [14].

There are many known forms for carbon structures in nature, like diamond, graphite, graphene, and fullerenes (buckyballs; Fig. 4). CNTs can be imagined as a rolled graphene sheet whose structure is made of one layer of carbon atoms bonded by carbon sp^2 bonds in a hexagonal pattern. Graphene sheets were investigated for the first time in 2004 by the 2010 Nobel Prize winners in physics, Andre Geim and Konstantin Novoselov, Russian scientists from the University of Manchester. CNTs can be assumed to be a graphene sheet rolled in a cylindrical (tube) shape and closed at both ends by half fullerenes or another carbon structure.

These rolled tubes can be formed as a single tube with one cylinder, called single-walled carbon nanotubes, or may be made from multiple layers, as if they have many cylinders inside each other (from 2 to 20 concentric layers), called multi-walled carbon nanotubes.

(a) (b)

Fig. 5 shows schematic drawings for an SWCNT and an MWCNT. The size of the CNTs is in nano scale; the diameter could vary from 1 to 4 nm for SWCNTs and 5 to 50 nm or more for MWCNTs, and the length can extend into several micrometers. CNTs have different structural

patterns for the carbon atoms; the orientation of the carbon hexagonal structure has different names, like armchair, zigzag, and chiral. Fig. 6 shows three different structural orientations for CNTs.

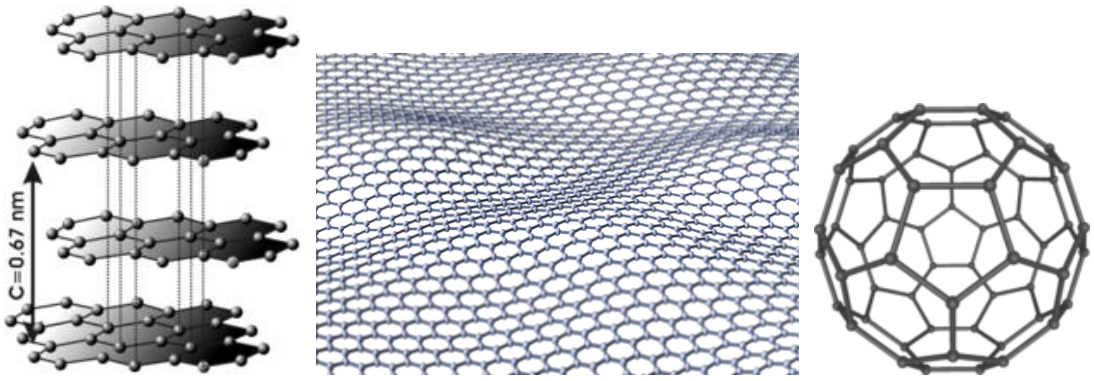

(a) (b) (c)

Fig. 4. Comparison between an (a) graphite structure [16], (b) graphene sheet [17], and (c) fullerenes (buckyball) structure [18].

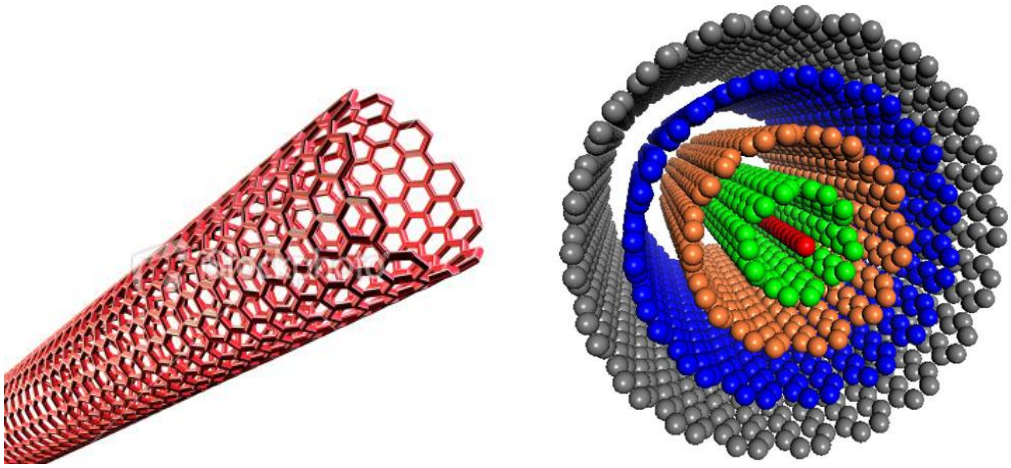

(a) (b)

Fig. 5. Schematic of an (a) SWCNT [19] and (b) MWCNT [20].

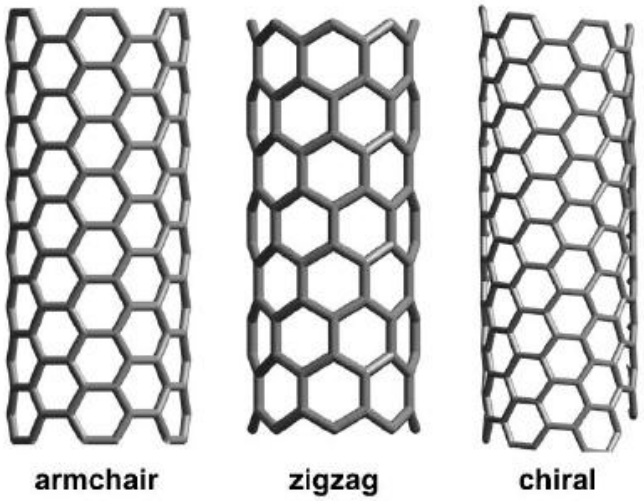

Fig. 6. CNT structural orientations: (a) armchair structure, (b) zigzag structure, (c) chiral structure [21].

1.2.2 Manufacturing of CNTs

There are three main approaches to manufacturing CNTs [22]: chemical vapor deposition (CVD), electric arc-discharge, and laser ablation (LA).

The chemical vapor deposition method is the most commonly used method; it is relatively less complicated and is cost efficient for mass production of CNTs. In addition, it produces CNTs with relatively high purity. This method is based on using a metal catalyst to initiate CNT formation by pumping high-carbon gases like acetylene, ethanol, or methane in a chamber using high pressure and temperature. The type and size of the metal catalyst, along with the pressure and temperature in the reactor, will determine the produced CNT's properties, including purity, length, and size.

In the electric arc-discharge method, both SWCNTs and MWCNTs can be produced by applying an electric arc through two carbon electrodes, which are surrounded by an inert gas. The high temperature from the arc (up to 3000^{o}C) will sublimate the carbon atoms and form the organized structure of the CNTs [23]. This method, however, will not provide a high purity of CNTs (around 30% pure CNTs by weight).

The laser ablation process produces a high purity of CNTs (around 30% pure CNTs by weight). This method uses a laser beam to evaporate a piece of graphite at a very high temperature within an inert gas. The evaporated gas is then cooled and solidified to form the

CNTs. The size of the CNTs will depend on the temperature of the reactor [24]. This method is the most expensive method; however, it provides uniform and pure CNTs.

1.2.3 Properties of CNTs

The unique structure and the nano scale of carbon nanotubes reduce the defects in their molecular structure as well as increase their surface-to-volume ratio. CNT properties would dramatically expand the number of mechanical, electrical, thermal, and chemical applications [9]. The applications for CNTs include structural and non-structural applications. Examples of non-structural functions include self-sensing for measurements of strain, temperature, damage, self-heating (for deicing), electromagnetic interference shielding, and even drug delivery for medical applications. For structural applications, the unique structure allows carbon nanotubes to have unique mechanical properties that make them promising reinforcements for many engineering materials [8].

The hexagonal structure of the carbon lattice in the CNTs provides a very strong structure, one that is stronger than diamond bonds. However, the van der Waals forces between the cylindrical tubes of the MWCNTs are much weaker and hence will allow the inner tubes to slide with respect to each other.

The measured tensile strength for multi-walled CNTs was reported to reach 63 GPa (about 100 times stronger than steel), with an ultimate strain capacity of more than 12% (about 60 times higher ductility than steel) and a Young's modulus of about 950 GPa [25]. Wong et al. [26] measured the flexural strength of MWCNTs—fixed as a cantilever beam—using an atomic force microscope (AFM) tip, and the results showed the capability of the MWCNT to elastically store and absorb strain energy. The average flexural strength reported was 14.2 ± 8.0 GPa. Yet, CNTs has a very low mass density that varies based on the purity, from 0.037 g/cm^3 with the super-growth CNTs [27] to about 1.3 to 1.4 g/cm^3 in conventional CNTs [9] (about 1/6 of the density of mild steel).

1.3 Literature Review

1.3.1 CNTs in Polymers, Metals, and Ceramics

The structural applications for CNTs have been mainly based on reinforcing material composites. The implementations of CNTs in polymeric materials have been widely used.

Significant enhancements in the mechanical properties of polymers/CNT composites have been reported by many researchers. The researches have implemented both treated and untreated CNTs into polymers/CNT nanocomposites. Good bonding strength between CNTs and the surrounding polymer matrix have been reported, and this enhancement in bonding increases the elastic modulus, toughness, and strength of the polymers/CNT composites [28, 29]. The electrical conductivity of polymers/CNT composites has increased significantly by the addition of CNTs up to 10^8 times. CNTs have also been implemented in metal nanocomposites for enhancing the electrical and mechanical properties of nanocomposites, such as CNT-reinforced aluminum composites and copper/CNT composites [30-34]. In addition, CNTs have been used as reinforcements in ceramics [35-38].

The dispersion of filaments and inclusions in composites is a major element in affecting the local characteristics of the matrix material, hence influencing the properties of the global composite. For polymers, effects of dispersion of inclusions on the mechanical and electrical properties of the composites are shown in the works of several researchers [39-43]. Also, some of the effects of dispersion in metals are shown in the works of Stoeffler et al. and Prasad et al. [44, 45], where the increase of the filament particle size compared to the matrix particle size resulted in poor dispersion, hence degrading the mechanical characteristics of the metal composites. This conclusion is important for the dispersion of CNTs in cementitious materials. The dispersion of filament-like fibers in cementitious materials has also been studied [46-48].

1.3.2 CNTs in Cementitious Materials

While much research has been done on CNTs/polymer composites, only a limited amount of research has been done on CNTs/cement composites. As mentioned previously, two major challenges need to be resolved in order to effectively obtain a successful CNT/cement composite: effective dispersion of the CNTs within the cement paste matrix, and adequate bonding or cohesive strength between the surface of the CNTs and the attached cement paste around them. Due to the high van der Waals forces caused by the large surface area/volume ratio, CNTs tend to attract to each other and agglomerate, making it difficult to disperse and separate them. Using an ultrasonic mixer with surfactants in an aqueous solution with a specific amount of energy and sonication time could achieve an acceptable dispersion of the CNTs within the cement paste. However, CNTs can dissolve in the solution or break down into smaller pieces if

an excessive amount of sonication energy is used. The compatibility of the surfactant used to disperse the CNTs with cement is another important issue. The hydration and the chemical reactions of cement could be badly affected; it could delay or even stop the hydration and the hardening process of the cement paste [49, 50].

Makar et al. [51] sonicated CNTs in ethanol for 2 hr and then sonicated the solution for another 5 hr after adding cement powder. After that, they evaporated the ethanol and grounded the resulted dried mixture. The scanning electron microscope (SEM) images for the grounded powder showed cement grains covered by the CNTs; however, some changes in the cement grain surface were noticed, and the authors attributed the changes to the ultrasonication process. On the other hand, other researchers, like Cwirzen et al. [52], tried to grow CNTs on the surface of cement particles directly in order to enhance dispersion and reduce the time and effort of mixing and dispersing the CNTs within the cement paste. Makar et al. [53] tested cement grains coated with SWCNTs before and after the hydration process, and the SEM images showed differences in the distributed non-hydrated cement particles and hydrated matrix. The SEM images also showed micro-crack bridging by the CNTs along with CNT pullout.

Li et al. [54, 55] tested acid-treated (H_2SO_4/HNO_3) functionalized MWCNTs and non-functionalized MWCNTs within cement composites of a 0.4 water/cement (w/c) ratio by dispersing the MWCNTs into plain water using an ultrasonic mixer and then mixing them with cement powder with a surfactant. They reported that the compressive and flexural properties for the functionalized MWCNTs/cement composite were 4% more than for the non-functionalized MWCNTs/cement composite. SEM images showed that the surface of the functionalized MWCNTs was covered by the calcium silicate hydrate (C-S-H), which increased the strength.

Cwirzen et al. [56] used two solutions of poly (acrylic acid) with gum Arabic to disperse treated and untreated MWCNTs with cement. They reported that the use of 0.8 wt% of gum Arabic delayed the cement hydration for 3 days but that this delay in the hydration did not affect the material strength. Flexural and compressive tests were conducted to evaluate the CNTs/cement composite mechanical properties. The nanocomposite was made of 0.045% MWCNTs by weight of the dry cement and cast into 10 mm by 10 mm by 60 mm molds for testing. The results showed improvements in the compressive strength by 50%.

Nasibulin et al. [57] provided a simple one-step process to grow carbon nanotubes and carbon nanofibers on cement particle surfaces using acetylene gas as the source of carbon in the chemical vapor decomposition technique. They used a continuous cement powder feeder rotating in a quartz tube. The CNT-cement coated paste was cast into 10 mm by 10 mm by 60 mm molds for testing. The experimental results showed enhancements in compressive strength by more than 100% and an increase in the electrical conductivity.

Shah et al. [58] improved the mechanical properties of MWCNTs/cement composites by ultrasonicating the MWCNTs in water with surfactants. The results showed an increase in the flexural strength by 8% to 40% and an increase in the elastic modulus by 15% to 55%. The reported optimum nanocomposite was achieved by using 0.1 wt% of dry cement with a water/cement ratio of 0.3.

Konsta-Gdoutos et al. [59] reported a comparison between long and short MWCNTs. The experimental work implemented concentrations of 0.025 and 0.08 wt% for long MWCNTs and 0.025 and 0.1 wt% for short MWCNTs. The experimental results implied that the concentrations of MWCNTs depend on their aspect ratios; optimum strength is obtained with the use of short MWCNTs at a concentration of 0.08 wt% and with long MWCNTs at concentrations less than 0.048 wt%.

In another publication, Konsta-Gdoutos et al. [60] suggested that mechanical properties were improved by proper dispersion, which was achieved by ultrasonicating the MWCNTs with a dispersant solution; less concentration is needed to improve the mechanical properties of long MWCNTs in cement composites than the concentration needed in short MWCNTs to reach the same level of mechanical properties.

Abu Al-Rub et al. [61] and Tyson et al. [62] investigated both CNFs and MWCNTs at different concentrations with cement paste (w/c ratio = 0.4) under a three-point flexural testing. They also investigated the functionalization effects on the CNFs and CNTs. Results were obtained at 7, 14, and 28 days from the day of casting and compared to plain cement specimens. Four mechanical properties were investigated: strength, ductility, modulus of elasticity, and toughness. The results showed that the CNFs/cement composites had better improvement in general than the MWCNTs/cement composites. The non-functionalized CNFs and MWCNTs showed a delay in gaining strength before the 28 days. However, most of the nanocomposites

showed improvements in ductility compared to the plain cement specimens. On the other hand, the functionalized CNFs and MWCNTs showed degradation in mechanical properties in general over time. The authors attributed the degradation to formation of weak hydration products, or harmful components like excessive formation of ettringite. SEM imaging was obtained to study the microstructure of the nanocomposites and to evaluate the nanofilament dispersion.

Luo et al. [63] tested MWCNTs with cement paste with fumed silica (FS; Grade I) at different concentrations of MWCNTs (0.1, 0.5, and 1 wt%). The dispersion of the MWCNTs was done by using a surfactant and ultrasonication. The nanocomposites were tested under three-point flexural testing with beam dimensions of 160 mm by 18 mm by 36 mm. The water/cement ratio was 0.46. The results of testing at 28 days showed improvements in the flexural strengths and the stress-intensity factor by 44.4% and 79.7%, respectively, with best enhancement for the 0.5 wt% of MWCNTs.

In another publication, Luo et al. [64] tested MWCNTs in cement paste using a surfactant and ultrasonication at a MWCNT/cement ratio of the same previous concentrations of 0.1, 0.5, and 1 wt%, and the results showed a 44.5% increase in the structural damping capacity of the MWCNT/cement composite compared to plain cement paste specimens.

Hunashyal et al. [65] tested beams of dimensions (20 mm × 20 mm × 80 mm) under a four-point bending test for composites of plain cement and carbon microfibers (CFs) with MWCNTs. The MWCNTs and the CFs were separately sonicated with a surfactant using an ultrasonicator for a long time (90 min for the MWCNTs and 20 min for the CFs). The sonicated solutions were then mixed with cement and sonicated again for another half hour. Next, the composite mixtures were cast, cured, and tested at 28 days. Four different cement paste composites (w/c ratio of 0.4) with relatively high amounts of MWCNTs were tested: 0.25, 0.5, 0.75, and 1 wt% of dry cement. The results showed improvements in strength, ductility, and toughness. The flexural strength increased by about 88% for the 0.75% MWCNTs specimens, compared to the plain cement specimens. It was reported that the ductility increased with the increase of the MWCNT content in the composites.

Generally, only some results showed improvements in the mechanical properties of the CNTs/cement composites due to the obstacles of good dispersion and bonding.

1.4 Research Objectives

The main objective of this research was to investigate the effects of different lengths (aspect ratio) and types (functionalization) of MWCNTs as nano reinforcements on the mechanical properties of a cement paste composite. The cementitious nanocomposite mechanical properties of interest in this study included flexural strength, ductility, modulus of elasticity, and modulus of toughness. Combining different types of MWCNTs at different concentrations to the cement paste was used to enhance the cement paste composite properties. Two aspect ratios were used (long and short MWCNTs) to investigate the effects of large and small aspect ratios and their behavior in cementitious nanocomposites. It was expected that the MWCNTs would enhance the strength and toughness by bridging the nano-cracks and limit the crack propagation at the nano level. The modulus of toughness was expected to improve due to the CNT pullout mechanism from the cement paste.

As noted in the literature, three challenging main points needed to be considered. First was the dispersion of the CNTs within the cement paste matrix. This was a very important element and was difficult to obtain since CNTs tend to agglomerate and bundle together. Second was the bonding between the CNTs and the cement paste. This was another important issue to be considered in order to fully utilize the CNTs and fully transfer the stresses from the cement matrix to the CNTs and hence effectively bridge the nano-cracks; otherwise, low pullout strength would occur and poor enhancement of the mechanical properties would be obtained. Third was the concentration of CNTs used in the composite. Low concentrations may not have been sufficient to fully reinforce the cement paste matrix, and high concentrations may have had dispersivity problems and been more costly.

This study mainly covered four tasks:

- Dispersion of CNTs within the cement paste nanocomposite.
- Examination of functionalization effects on bonding between the CNTs and the cement matrix.
- Testing of the mechanical properties of the CNTs/cement composite.
- Microstructural characterization of the cement nanocomposite using SEM and TEM imaging.

These tasks are discussed in the following chapters:

- Chapter 2 discusses the dispersion challenges of the CNTs within an aqueous solution with the use of a chemical surfactant and within cement paste. It also discussed the CNTs' surface functionalization methods and evaluation.
- Chapter 3 provides the details on mixing the CNTs with the cement paste and the preparation process for the CNTs/cement nanocomposites.
- Chapter 4 provides the results of the mechanical testing and a detailed discussion on the mechanical properties of the different batches of CNTs/cement nanocomposites. The microstructural characterization of the cement nanocomposites using SEM and TEM are discussed as well.
- Chapter 5 summarizes the work done, provides conclusions based on the results obtained, and provides plans for future research.

2. FUNCTIONALIZATION AND DISPERSION OF CARBON NANOTUBES

2.1 Introduction

In order to effectively utilize carbon nanotubes and make use of their extraordinary properties, they should be well dispersed within the reinforced matrix. Dispersion of CNTs means spreading the tubes individually within the matrix by separating the agglomerations and bundles. In this study, dispersion of CNTs within the cement paste was a major element in controlling the mechanical properties of the cement nanocomposite (as discussed in the next sections). Poor dispersion of these nanofilaments within the matrix will not enhance the nanocomposite properties; in fact, it might significantly degrade and deteriorate the matrix properties. Carbon nanotubes in their dry state bundle together due to the van der Waals forces. These interfacial forces at the nano scale are strong enough to pull the nanotubes back to stick together, even after being dispersed in an aqueous solution. Chemical surfactants that provide non-covalent bonds have been used to reduce the surface tension of the solution and keep the CNTs suspended and unbundled within the solution after they have been dispersed (separated) by mechanical dispersion. Regular hand soap is considered a good chemical surfactant for nanofilaments. Two main categories of dispersing techniques of nanofilaments have been used: mechanical dispersion and chemical treatment. A third technique that has been used to guarantee a good dispersion of CNTs and CNFs within cement paste is growing CNTs/CNFs directly on cement particle surfaces [57]; in this method, the CNTs are covered and attached on the surface of cement particles without the need for any further dispersion or sonication process.

2.2 Mechanical Dispersion of CNTs

Mechanical dispersion alone using an ultrasonic wave mixer without any chemical surfactants is not effective for keeping CNTs suspended and dispersed. However, mechanical dispersion (using an ultrasonic wave mixer) is adequate to break the van der Waals forces between the CNTs and separate them in the aqueous solutions. The ultrasonic wave mixer (Fig. **7**) induces high energy into the solution with very high frequency waves (vibrations), causing micro and nano cavitations (vacuum bubbles) to be formed among the solution molecules. These micro/nano vacuum bubbles will implode when they touch the CNT surfaces. The imploded bubbles will cause a huge vacuuming force that will pull the nanotubes away into the solution; hence, the CNTs will be separated from each other and in the liquid. However, if no surfactant is

used in the solution, the suspended CNTs will start to agglomerate and bundle again. In order to disperse the CNTs effectively, sufficient energy and sonication time should be applied. If excessive amounts of energy, sonication time, or both are introduced into the CNT solution, the huge forces from the imploded micro bubbles will break (shorten) the nanotubes. Optimizing the sonication process will require providing the optimum combination of sonication energy, duration, volume of solution, concentration of nanofilaments, temperature, amount, and type of chemical surfactant (anionic, cationic, or nonionic) used in the solution.

Fig. 7. Ultrasonic wave mixer from Sonics & Materials, Inc. used to mechanically disperse CNTs within aqueous solutions [66].

2.3 Chemical Treatment of CNTs

The second technique is the chemical treatment of the surface of CNTs. This technique is widely used. Many different approaches have been used for chemical treatment (functionalization) of CNT surfaces, and many of them show good results in effectively dispersing CNTs within the matrix and improving bonding between the CNTs and the surrounding matrix. Along with the mechanical dispersion of CNTs, the chemical treatment of the surface of CNTs will help in improving the efficiency of dispersion and the bonding between the CNTs and with the material matrix. There are two main types of chemical treatment: covalent bonding and non-covalent bonding (functionalization).

2.3.1 Non-Covalent Functionalization

As mentioned before, the use of chemical surfactants in the sonication solution is the most common non-covalent functionalization approach. The existence of the surfactant will introduce non-covalent bonding or treatment for the CNT surface and the surrounding liquid. The main purpose of these chemical surfactants is to reduce the surface tension of the water, thereby helping to separate the CNTs and keep them suspended and separated within the solution. The non-covalent functionalization approach provides the least amount of damage to the CNT surfaces since no defects are caused by the chemical surfactant to the surface of the CNTs and the only damage (breakage) will be due to excessive sonication power induced.

Chemical surfactants are amphiphilic; they have two side groups in their chemical structure: hydrophilic (polar) and hydrophobic (nonpolar) [67]. The hydrophobic side of the amphiphilic surfactants will be attracted to the CNT surface (which is hydrophobic), where the hydrophilic end group will be attached to water molecules. Hence, the surfactant will pull the CNTs away from each other toward the water in the aqueous solution and the nanofilaments will stay suspended in the solution because of these non-covalent bonds.

While the focus of this study was on the CNTs/cement nanocomposites, it is important to mention that most of the CNT composite and dispersion research has focused on polymer nanocomposites. Many researchers have combined CNTs within different types of polymers successfully [12, 67-72]. Many different surfactants have been used to disperse CNTs within polymers. For example, Bandyopadhyaya et al. [73] ultrasonicated SWCNTs for 20 min with a water solution with the addition of gum Arabic as a surfactant. They achieved homogeneous dispersions for the CNTs because of the absorption of the surfactant. Islam et al. [74] successfully dispersed high mass fractions of CNTs in different surfactants like sodium dodecylbenzene sulfonate (NaDDBS)—which is a main component of laundry detergents—Triton X-100, and sodium dodecyl sulfate (SDS). While these surfactants and many others can be used in polymers, there is a very limited number of surfactants options that can be used with cementitious materials. The nature and chemistry of cement and its hydration process require certain surfactants that are compatible with cement since many surfactants will delay or stop the hydration process of cement paste [56]. It has been shown by Yazdanbakhsh et al. [49] that using sodium dodecylbenzene sulfonate as a surfactant with cement introduces much more air

entrained in the cement paste (five times more than normal range), thereby hindering the initial set of the cement paste for 24 hr.

One of the most successful surfactants that is compatible with cement without affecting the hydration process was proposed by Yazdanbakhsh et al. [49]. It has been shown that using an ultrasonic mixer with a commercial superplasticizer, ADVA Cast 575 (polycarboxylate-based water-reducing admixture), to disperse CNTs in the mixing water of cement paste provided a relatively good dispersion of the CNTs within the water. In this study, this technique of using ADVA Cast 575 superplasticizer as a surfactant to disperse MWCNTs was employed. The details of the experimental work done in this study for the CNTs/cement composites are discussed the next sections.

2.3.2 Covalent Functionalization

Covalent functionalization is widely used in the world of nanocomposites; it is not only a powerful tool for CNT and CNF dispersion but also opened the door to many applications of different nanocomposites by increasing the reactivity and bonding between functionalized CNTs and the hosting matrix. Covalent functionalization has effectively utilized these nanofilaments into usable composite materials.

Many different approaches have been used to functionalize CNTs for cement nanocomposites, like air oxygen treatment [75-77], acid treatment [78], ozone treatment [79, 80], and plasma oxidation [76, 81-84]. The main purpose of these processes is to provide a side group (functional group) at the surface of CNTs to improve dispersion and increase the reactivity and bonding strength between functionalized CNTs and the matrix by covalent bonds. The most common functional groups used in CNTs/cement nanocomposites are the oxygen groups, which include hydroxyl, carboxyl, carbonyl, and ester side groups. Other side groups include halogen groups, like fluoro and chloro side groups, in addition to hydrocarbyl groups, which include alkenyl and alkyl side groups. Ago et al. [81] used X-ray photoelectron spectroscopy (XPS) to analyze the surface of MWCNTs and proposed the formation of hydroxyl and carbonyl groups using gas-phase treatment and carboxylic acid groups using liquid-phase functionalization.

The functionalization of CNTs targets one of the following locations on the surface of CNTs—the end caps [85, 86], the defect sites [87], or the whole surface—without introducing defects sites on the surface (sidewall functionalization) [88].

The defect site functionalization includes using a strong oxidizing agent (like sulfuric acid) to attack and defect small locations on the surface of the CNTs. Usually a mixture of sulfuric and nitric acid is used for this type of functionalization. The level of functionalization depends on many factors, like the sulfuric/nitric acid ratio. The higher the concentration of the sulfuric acid, the more defects on the CNT surface. After that, the nitric acid interacts with these defected sites and provides the functional group attached to the defected sites by covalent bonds [81, 88-91].

Wang et al. [92] functionalized SWCNTs using sulfuric/nitric acid treatments. CNTs were mixed at a concentration of 10-20 mg/20 ml of 1:1 solution of the sulfuric and nitric acid. After that, the CNT/acid solution was functionalized by microwave radiation at 450 W for 1 to 20 min at a pressure of 20 psi. The Raman and Fourier transformation infrared (RTIR) spectroscopy showed that the optimum microwave time was 3 min to prevent excessive damage of the CNTs. After drying the solution, SEM images were taken for the CNTs. The images showed an average length of 1 μm, which is smaller than the original length of the CNTs. This indicates that the acid treatment along with the high energy of microwave radiations damaged the CNTs and broke them into smaller pieces.

End cap functionalization is similar to defect site functionalization, but without using sulfuric acid to attack and defect the surface of the CNTs. This means that the oxidizing agent interacts only with pre-defected locations on the surface of the CNTs (if they exist) and functionalizes the end caps at the ends of the CNTs.

The last approach that is widely used for different types of nanocomposites is the sidewall functionalization. In this method, many different chemicals can be used to functionalize the surface of CNTs [93], but there is no need to use a strong acid for the functionalization. These chemicals include the use of salts like benzenediazonium salts [93], oleum (pyrosulfuric acid) [94], or gases such as fluorine gas [95].

Other techniques that have been used for covalent functionalization include ozone and plasma treatments. These techniques have shown positive results of dispersion with minor defects for CNT and CNF surfaces. For example, Fu et al. [96] showed an increase in the CNF surface oxygen content using ozone treatment by changing the surface oxygen configuration from C − O to C = O. The ozone treatment process included immersing the fibers in acetic acid,

H_2O_2, and an NaOH solution, then washing and trying the fibers, and finally exposing the fibers to O_3 gas for 5 min at a temperature of 160°C. Chen et al. [97] used microwave-excited Ar/H_2O surface-wave plasma to functionalize the surface of MWCNTs. The results showed enhancement in the surface oxygen content without damaging the MWCNT surfaces.

Although it is very challenging to obtain good dispersion within cementitious composites, it is more challenging to evaluate quantitatively the level of dispersion of nanofilaments within many matrices, especially within cement paste. Only a few works have tried to quantitatively define the level of dispersion [49, 50, 98]. However, experimentally, SEM and TEM imaging could give some idea on how CNTs are qualitatively dispersed within the matrix. Some researchers assessed the dispersion of nanofilaments in cement paste by measuring the electrical resistivity of the composite and comparing it with the electrical resistivity of the plain cement paste [99].

2.4 Dispersion and Acid Treatment of MWCNTs (Experimental Work)

2.4.1 Dispersion

In order to study the dispersion of the MWCNTs used in this study, two identical solutions of deionized water, with MWCNTs at 0.25 wt% by weight of water and ADVA Cast 575 surfactant (superplasticizer) at 1.25 wt% by weight of water, were made. The first CNT solution was dispersed by mechanical shaking by hand for 7 min. The other CNT solution was dispersed by ultrasonication at a power of 78.64 W (70% of maximum amplitude) for 20 min.

The dispersing results indicated that the mechanical shaking by hand resulted in very poor dispersion. Large areas of agglomerations and bundles of CNTs were seen in the mechanical shacked solution. In just a few minutes, the CNTs had bundled again and settled down in the suspension. On the other hand, the sonicated solution showed a uniform stable distribution of the CNTs within the solution. In order to visually evaluate the dispersion of the CNTs within the solution, cryo-TEM images for the dispersion were obtained at frozen liquid nitrogen temperatures (-196^{o}C) by an FEI Tecnai F20 transmission electron microscope. Fig. 8 shows a relatively good dispersion of the CNTs within the aqueous solution. No significant clumps and agglomerations were noticed.

In general, CNTs are very difficult to disperse well in any media. Ultrasonication is a good means to guarantee relatively good dispersion of CNTs. However, breakage of CNTs could occur due to excessive sonication power induced.

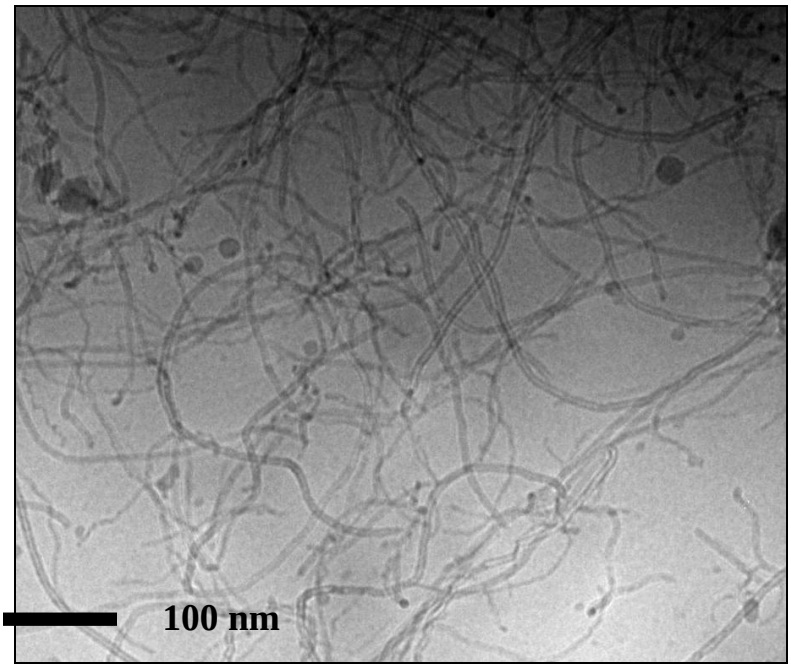

Fig. 8. Cryo-TEM image for the MWCNTs dispersed in a water/surfactant solution. No obvious agglomerations of the MWCNTs were noticed after ultrasonication (picture courtesy of Bryan M. Tyson) [100].

2.4.2 Acid Treatment and Defect Site Functionalization

Acid treatment using sulfuric/nitric acids was the technique adopted in this study for functionalizing the MWCNTs that were used in the CNT/cement composite fabrication (as shown in the following sections).

Four main variables control the acid functionalization process. First is the concentration of each of the acids used, i.e., the ratio between the sulfuric and nitric acids. The sulfuric acid (H_2SO_4) creates small defect sites on the surface of the CNTs, and the nitric acid (HNO_3) oxidizes these defect sites by providing a functional group (like carboxylic acid groups in this study). Increasing the concentration of the sulfuric acid introduces more defects (roughness) on the CNT surfaces. Hence, by changing the sulfuric/nitric acid concentrations, the level of

functionalization can be controlled. However, excessive surface treatment by sulfuric acid could break (shorten), damage, dissolve, or deteriorate the mechanical properties of the CNTs.

Another important element in the acid functionalization process is the temperature of the solution (reaction temperature). An appropriate temperature should be maintained during the functionalization process. A high temperature would increase the reaction speed, and a low temperature could slow it down. The duration of the acid treatment of the CNTs is another variable. The more the CNTs stay in contact with the acids, the more the functionalization will be introduced to the CNT surfaces. Finally, the CNT/acid ratio affects the severity of the functionalization process. If the CNT concentration is relatively high, then more acids will be needed to complete the chemical reactions.

In this study, the complete acid functionalization process for MWCNTs was carried out through three main stages [100]. The first step was to place the untreated MWCNTs in a solution of sulfuric and nitric acids. Then the CNT/acid solution was placed in an oil bath at a constant temperature of 85^{o}C. The sulfuric acid/nitric acid ratio was 2:1, where the CNT/acid concentration was 100 mg of MWCNTs for every 100 ml of the acid solution. The acid treatment of the CNTs lasted for 60 min.

The next step after the acid treatment was to dilute the acidic solution and wash the CNTs. The dilution and washing were done using deionized water. The CNTs were placed in a filter with a 0.45 μm pore size and washed by the deionized water multiple times until the pH value of the washing water reached almost the neutral value between 6.0 and 7.0, which was the pH for the deionized water used.

The last step was to dry the functionalized MWCNTs. Oven drying at a temperature of 60^{o}C was used with a relative humidity set to approximately 0%. The drying process took 1 to 3 days and lasted until the CNTs were completely dried with no change in the weight. The functional group introduced to these MWCNTs was the carboxylic acid group (COOH). These CNTs will be denoted as MWCNTs (COOH) in the remainder of this report.

2.4.3 Functionalized MWCNT Characterization

After the functionalization process was complete, the functionalized MWCNTs (COOH) were analyzed by an X-ray photoelectron spectroscopic in order to measure the oxidization level

at the surface of the functionalized MWCNTs (COOH). The ratio of C1s to O1s was calculated in order to properly calculate the oxidation level. The XPS results (Table 1) showed that the functionalized MWCNTs (COOH) increased the amount of oxygen atoms by 10 times compared to the untreated ones.

In order to widen the area of this research, two new batches of MWCNTs were included. The new batches had a higher aspect ratio, and the functional group for the long MWCNTs (OH) was provided by Cheap Tubes, Inc. [101]. Four different batches were used in this study: untreated short MWCNTs, untreated long MWCNTs, treated short MWCNTs (COOH), and treated long MWCNTs (OH). Table 1 shows a summary of the atomic mass percentages of carbon and oxygen for the four different types of MWCNTs used.

Table 1
The atomic mass percentages of carbon and oxygen for the MWCNTs.

Sample	Carbon %	Oxygen %
Untreated short MWCNTs	98.78[◊]	1.22[◊]
Untreated long MWCNTs	97.44*	-
Treated short MWCNTs (COOH)	87.80[◊]	12.20[◊]
Treated long MWCNTs (OH)	94.42*	5.58*

*Using energy dispersive X-ray spectroscopy [101].
[◊]Data from [100].

In order to evaluate the functionalization effects on the surface of the functionalized short MWCNTs (COOH) and long MWCNTs (OH), SEM images were taken at a high magnification. Fig. 9 shows a comparison between the untreated MWCNTs and the treated short MWCNTs (COOH) and long MWCNTs (OH). The images show that there was no noticeable damage (defects or cuts) introduced on the surface structures for either of the functionalized MWCNTs. In addition, similar surface characteristics were noted, with no significant differences between the untreated and the treated MWCNTs.

However, the mechanical properties of the functionalized and non-functionalized MWCNTs in the cement composites were different. The mechanical properties of the CNTs/cement composites will be discussed in Chapter 4.

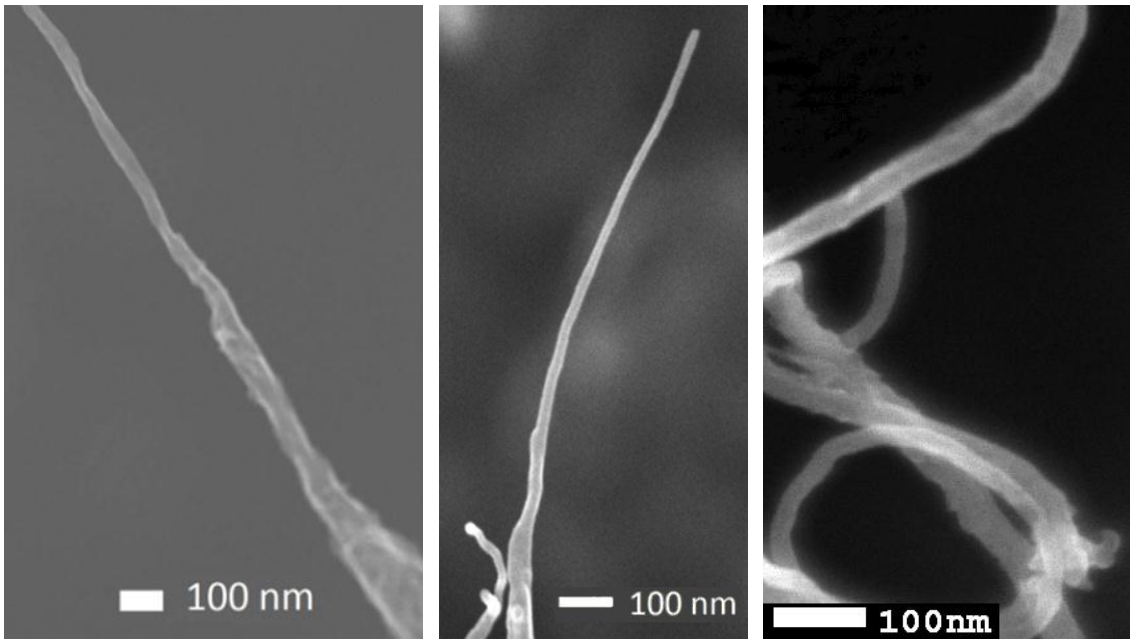

(a) (b) (c)

Fig. 9. SEM images for comparison of (a) an untreated MWCNT, (b) an acid-treated short MWCNT (COOH), and (c) a treated long MWCNT (OH). All the MWCNT surfaces look similar, indicating no severe damage (defects) for the functionalized MWCNTs (pictures a and b courtesy of Bryan M. Tyson) [100].

In summary, using the proper chemical surfactant is helpful for maintaining the dispersion of CNTs; however, the surfactant has to be compatible with cement. Excessive amounts of a surfactant will enhance the dispersivity of CNTs and reduce the amount of ultrasonication power and time but will have negative effects on the cement paste hydration process. Less surfactant means more energy (sonication) is needed for effective dispersion, but more energy will cause breaking and dissolving of the CNTs. An optimum level of both surfactant and ultrasonication must be achieved, and more investigations are needed. In addition, the CNT functionalization process is very important in order to improve dispersion and enhance bonding between CNTs and the surrounding matrix. Providing the specific type of the functional group that will bond with the matrix and optimizing the level of functionalization is crucial, such as providing sufficient side functional groups without excessively damaging the CNTs. A combination of all these parameters will result in effectively utilizing the unique properties of the CNTs.

3. MIXING CARBON NANOTUBES IN AN AQUEOUS SOLUTION WITH CEMENT TO MAKE THE NANOCOMPOSITE

3.1 MWCNT Materials

3.1.1 Long MWCNTs

The long functionalized (OH functional group) and the long non-functionalized multi-walled CNTs used in this study were provided by Cheap Tubes, Inc. [101] and had batch names SKU 030201 and SKU 030101, respectively. The long MWCNTs were produced using the catalytic chemical vapor deposition (CCVD) process. The OH represents the hydroxyl functional group. The physical properties provided by the manufacturer are shown in Table 2. The average aspect ratio (length/diameter ratio) for the long MWCNTs was 1250 to 3750.

3.1.2 Short MWCNTs

The functionalized (COOH functional group) and non-functionalized short MWCNTs were NC7000 multi-walled carbon nanotubes provided by Nanocyl, Inc. [102] and were also produced using the CCVD process. The COOH represents the carboxyl functional group. The physical properties are shown in

Table **3**. The average aspect ratio (length/diameter ratio) for the short MWCNTs was about 157. The functionalized MWCNTs were acid treated using sulfuric and nitric acids in order to get carboxylic functional groups, as discussed in the previous section.

Table 2
Physical properties for the long treated MWCNTs (OH) and long untreated MWCNTs.

	Long CNTs (OH)	Long CNTs
Outer Diameter	< 8 nm	< 8 nm
Length	10-30 μm	10-30 μm
Specific Surface Area	> 500 m^2/g	> 500 m^2/g
Purity	> 95%	> 95%
OH Content	5.58 wt%	--

Table 3
Physical properties for the short MWCNTs (COOH) and short untreated MWCNTs.

	Short CNTs (COOH)	Short CNTs
Outer Diameter	9.5 nm	9.5 nm
Length	1.5 μm	1.5 μm
Specific Surface Area	250-300 m^2/g	250-300 m^2/g
Purity	≥ 90%	≥ 90%
COOH Content	12.20 wt%	--

3.1.3 Portland Cement and Superplasticizer

The cement used in all mixtures was the commercial Type I/II Portland cement. A commercial water-reducing admixture (polycarboxylate), provided by Grace Corporation and named ADVA Cast 575, was used as a superplasticizer. This superplasticizer was used in this study as a surfactant to disperse the CNTs within the aqueous solution.

3.1.4 Mixing Water

The mixing water used for all batches was water deionized using a reverse osmosis water filtering technique. The measured pH value for the water was about 5.5 to 6.0.

3.2 Methodology

3.2.1 Carbon Nanotube Solution Preparation

The preparation process of the nanocomposite cement mixture started by weighing the required amount of the CNTs using an accurate scale (Fig. 10). The required quantities of the mixing water and the surfactant (ADVA Cast 575 superplasticizer) were measured and added together with the CNTs into a water-jacketed beaker with a capacity of 250 ml (Fig. 11). The dispersion process was performed using an ultrasonic mixer from Sonics & Materials, Inc. (Fig. **12**). The high frequency of the ultrasonic waves that transferred through the 13 mm titanium alloy probe to the liquid medium with a maximum power that could reach 500 W and a frequency of 20 kHz provided a good level of dispersion of the CNT filaments in the water. Under adequate ultrasonic wave power and for a certain period of sonication time, the high

energy put into the mixture broke the agglomerations and clumps of the CNTs by breaking the chemical bonding of the van der Waals forces between the nanofilaments.

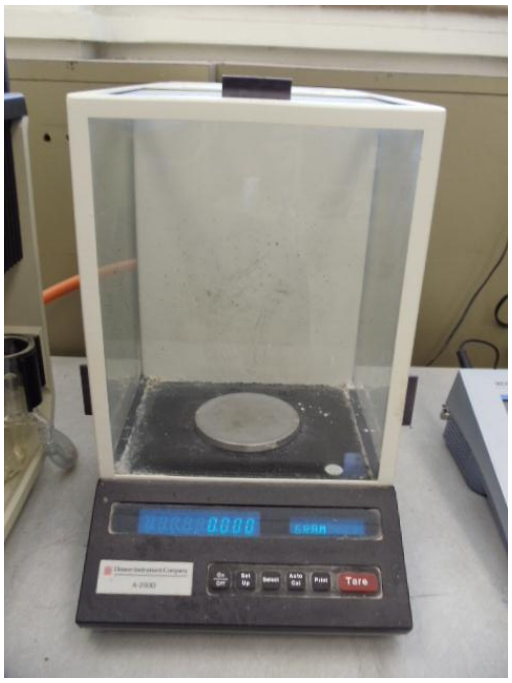

Fig. 10. Accurate scale used to weigh the CNTs.

The high energy introduced into the solution heated it up and caused part of the mixture water to evaporate. In order to reduce the solution temperature, a water jacket of flowing tap water at room temperature surrounding the beaker was used to help reduce the temperature below 45^{o}C throughout the dispersing period. The amount of power and period of dispersion was a critical element for achieving a good dispersion of CNTs; less energy and time could not guarantee a good dispersion, while more energy and time would dissolve and break the nanofilaments. The sonication power for all the different types of MWCNT solutions was 78.64 W (70% of maximum amplitude), and the power per solution volume was 0.4626 W/ml of the solution. The sonication period for the different MWCNT lengths varied from 20 to 30 min.

Fig. 11. Water-jacketed beaker (250 ml) used to sonicate the CNTs within the water using the ultrasonic mixer. Constant flow of the water jacket reduced the temperature of the solution and helped prevent excessive evaporation.

Fig. 12. Ultrasonic wave mixer from Sonics & Materials, Inc. used for CNT dispersion [66].

3.2.2 Mixing Carbon Nanotube Solutions with Portland Cement

The required amount of sonicated CNT solution was poured into a variable-speed planetary kitchen blender (Oster Fusion™), as shown in Fig. 13. Due to the small mix quantities made, the use of the standard Hobart mixer would not have been effective because of its

relatively large mixing bowl. In the previous step, the cement powder was weighed and kept in another beaker. The blender was started with the dispersed solution only, and then the cement powder was added gradually to the CNT solution. After adding the cement powder, the mixing time was a total of 7 min: 3 min at low speed, 1 min at medium speed, and another 3 min at low speed. Another mixing protocol was tried where the CNT solution was added to the cement powder in the blender. However, that protocol caused agglomerations of some parts of the unhydrated cement, which then stuck on the blender jar walls. This required a pause in the mixing process and a scraping of the stuck cement agglomerations to guarantee homogeneous mixing. However, the products of both mixing protocols did not show any significant effects on the mechanical properties from flexural testing.

Fig. 13. Variable-speed planetary mixing blender (Oster Fusion™).

3.2.3 Casting the Nanocomposite into the Molds

Immediately after mixing was done, the composite cement paste was poured into a plastic bottle and placed into a small air vacuuming chamber for 3 min (Fig. 14). The air vacuuming helped get rid of the entrapped air bubbles that formed during the mixing process.

Fig. 14. Vacuuming chamber and the air pump.

Next, the composite cement paste was poured into small vertical acrylic molds of a square cross-section that had been placed on top of a vibrating table, as shown in Fig. 15. The vibration during casting the cement paste helped to fill the molds smoothly and reduce the air voids and entrapped air bubbles. This was important in order to get solid uniform cross-sections of the material throughout the length of the small beams and to not have defects due to air voids that would significantly affect the mechanical strength of the composite.

Fig. 15. Vibration table used for casting the composite cement paste.

The used extruded acrylic molds were chosen for their smooth surfaces and small dimensional tolerances. Acrylic as a polymer will not absorb the mix water from the cement paste like some other polymeric materials. The molds' inner cross-section dimensions were square (6.5 mm × 6.5 mm), as shown in Fig. 16. The molds were bought as long extruded tubes and then were cut into the desired length of about 200 mm. Small square flat pieces (~ 2.5 cm × 2.5 cm) of acrylic were glued to the bottom of the acrylic tubes to seal the bottom and to serve as a standing base.

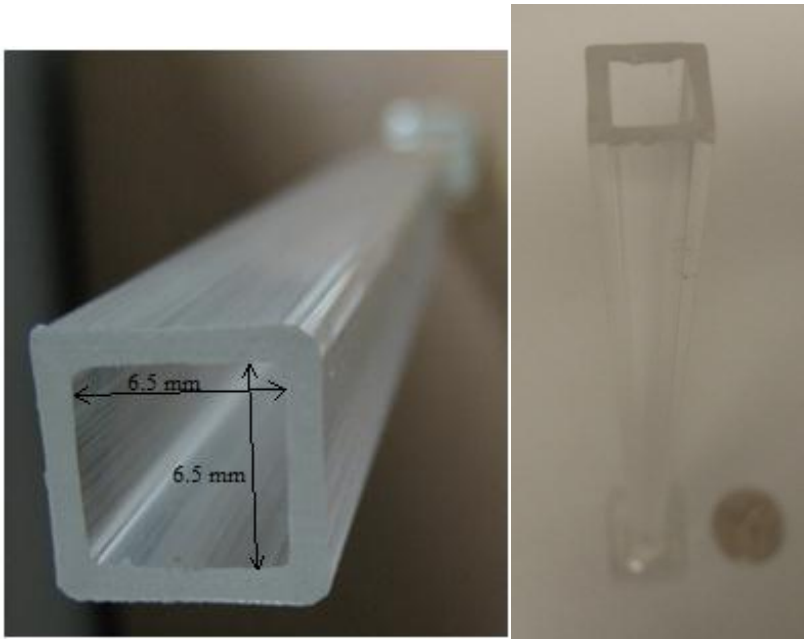

Fig. 16. View of the square acrylic mold.

The cast specimens were then allowed to air cure in the molds at room temperature for 7 days before demolding. Since only the upper side of the molds, which had a very small cross-sectional area, were exposed to air, the mix water content loss was minimal.

After 7 days from casting, the specimens were demolded using a special soldering iron. The soldering iron used was provided by a custom-made cutting edge made of copper, with a power of 200 W and temperature of 537^{o}C (1000^{o}F), as shown in Fig. 17. The sides of the acrylic molds were cut using the soldering iron by melting the acrylic at the cutting lines on the four sides.

Fig. 17. Soldering iron of 200 W power used for demolding the specimens from the acrylic molds.

3.3 Cement Composite Batches

Ten different CNT-reinforced Portland cement paste batches were produced during the course of this study. The first batch was the plain cement batch (reference) sample; the other nine batches covered all different MWCNTs/cement composites. These included five batches using non-functionalized MWCNTs and four batches using functionalized MWCNTs. The different batches included different CNT aspect ratios (long and short) and three different concentrations of the CNTs by weight of dry cement (0.04%, 0.1%, and 0.2%). All specimens including the plain cement reference sample had a water/cement ratio of 0.4. A summary of the mix design for all batches is shown in Table 4. For each testing day (7, 14, and 28 days), four or five replicates (samples) of each specimen were made to get a representative average value from the flexural testing. Between 12 to 15 replicates (samples) for each batch were cast. However, a batch of 0.2% long MWCNTs could not be produced due to the difficulty in achieving satisfactory dispersion of the long MWCNTs within the aqueous solution.

The plain cement paste (reference) specimen was made with a water/cement ratio of 0.4, with the addition of 0.1% of superplasticizer by the weight of cement. This amount of superplasticizer was equal to 25% of what had been added to the other MWCNTs/cement composite specimens. The reason why more superplasticizer had been used in all other MWCNTs/cement composites was that larger amounts of superplasticizer, which was used as a surfactant, were needed in the nanocomposites in order to improve the dispersion of the nanofilaments (see [49] and [98] for more details).

Table 4
Mix design of the functionalized and non-functionalized MWCNT test specimens.

Test Specimens	Superplasticizer: % weight of cement	CNTs: % weight of cement	Ultrasonication time (minutes)
Plain Cement (Reference)	0.1	0.0	-
Short CNTs 0.04	0.4	0.04	20
Short CNTs 0.1	0.4	0.1	30
Short CNTs 0.2	0.4	0.2	30
Long CNTs 0.04	0.4	0.04	30
Long CNTs 0.1	0.4	0.1	20
Short CNTs (COOH) 0.1	0.4	0.1	30
Short CNTs (COOH) 0.2	0.4	0.2	30
Long CNTs (OH) 0.04	0.4	0.04	30
Long CNTs (OH) 0.1	0.4	0.1	20

4. EXPERIMENTAL RESULTS AND MICROSTRUCTURAL CHARACTERIZATION

4.1 Testing Fixture

A custom-made flexural testing apparatus [100] was needed due to the small scale of the specimens (beams) in order to accurately capture the stress-strain behavior of the nanocomposites. The testing apparatus used was a three-point bending testing frame made of 6061 aluminum, with dimensions of 170 mm by 25 mm by 114 mm and a flexural span of 160 mm. Fig. 18 shows the frame dimensions. The frame was fixed with an actuator (NSA12 from Newport Corp.), a load cell (from Strain Measurement Devices) of 2.5 kg capacity to measure the applied force, and a linear variable differential transformer (LVDT; from Macro Sensors) to measure the displacement (deflection) at mid-span of the beam and was connected to a data acquisition board (DAQ; from National Instruments) and a micro-stepping controller (from Newport NSC200) to control and smooth the actuator motion.

A LabView program [103] was written to control the actuator and to record the measured load vs. displacement data. The testing frame setup showing the testing frame components is shown in Fig. 19.

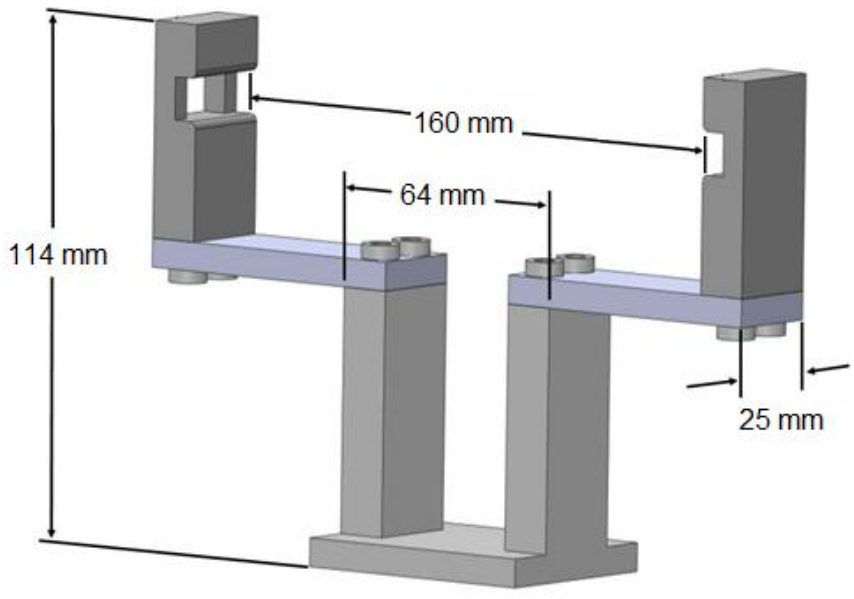

Fig. 18. Three-point bending testing frame dimensions (picture courtesy of Bryan M. Tyson).

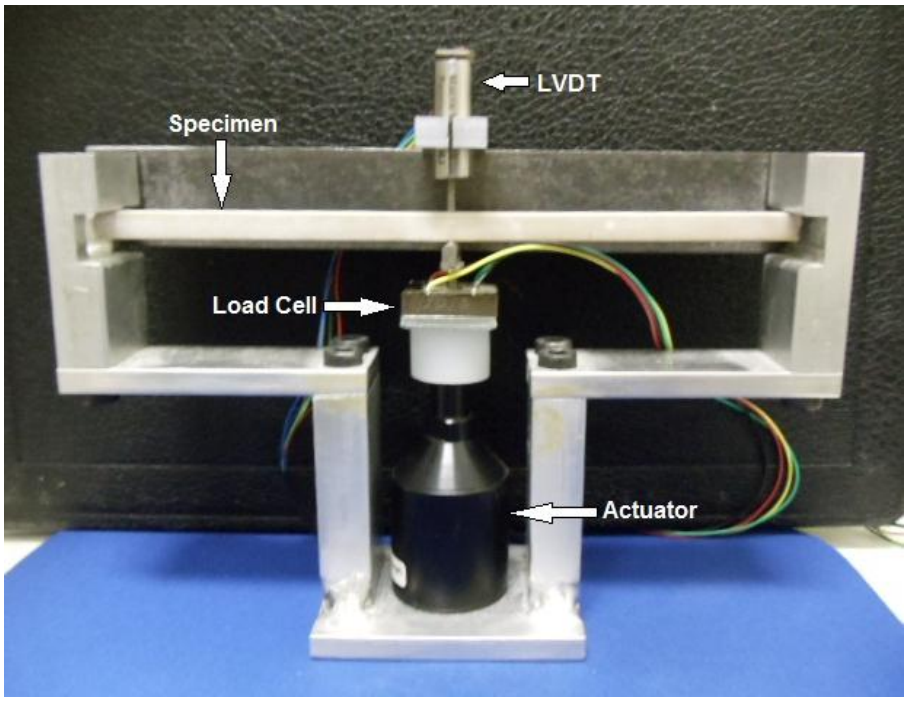

Fig. 19. Testing frame setup, showing the aluminum frame, the specimen, the LVDT, the load cell, and the actuator.

The LVDT had a very high resolution that allowed it to capture micro displacements with an error tolerance of ±0.002 mm and maximum displacement range of 5.0 mm. The load cell had a relatively small load capacity of 24.5 N in order to provide high resolution for the load data recorded. The Newport NSA12 actuator had a motion speed range of 0.001 mm/s to 0.9 mm/s. This allowed higher accuracy for static loading (very low loading speed), which allowed for measuring the mechanical properties like elastic modulus, strength, and toughness. Fig. 20 shows the actuator and the load cell with a loading bar on the top to uniformly distribute the applied force across the beam width at mid-span.

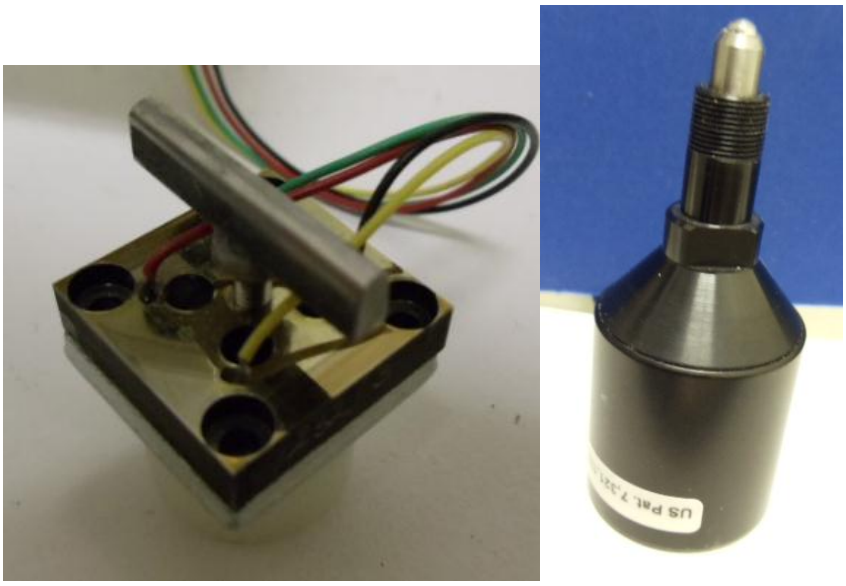

Fig. 20. The 2.5 kg capacity load cell with a small loading bar welded at top of adjustable screw (left) and the Newport NSA12 actuator (right).

All tests were performed at a loading speed of 0.003 mm/s. More information about the actuator specifications are shown in Table 5. The simply supported beams under three-point bending were loaded from the bottom by the actuator, the load cell was mounted on the actuator so that it pushed the specimen up (cambering up), and the LVDT measured the deflection of the beam at mid-span from the top. For more information about the testing fixture, refer to the discussion in Tyson [100].

Table 5
Newport NSA12 actuator specifications.

Feedback	Open loop, no encoder
Axial Load Capacity (N)	25
Maximum Speed (mm/s)	0.9
Travel Range (mm)	11
Minimum Incremental Motion (μm)	0.2
Drive Screw Pitch (mm)	0.3048

4.2 Data Analysis

The loads (in kilograms) and displacements (in millimeters) were measured and recorded by the software and then converted to stresses and strains using the Euler-Bernoulli elastic beam theory in order to calculate mechanical properties:

$$\sigma_i = \frac{LC}{4I} \cdot F_i \qquad \text{and} \qquad \varepsilon_i = \frac{12C}{L^2} \cdot y_i \tag{1}$$

where σ_i is the flexural tensile stress at the extreme tension fibers of the beam at each load step; ε_i is the elastic strain at the extreme tension fibers of the beam at each load step; L is the span length of the beam (160 mm); C is the half-depth of the beam cross-section ($6.5/2$ mm); I is the second moment of area of the square cross-section beam ($6.5^4/12$ mm^4); F_i is the applied force measured by the load cell at mid-span length at each load step (N); and y_i is the displacement measured by the LVDT at mid-span length at each load step (mm).

Data were analyzed and stress-strain diagrams were generated using Matlab software and Microsoft Excel spreadsheets. The Excel software was used to generate the stress-strain diagrams and all the statistical analyses: the mean value, standard deviation, and standard error of the mean. Matlab was used for curve fitting and smoothing. The modulus of toughness of the beams was calculated by integrating the stress-strain curve function (total area under the stress-strain diagram).

4.3 Mechanical Properties

For each different batch, three to five replicates were tested at 7, 14, and 28 days from the casting day. Stress-strain diagrams were obtained for each single sample. The average value for the replicates for each batch was computed for four major mechanical characteristics: maximum flexural strength, ultimate strain capacity (ductility), modulus of elasticity (Young's modulus), and modulus of toughness. The results for the different nine nanocomposite batches were compared along with the plain cement (reference) batch.

Examples of long vs. short non-functionalized MWCNT composite stress-strain curves at 7 days are shown in Fig. 21 along with the plain cement reference sample. The material behaved

linearly until fracture, and both the long and short nanocomposites at different concentrations showed an increase in both the strength and ductility.

Most of the nanocomposites showed a change in the material characteristics at 14 days, as seen in Fig. 22. The plain cement stress-strain curve was almost linear, similar to the 7 day behavior. However, most of the nanocomposites showed softening and multi-peak behavior. After the first crack, the material softened or yielded in some cases and sometimes showed a gradual increase in the strength to become higher than the first-crack strength. This behavior clearly indicated the CNT pullout action, which increased the composite ductility and toughness.

Fig. 23 shows examples of the behaviors after 28 days. The plain cement sample showed softening and nonlinearity post-peak. The non-functionalized nanocomposites showed a significant increase in strength and ductility compared to the plain cement reference sample. The progressive CNT pullout could be seen in most of the samples, and the increase in strength after the first crack showed how the CNTs were effectively bridging the cracks and enhancing the mechanical properties of the material.

Examples of long vs. short functionalized MWCNT composite stress-strain curves are shown in Fig. 24, Fig. 25, and Fig. 26 for the results at 7, 14, and 28 days, respectively. Similar to the non-functionalized nanocomposites, most of the nanocomposites showed a linear trend with a higher strength and ductility with respect to the plain cement reference sample. However, the 0.04% long MWCNT (OH) at 7 days showed softening and nonlinearity in the material with multi-peak behavior, and it had low strength and high ductility compared with the plain cement reference sample. A similar general trend between the functionalized and non-functionalized nanocomposites at 14 days and 28 days was seen. Multi-peak behavior and an increase in the strength after the first crack drop was clearly noticed, which indicates how CNTs can improve the mechanical properties of the cement paste by effectively bridging the cracks and increasing the toughness through the progressive tube pullout. Some of the nanocomposites showed a linear behavior with a brittle failure at a higher strength and ductility compared to the plain cement sample.

More details on the comparison between long and short MWCNT nanocomposites' mechanical properties are discussed in the following subsections.

The stress-strain diagrams for the samples of all different batches are shown in the Appendix.

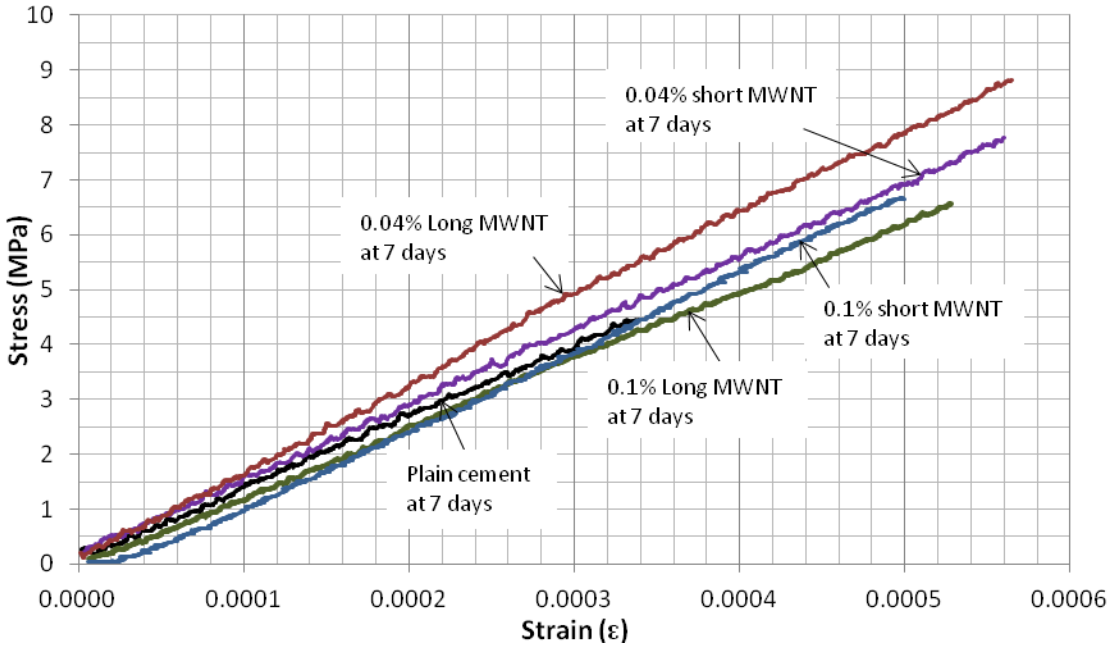

Fig. 21. Example of stress-strain curves for the plain cement and the non-functionalized short and long MWCNT specimens at 7 days.

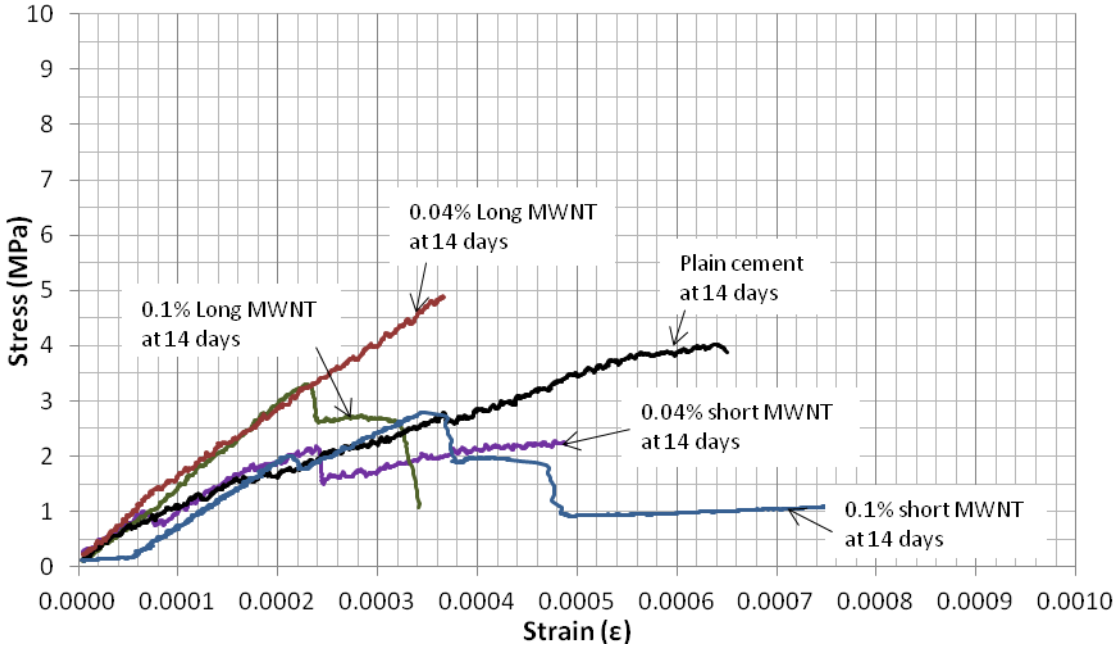

Fig. 22. Example of stress-strain curves for the plain cement and the non-functionalized short and long MWCNT specimens at 14 days.

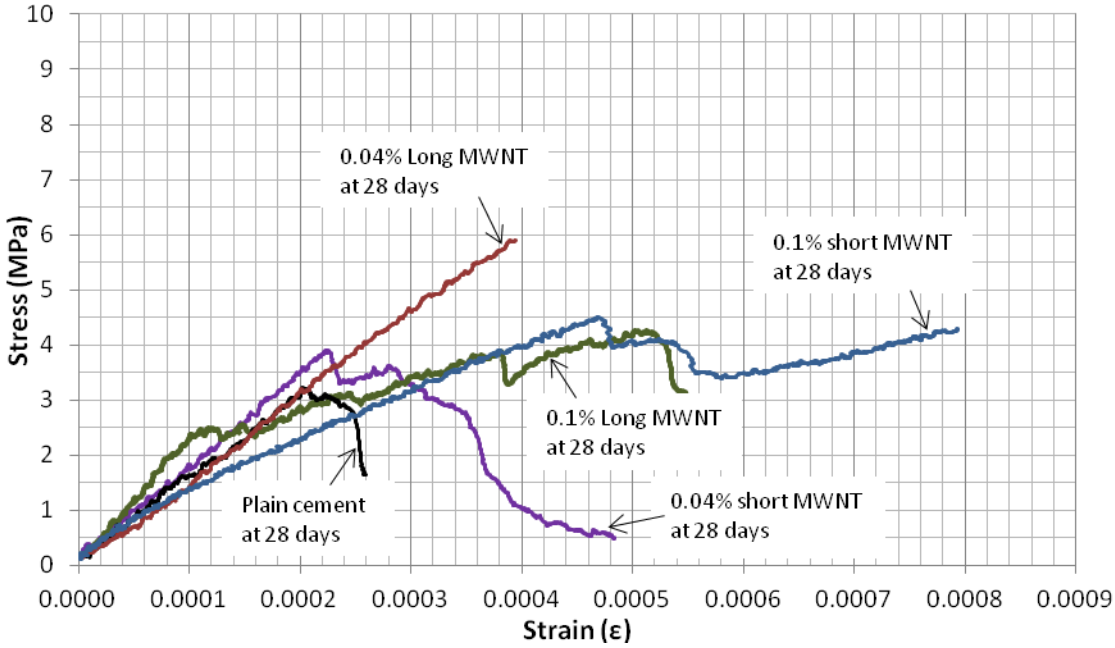

Fig. 23. Example of stress-strain curves for the plain cement and the non-functionalized short and long MWCNT specimens at 28 days.

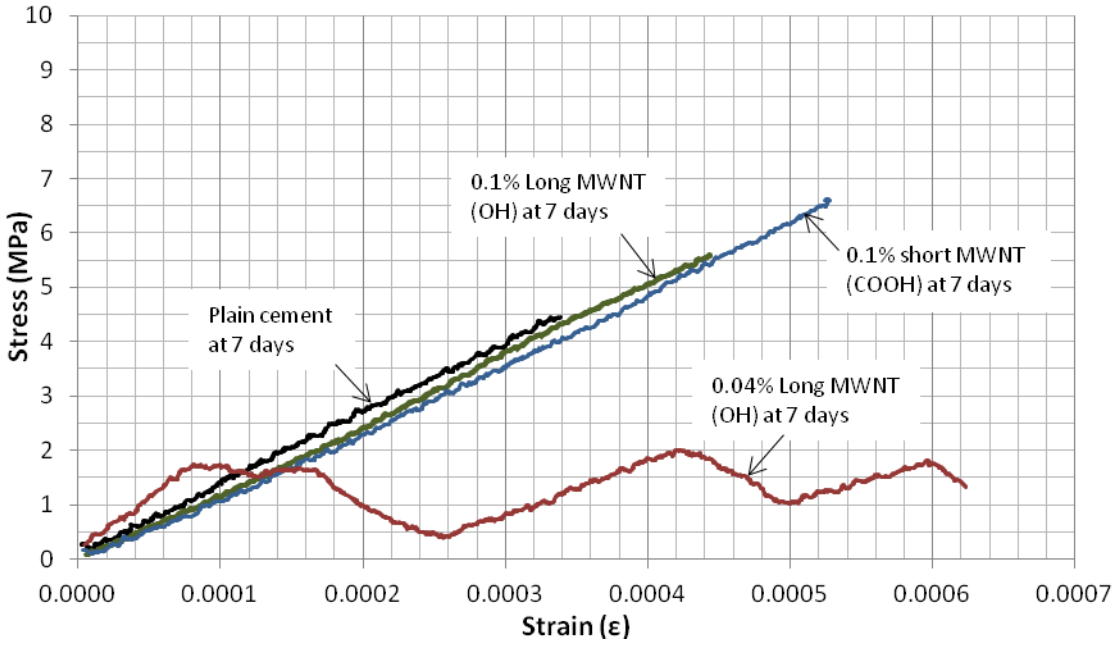

Fig. 24. Example of stress-strain curves for the plain cement and the functionalized short and long MWCNT specimens at 7 days.

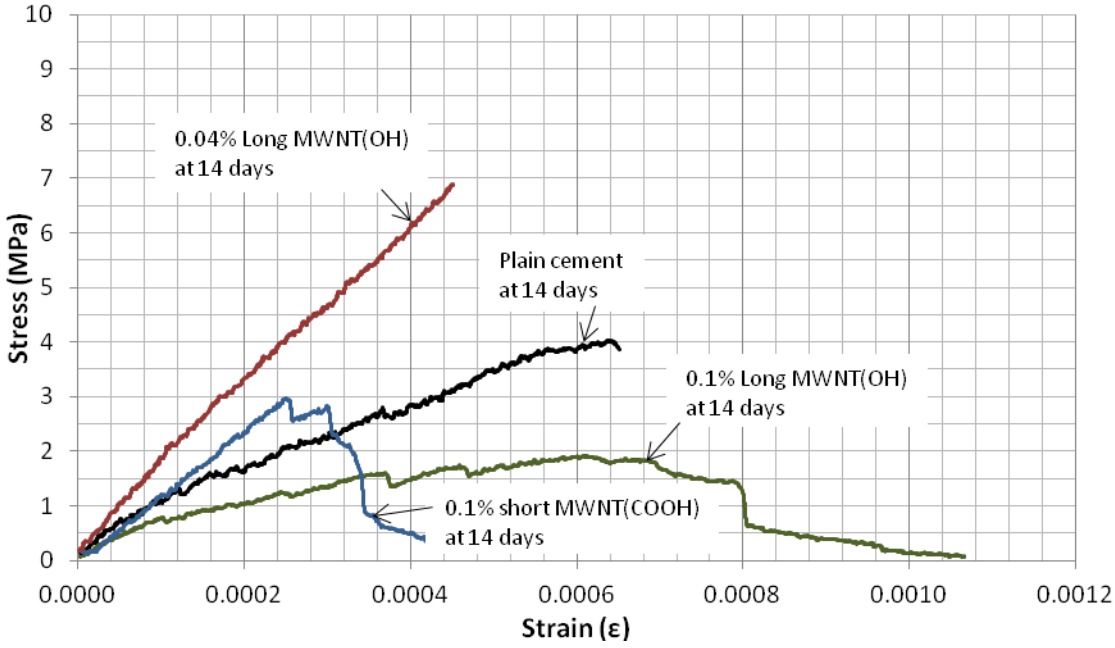

Fig. 25. Example of stress-strain curves for the plain cement and the functionalized short and long MWCNT specimens at 14 days.

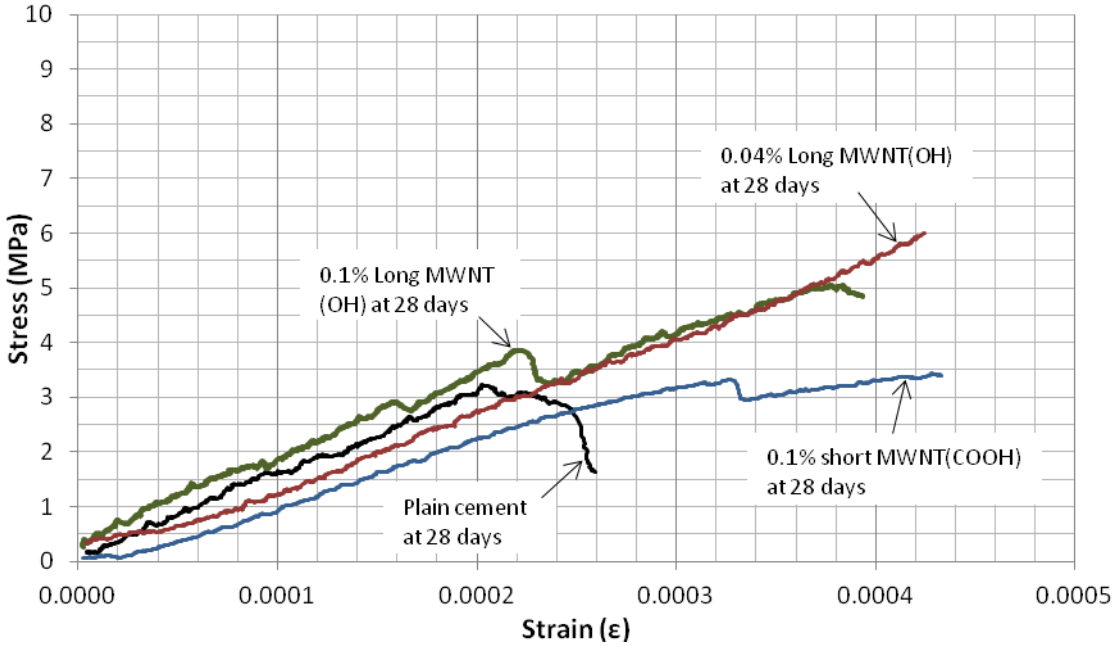

Fig. 26. Example of stress-strain curves for the plain cement and the functionalized short and long MWCNT specimens at 28 days.

4.3.1 Long vs. Short Non-Functionalized MWCNT Nanocomposites

In this section, a detailed analysis for the data obtained from the mechanical testing is discussed, comparing the four mechanical properties of the long and short non-functionalized MWCNT nanocomposites with respect to the plain cement (reference) specimen. Summary tables for the average values of all different batch results are shown in

Table **6** through Table 9 for average ultimate flexural strength, average ultimate strain, average modulus of elasticity, and average modulus of toughness, respectively.

Table 6
Average ultimate flexural strength for the functionalized and the non-functionalized MWCNT test specimens (MPa).

Specimen	Day		
	7	14	28
Plain Cement (Reference)	4.50	4.51	3.22
Short CNTs 0.04	7.49	3.49	3.77
Short CNTs 0.1	5.19	2.39	4.36
Short CNTs 0.2	2.76	3.26	11.87
Long CNTs 0.04	5.47	5.64	4.94
Long CNTs 0.1	6.10	2.96	5.30
Short CNTs (COOH) 0.1	6.36	2.89	4.02
Short CNTs (COOH) 0.2	9.54	2.79	1.96
Long CNTs (OH) 0.04	1.37	6.82	5.88
Long CNTs (OH) 0.1	5.35	1.59	3.70

Table 7
Average ultimate strain capacity for the functionalized and the non-functionalized MWCNT test specimens (%).

Specimen	Day		
	7	14	28
Plain Cement (Reference)	0.0339	0.0603	0.0414
Short CNTs 0.04	0.0511	0.0498	0.0520
Short CNTs 0.1	0.0471	0.0894	0.0651
Short CNTs 0.2	0.0780	0.1040	0.0635
Long CNTs 0.04	0.0460	0.0539	0.0318
Long CNTs 0.1	0.0520	0.0401	0.0430
Short CNTs (COOH) 0.1	0.0471	0.0634	0.0409
Short CNTs (COOH) 0.2	0.0736	0.0453	0.0476
Long CNTs (OH) 0.04	0.0652	0.0471	0.0440
Long CNTs (OH) 0.1	0.0448	0.0840	0.0459

Table 8
Average modulus of elasticity for the functionalized and the non-functionalized MWCNT test specimens (GPa).

Specimen	Day		
	7	14	28
Plain Cement (Reference)	13.69	10.47	14.38
Short CNTs 0.04	12.49	12.17	12.40
Short CNTs 0.1	15.45	10.77	15.20
Short CNTs 0.2	14.36	8.72	16.98
Long CNTs 0.04	11.83	11.43	15.25
Long CNTs 0.1	7.51	8.50	12.99
Short CNTs (COOH) 0.1	12.71	11.93	11.90
Short CNTs (COOH) 0.2	11.99	11.02	8.58
Long CNTs (OH) 0.04	13.87	15.78	17.30
Long CNTs (OH) 0.1	6.79	3.48	14.39

Table 9
Average modulus of toughness for the functionalized and the non-functionalized MWCNT test specimens (kPa).

Specimen	Day		
	7	14	28
Plain Cement (Reference)	0.758	1.524	0.589
Short CNTs 0.04	1.926	1.003	1.013
Short CNTs 0.1	1.142	1.158	1.790
Short CNTs 0.2	1.083	1.704	3.712
Long CNTs 0.04	1.401	1.623	0.875
Long CNTs 0.1	0.946	0.347	0.797
Short CNTs (COOH) 0.1	1.537	0.709	0.860
Short CNTs (COOH) 0.2	3.380	0.769	0.596
Long CNTs (OH) 0.04	0.520	1.700	1.362
Long CNTs (OH) 0.1	0.711	0.474	0.533

For comparison purposes, results for plain cement as well as the long and short non-functionalized MWCNT nanocomposites are shown in Fig. 27 through Fig. 30 for average ultimate flexural strength, average ultimate strain, average modulus of elasticity, and average

modulus of toughness, respectively. The column charts include the standard error of the mean, which is a statistical measure for the deviation (error) from the true mean value ($\bar{x}$), taking into account the number of samples (n) for each data point. The standard error of the mean is the value of the sample standard deviation (σ) divided by the square root of the number of the samples (n), such that:

$$Std.\,Error_{\bar{x}} = \frac{\sigma}{\sqrt{n}} \tag{2}$$

At 7 days, most of the non-functionalized MWCNTs/cement composites showed an increase in the flexural strength, ductility, and modulus of toughness when compared to the plain cement (reference) specimen. The highest improvement in the flexural strength was seen in the short 0.04% MWCNT specimens with an increase of 66% compared to the plain cement specimen. The long 0.1% MWCNT, short 0.1% MWCNT, and long 0.04% MWCNT flexural strength also increased, by 35%, 15%, and 22%, respectively. The short 0.2% MWCNT specimens showed a decrease in their flexural strength by 38% but showed the highest improvement in ductility (ultimate strain) with an increase of 130% with respect to the plain cement specimen. All specimens of different batches showed increase in ductility.

The modulus of elasticity values for most of the specimens at 7 days were close to the plain cement sample. However, the short 0.1% MWCNT and short 0.2% MWCNT showed a slight increase of 13% and 5%, respectively, compared to the plain cement sample. All nanocomposite specimens showed an improvement in modulus of toughness. The highest improvement in modulus of toughness was provided by the short 0.04% MWCNT with a significant increase of 154% compared to the plain cement sample.

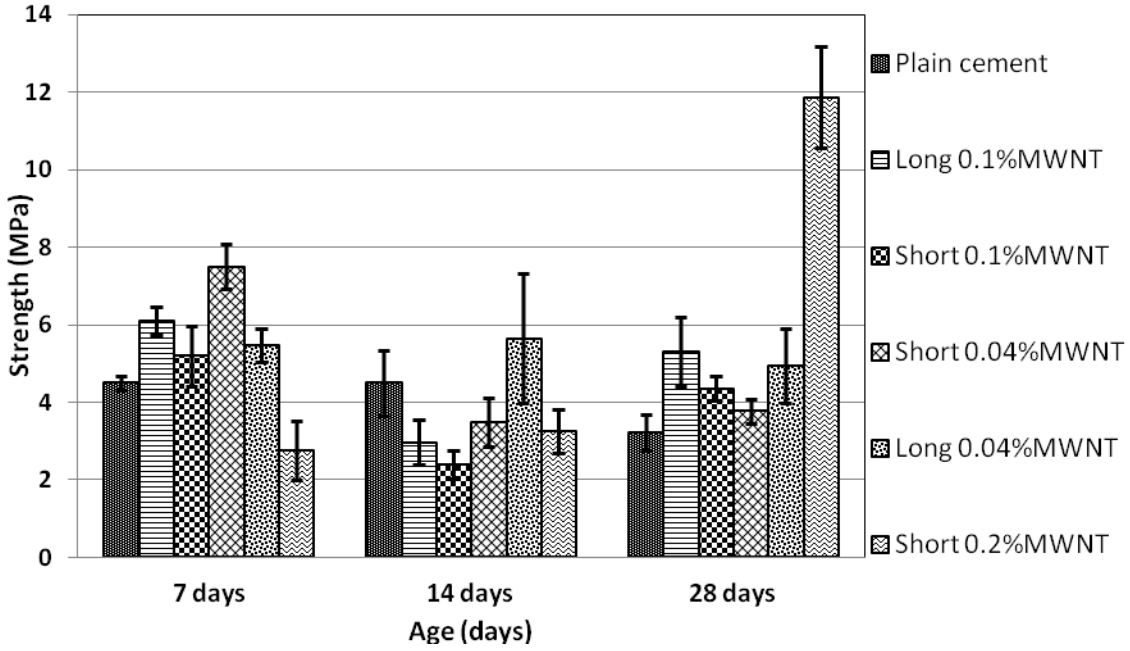

Fig. 27. Average flexural strength results for the plain cement and the non-functionalized short and long MWCNT composite specimens with the standard error of the mean.

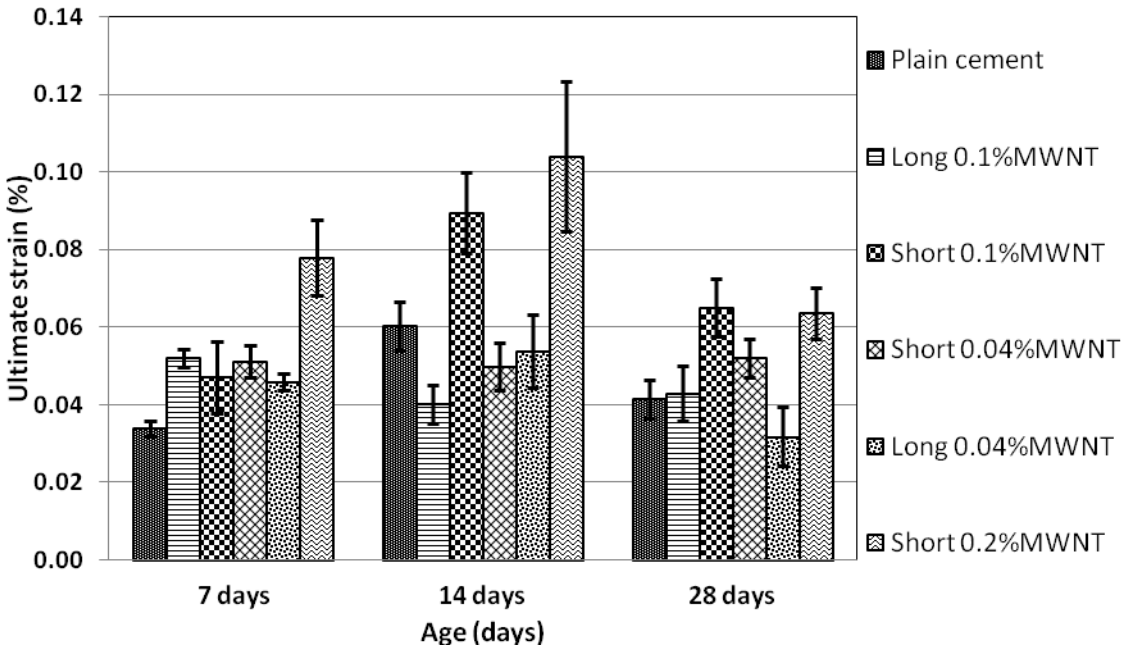

Fig. 28. Average ultimate strain results for the plain cement and the non-functionalized short and long MWCNT composite specimens with the standard error of the mean.

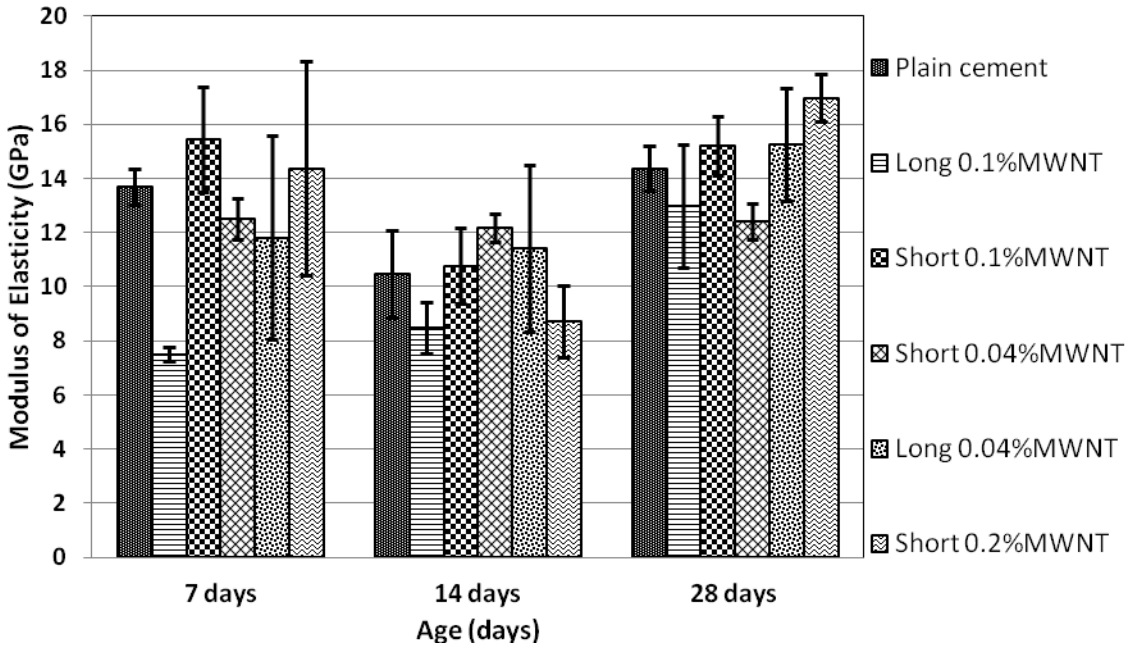

Fig. 29. Average modulus of elasticity results for the plain cement and the non-functionalized short and long MWCNT composite specimens with the standard error of the mean.

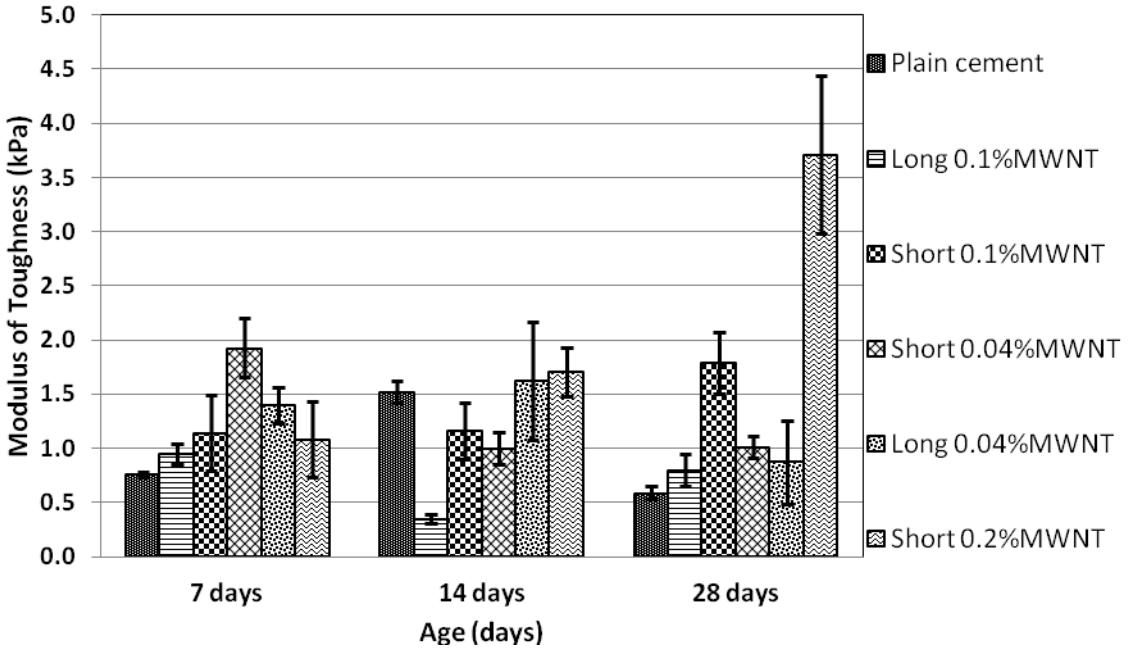

Fig. 30. Average modulus of toughness results for the plain cement and the non-functionalized short and long MWCNT composite specimens with the standard error of the mean.

On the other hand, considerable changes in the behavior of the nanocomposites were observed at 14 days. A large drop in the flexural strength of most of the composites to be less than the plain cement sample strength occurred, except for in the long 0.04% MWCNT, which showed an increase in the average strength by 25% compared to the plain cement sample. The lowest flexural strength was recorded for the short 0.1% MWCNT, with a degradation of 89% with respect to the plain cement sample. Some of the nanocomposites showed a decrease in ductility, while others showed an increase. The highest ductility obtained after 14 days was for the short 0.2% MWCNT with an increase of 72% from the corresponding value of the plain cement sample.

At 14 days, there were no significant changes in the general behavior of the composites regarding the modulus of elasticity values with respect to the plain cement samples, but in general, most of the specimens showed a decrease in the modulus of elasticity compared to the values at 7 days. Degradation in modulus of toughness values was observed in many of the nanocomposites compared to the plain cement sample, and a large decrease was noticed in the long 0.1% MWCNT with 339% degradation from the corresponding value of the plain cement sample.

After 28 days, all composites retrieved their strength values to become higher than the values at 14 days, and all showed higher strength than the plain cement sample. However, the short 0.2% MWCNT showed a significant increase in the flexural strength, specifically increasing by 269% compared to the plain cement sample value. The long 0.1% MWCNT also increased by 65%. Most of the nanocomposites showed a reduction in ductility in general when compared to the ductility at 14 days. The highest ductility at 28 days was for the short 0.1% MWCNT and short 0.2% MWCNT, with 86% and 81%, respectively, which was more than the plain cement sample. However, the short 0.04% MWCNT showed almost a constant value in ductility from 7 days through 28 days.

All specimens showed an increase in their modulus of elasticity values at 28 days compared to the 14 day values, and the short 0.2% MWCNT had the highest increase, 18%, compared to the plain cement sample. All the non-functionalized MWCNT nanocomposites showed a significant improvement in modulus of toughness compared to the plain cement

sample. Due to the large increase in the flexural strength of the short 0.2% MWCNT, it had the highest modulus of toughness value, with an increase of 530%, and the short 0.1% MWCNT improved by 204% compared to the plain cement sample at 28 days.

Generally, the same trend was seen for the variation of flexural strength and modulus of elasticity with variation in age and MWCNT concentration: an increase at 7 days, a decrease at 14 days, and then an increase at 28 days. The same trend of variation in the ductility and toughness was also seen with variation in age and MWCNT concentration: low values at 7 days, an increase at 14 days, and then a decrease at 28 days. Generally, an increase in strength corresponded to an increase in ductility and toughness. Moreover, generally, the short MWCNTs led to better enhancements in the stress-strain response. This might be attributed to the better dispersivity of the short CNTs within the cement paste compared to the long CNTs.

4.3.2 Long vs. Short Functionalized MWCNT Nanocomposites

This section includes a detailed discussion of the results from the data obtained from the mechanical testing, comparing the four mechanical properties of the long and short functionalized MWCNT nanocomposites with respect to the plain cement (reference) specimen. Summary tables for the average values of all different batch results were shown in

Table **6** through Table 9 for average ultimate flexural strength, average ultimate strain, average modulus of elasticity, and average modulus of toughness, respectively.

For comparison purposes, results for the plain cement as well as the long and short functionalized MWCNT nanocomposites are shown in Fig. 31 through Fig. 34 for average ultimate flexural strength, average ultimate strain, average modulus of elasticity, and average modulus of toughness, respectively. The four mechanical properties are shown at 7, 14, and 28 days with the standard error of the mean.

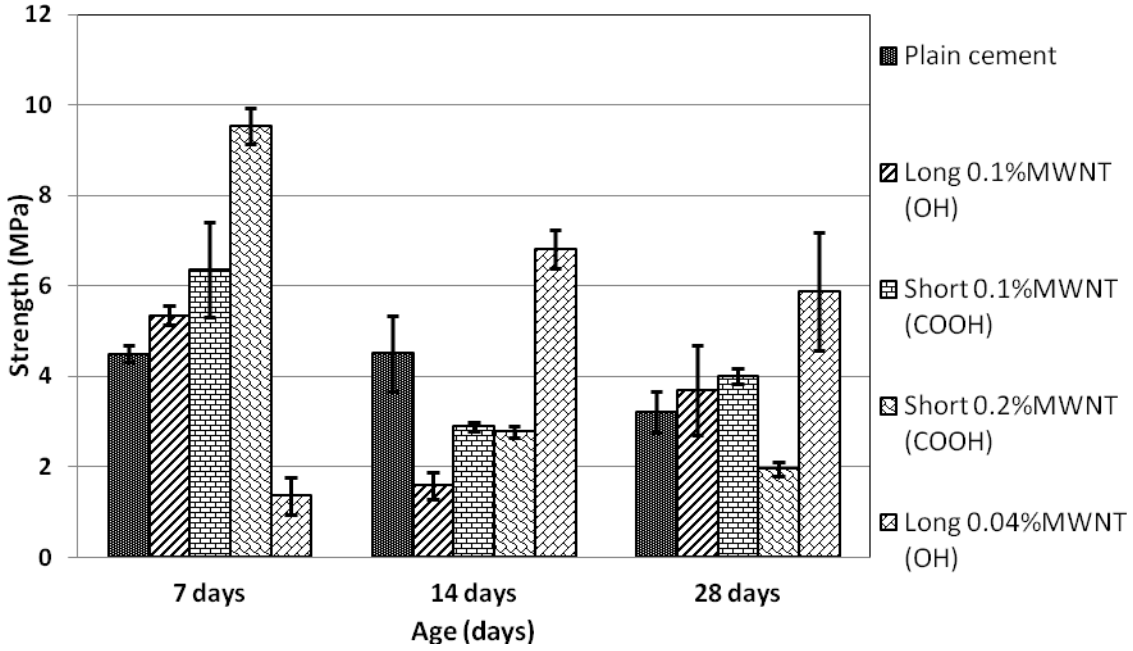

Fig. 31. Average flexural strength results for the plain cement and the functionalized short and long MWCNT composite specimens with the standard error of the mean.

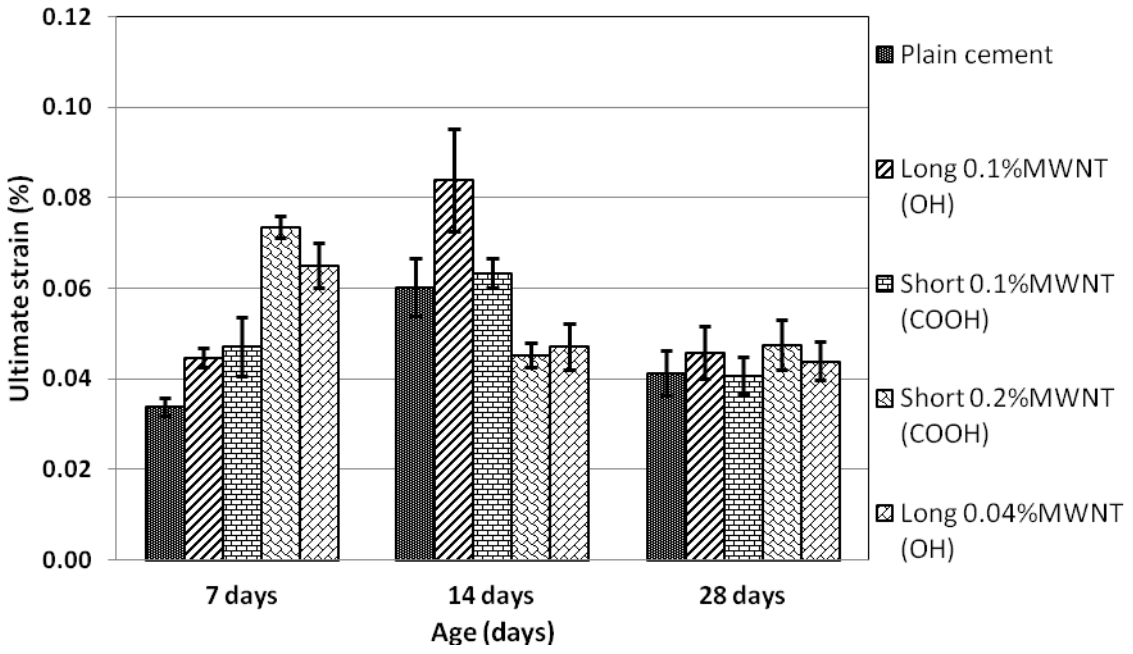

Fig. 32. Average ultimate strain results for the plain cement and the functionalized short and long MWCNT composite specimens with the standard error of the mean.

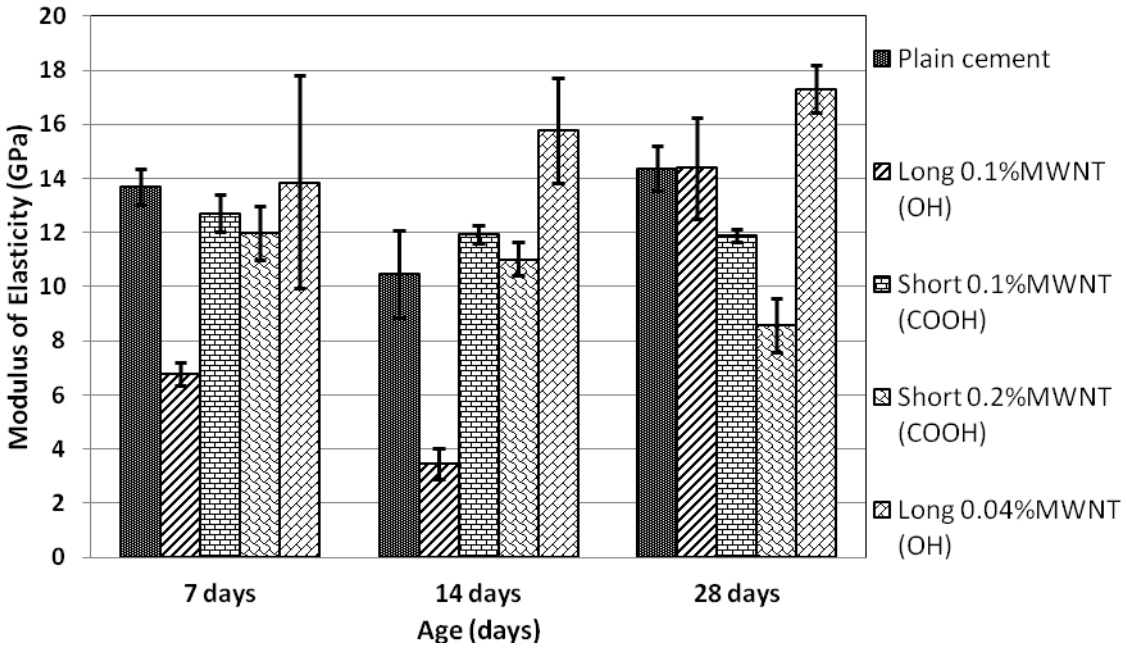

Fig. 33. Average modulus of elasticity results for the plain cement and the functionalized short and long MWCNT composite specimens with the standard error of the mean.

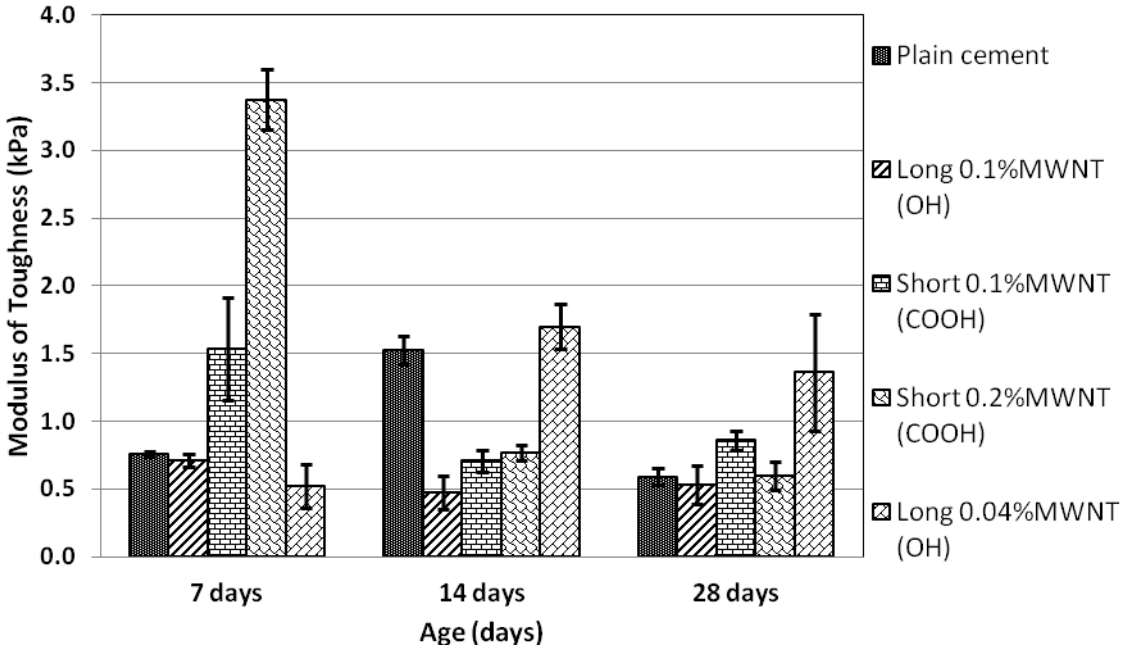

Fig. 34. Average modulus of toughness results for the plain cement and the functionalized short and long MWCNT composite specimens with the standard error of the mean.

At 7 days, most of the functionalized MWCNTs/cement composites showed improvements in the flexural strength and ductility and some showed improvement in modulus of toughness when compared to the plain cement sample. The highest improvement in the flexural strength was seen for the short 0.2% MWCNT (COOH) specimens with an increase of 112% compared to the plain cement specimen. The long 0.1% MWCNT (OH) and the short 0.1% MWCNT (COOH) flexural strength also increased by 19% and 41%, respectively. The long 0.04% MWCNT (OH) specimens showed a huge decrease in their flexural strength by 228% compared to the plain cement specimens.

All specimens of different batches showed an increase in ductility. The highest ductility was seen for the short 0.2% MWCNT (COOH) and the long 0.04% MWCNT (OH) specimens with an increase of 118% and 89%, respectively, with respect to the plain cement sample. The modulus of elasticity values for most of the specimens were close to the plain cement sample. However, the long 0.1% MWCNT (OH) showed a decrease in the elastic modulus by 102% compared to the plain cement sample. Only the short 0.1% MWCNT (COOH) and short 0.2% MWCNT (COOH) showed improvement in modulus of toughness with an increase of 103% and 346%, respectively, compared to the plain cement sample.

Considerable changes in the behavior of the composites were observed at 14 days. A large drop in the flexural strength of most of the nanocomposites to be less than the plain cement sample strength occurred, except for the long 0.04% MWCNT (OH), which showed an increase in the average strength by 51% compared to the plain cement sample. The lowest flexural strength was recorded for the long 0.1% MWCNT (OH), with a degradation of 184% with respect to the plain cement sample. Some of the nanocomposites showed a decrease in ductility while others showed an increase at 14 days. The highest ductility obtained after 14 days was for the long 0.1% MWCNT (OH) with an increase of 42% from the corresponding value of the plain cement sample. The short 0.1% MWCNT (COOH) showed a ductility close to the plain cement sample, while the short 0.2% MWCNT (COOH) and the long 0.04% MWCNT (OH) showed a decrease in ductility.

Fig. 33 shows that, in general, there were no significant changes in the general behavior of the composites regarding the modulus of elasticity values with respect to the plain cement

sample. However, the long 0.1% MWCNT (OH) showed more degradation in modulus of elasticity, and the long 0.04% MWCNT (OH) showed an increase compared to the plain cement sample and to the 7 day values.

A significant degradation in modulus of toughness values was observed in most of the nanocomposites compared to the plain cement sample. The lowest modulus of toughness was noticed in the long 0.1% MWCNT (OH) with a 222% degradation from the corresponding value of the plain cement sample. However, a significant increase in modulus of toughness was seen for the long 0.04% MWCNT (OH) with respect to its value at 7 days.

When investigating the results at 28 days, some of the nanocomposites showed an increase in the flexural strength while others showed a decrease compared to the values at 14 days, but most of the nanocomposites ended with a higher strength than the plain cement sample. The long 0.04% MWCNT (OH) showed the highest flexural strength at 28 days, specifically with an improvement of 83% compared to the plain cement sample. All of the nanocomposites showed a higher ductility than the plain cement sample at 28 days. The highest ductility at 28 days was for the short 0.2% MWCNT (COOH) and the long 0.1% MWCNT (OH) with an increase of 36% and 31%, respectively, compared to the plain cement sample. However, all of the nanocomposites' ductility values were close to each other at 28 days. Only the long 0.04% MWCNT (OH) showed a significant increase in the elastic modulus, compared to the plain cement sample, of 20%. Unlike the non-functionalized MWCNT nanocomposites, only the long 0.04% MWCNT (OH) showed a significant improvement in modulus of toughness, by 131%, compared to the plain cement sample. The rest of the nanocomposites showed a similar modulus of toughness to the plain cement sample, but the short 0.1% MWCNT (COOH) showed an increase of 46% compared to the plain cement sample.

4.4 Results and Discussion

The experimental results obtained for different batches clearly showed the variation in the mechanical properties between the functionalized and non-functionalized short and long MWCNT nanocomposites over time. It was noticed that these nanofilaments at very small concentrations could change and vary the cement paste behavior extremely by hardening, softening, stiffening, or weakening. In order to gain insight into the mechanical behavior of these MWCNT nanocomposites in general, and to observe the real effects of the aspect ratio of the

MWCNTs on the mechanical behavior of the cement nanocomposites, a different arrangement of the data presentation is provided in the following pages. This is done by comparing the same mechanical characteristics for long and short MWCNTs in two figures on the same page. The data point of the short 0.2% MWCNT was removed from this comparison—for strength and modulus of toughness—because it had much higher strength and modulus of toughness than all other batches.

4.4.1 Long vs. Short MWCNTs

Fig. 35 and Fig. 36 show that at 28 days, almost all of the MWCNT composites had increased the flexural strength of the cement nanocomposites. At 28 days, the long MWCNTs had increased the flexural strength more than the short MWCNTs, although the short MWCNTs improved the flexural strength more at 7 days. This behavior matches expectations in that the longer fibers will need more energy (force) to be pulled out from the matrix. At 28 days, the functionalized MWCNTs (OH) and MWCNTs (COOH) at higher concentrations (mass fraction) did not effectively increase the flexural strength of the cement nanocomposites.

Fig. 37 and Fig. 38 show that at all ages—7, 14, and 28 days—the ultimate strain (ductility) of the short MWCNT nanocomposites was more than the ultimate strain of the long MWCNT nanocomposites. This was not an expected behavior since it was thought that the longer fibers have longer friction surfaces and would provide more ductility to the matrix. However, the author believes that this might be because of the dispersion variations between the long and short MWCNTs. Since a better level of dispersion can be achieved in the short MWCNTs, then a better distribution of the nanotubes in the composite material would be more critical to ductility than length (aspect ratio). Also, at 28 days, the short functionalized MWCNTs (COOH) did not help that much in improving the ductility, compared to the short non-functionalized MWCNTs.

Fig. 39 and Fig. 40 show a slightly better improvement in modulus of elasticity for the long MWCNT nanocomposites over the short ones at 28 days. More consistent results were seen for the short MWCNT nanocomposites over the long ones at 7 and 14 days.

Fig. 41 and Fig. 42 show a higher modulus of toughness for the short MWCNT nanocomposites over the long MWCNT nanocomposites at 7 days. However, no significant

differences in toughness were noticed between the long and short MWCNT nanocomposites at 28 days.

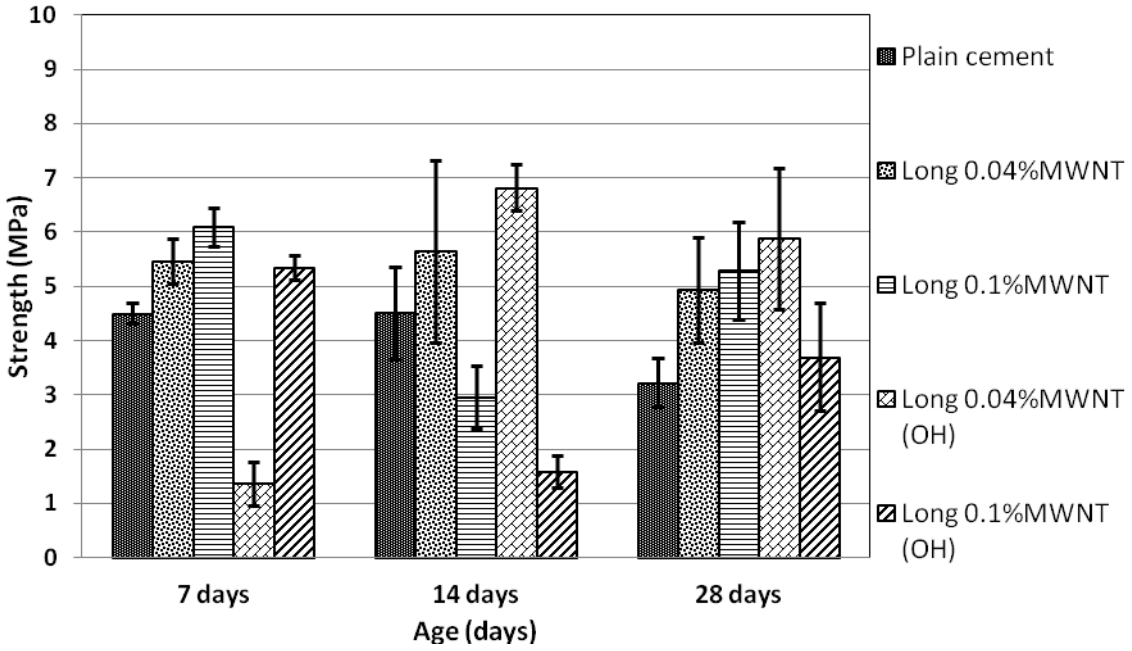

Fig. 35. Average flexural strength results for the plain cement and the long MWCNT composite specimens with the standard error of the mean.

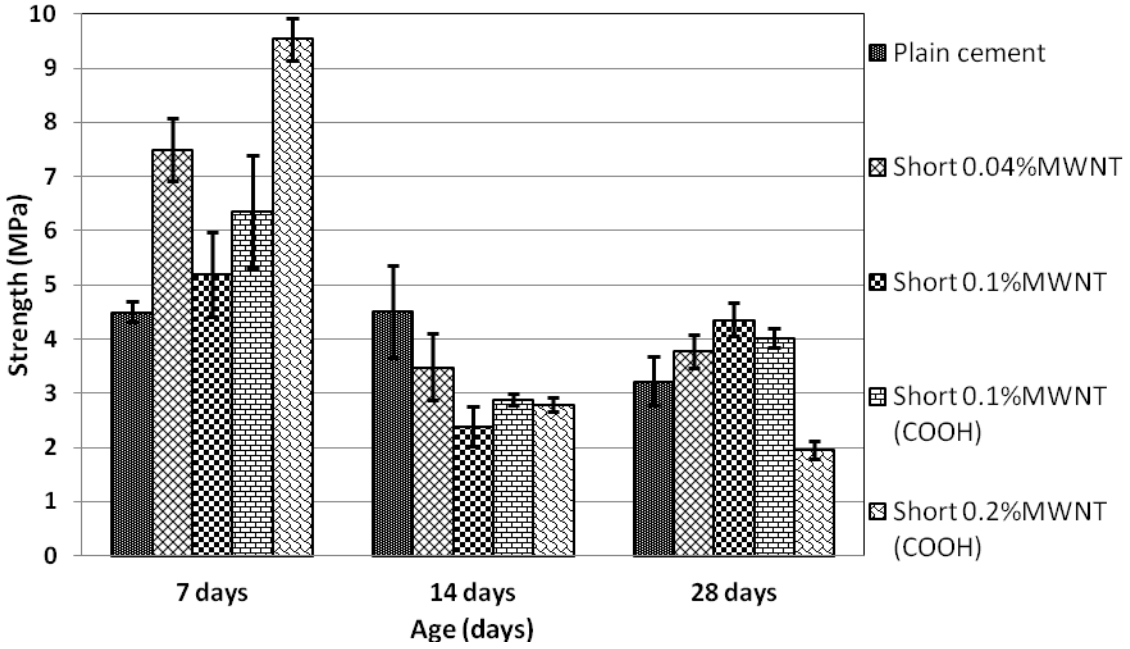

Fig. 36. Average flexural strength results for the plain cement and the short MWCNT composite specimens with the standard error of the mean.

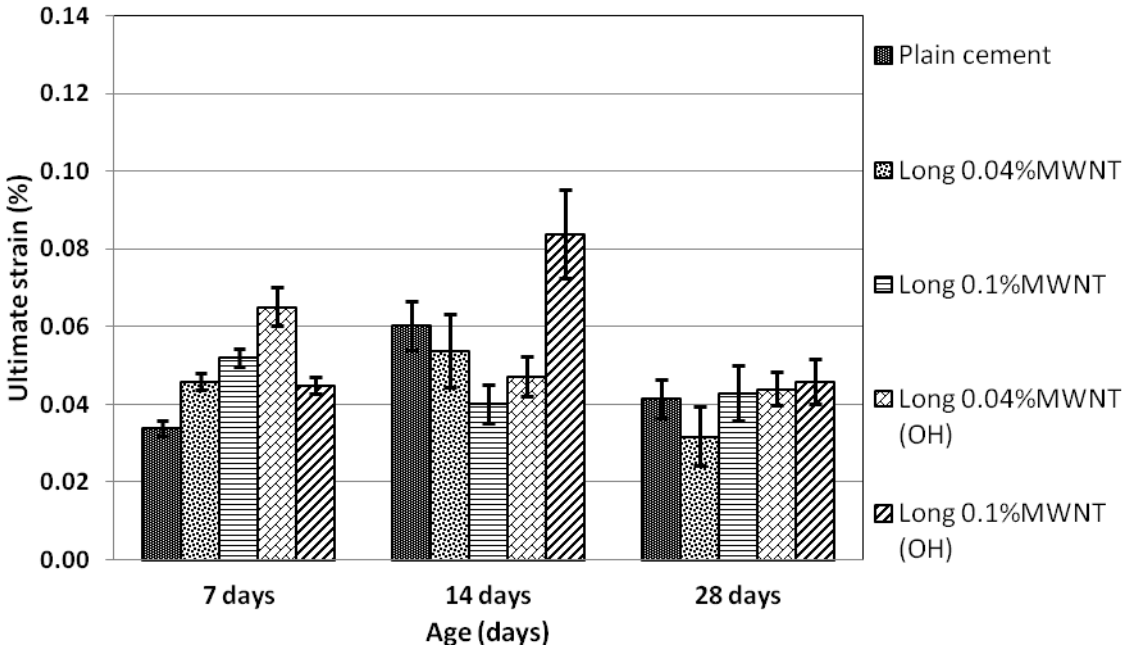

Fig. 37. Average ultimate strain results for the plain cement and the long MWCNT composite specimens with the standard error of the mean.

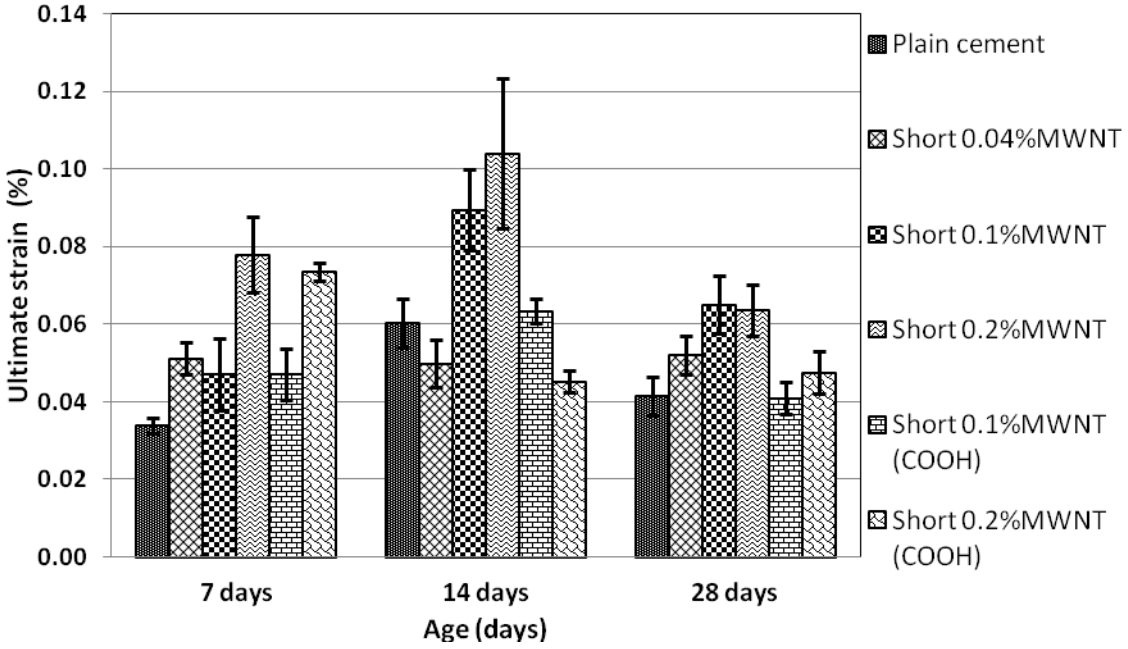

Fig. 38. Average ultimate strain results for the plain cement and the short MWCNT composite specimens with the standard error of the mean.

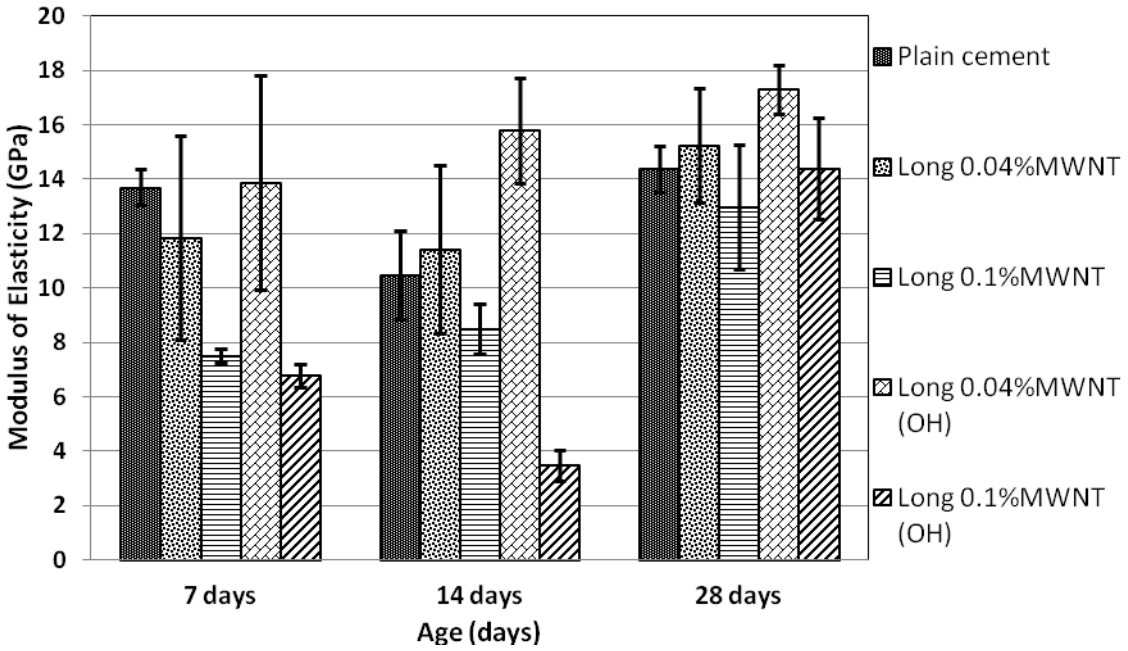

Fig. 39. Average modulus of elasticity results for the plain cement and the long MWCNT composite specimens with the standard error of the mean.

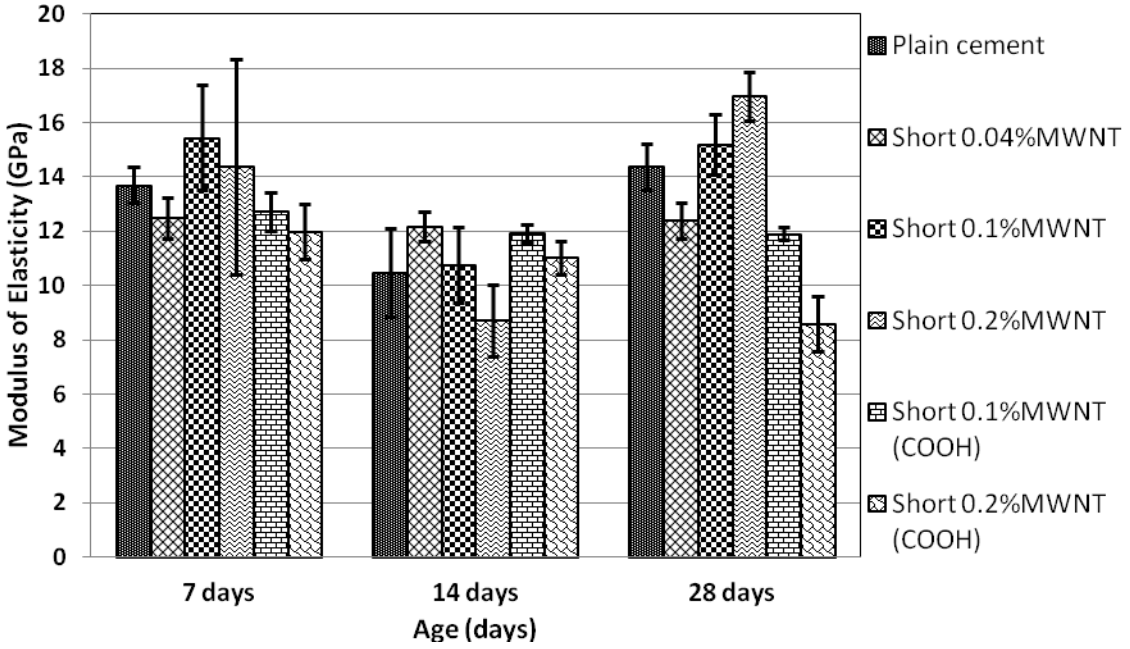

Fig. 40. Average modulus of elasticity results for the plain cement and the short MWCNT composite specimens with the standard error of the mean.

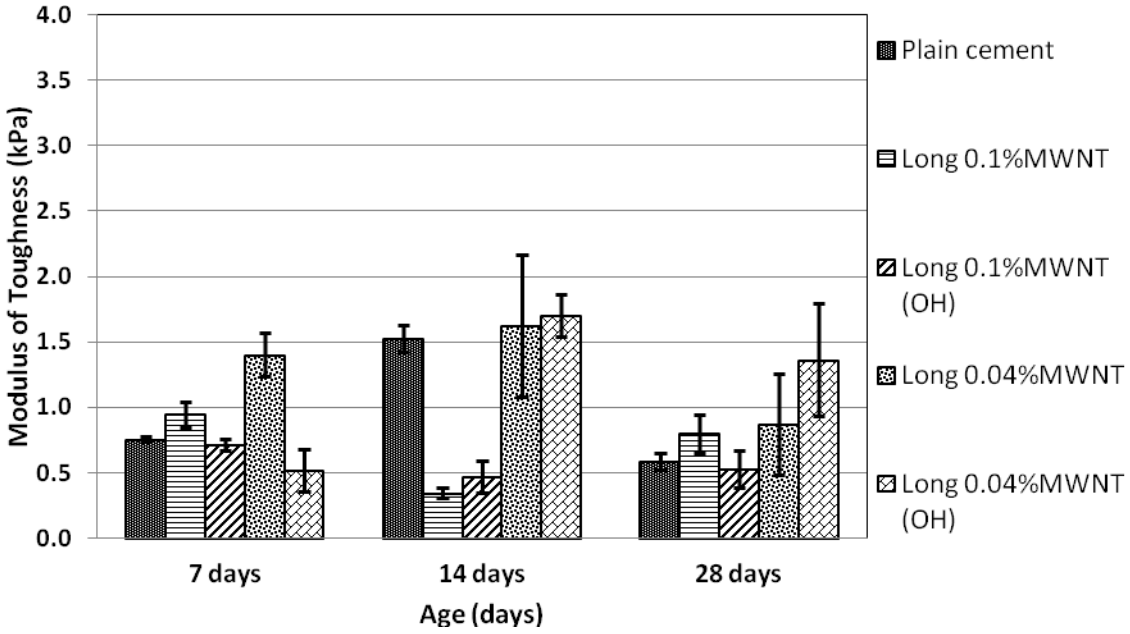

Fig. 41. Average modulus of toughness results for the plain cement and the long MWCNT composite specimens with the standard error of the mean.

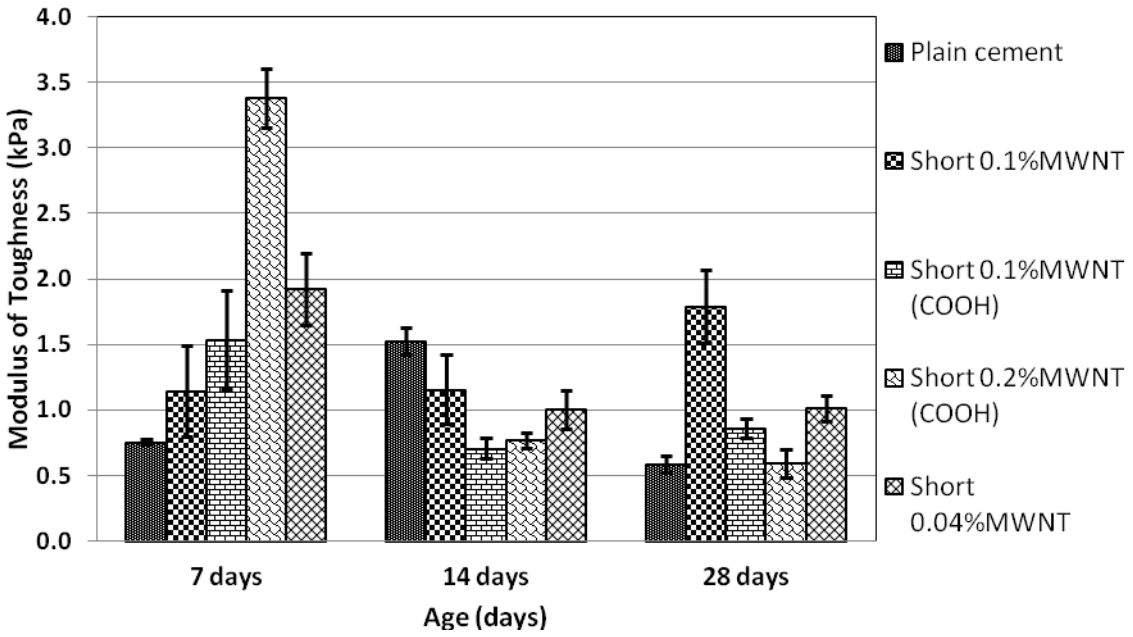

Fig. 42. Average modulus of toughness results for the plain cement and the short MWCNT composite specimens with the standard error of the mean.

4.4.2 MWCNT Pullout and Result Variability

Based on the observation of the stress-strain diagrams of all specimens, multi-peak behavior related to CNT pullout from the cement paste matrix was seen. This action was important to increase the fracture energy stored in the composite (strain energy) in order to directly increase the strain capacity (ductility) and the modulus of toughness (fracture resistance). However, the pullout process did not necessarily improve the strength since some of the stress-strain curves showed a constant strength or yielding plateau after the first crack without any increase in the strength, while other specimens showed an increase in the strength after the first crack, as was seen in Fig. 22 through Fig. 26. This might be attributed to the dispersivity of the CNTs within the hydrated cement paste.

When investigating the amount of deviations from the mean value (standard error of the mean), it was noticed that although all the samples (replicates) of the same batch were identical and cast at the same time from the same mix, there was, in many cases, a noticeable variability in the results from one sample to another of the same composite. This could be due to the size of the specimens and the uniformity of the mixture. The small size of the specimens (beams) made

them more sensitive (size effect) to the existence of any small impurities, like air bubbles or small voids. On the other hand, the uniformity of the distribution of the MWCNTs within the aqueous solution did not guarantee a uniform distribution of the nanofilaments within the cement paste composites; hence, the stress distribution in the cross-sections along the composite beam length was not uniform and caused variability in the flexural behavior from sample to sample.

4.4.3 Weakening Due to Functionalization

Many hypotheses have been proposed to explain the degradation of the functionalized CNT nanocomposites compared to the non-functionalized CNT composites. For example, Musso et al. [104] reported that the degradation in the flexural strength in many specimens could be related to a decrease in the formation of the C-S-H as one of the main products of the cement hydration. C-S-H has many different chemical structures, for example $Ca_5Si_6O_{16}(OH)_2 \cdot 4H_2O$ and $Ca_5Si_6(O,OH)_{18} \cdot 5H_2O$. C-S-H is the main contribution to the strength of the cement hydrate in different stages of hydration [104, 105]. Degradation in the compressive strength has been noticed in composites with functionalized CNT specimens. Musso et al. [104], using thermo-gravimeter analysis (TGA), showed that less amounts of C-S-H were produced in the composite with the presence of the functionalized CNTs in the composite.

Another hypothesis to explain the deterioration of the mechanical properties of the functionalized CNTs/cement composites is the excessive formation of ettringite hypothesis [61, 100]. Ettringite ($3CaO\_Al_2O_3\_3CaSO_4\_32H_2O$) is one of the typical products of cement hydration. It is a needle-shaped crystalline structure that is produced be the hydration of tricalcium aluminate (C_3A) with gypsum (another component of Portland cement used to control the hydration process and prevent the flash set of the cement paste). Naturally, ettringite expands and causes internal stresses that could lead to micro-cracks in the matrix of the hydrated cement paste. Due to the acid treatment of CNTs, sulfate residue could be left on the surfaces of CNTs that are not perfectly washed. The existence of sulfate will cause excessive formation of ettringite in locations near the CNTs in the matrix, hence weakening the material surrounding the CNTs and, as a result, causing degradation in the composite mechanical properties. More details on ettringite at the microscopic scale are provided in the next section.

4.4.4 Effect of the Cement Paste Curing Method and the Superplasticizer

The last point in this discussion is about the overall degradation in the mechanical properties (strength, ductility, and toughness) of most of the nanocomposites and the plain cement specimen from 14 days to 28 days. As seen in Fig. 35 through Fig. 42, most of the specimens, including the plain cement, showed a decrease in the mechanical properties at 28 days compared to 14 days. This behavior is abnormal since it is well known that cement paste gains strength with time. The curing method used for all specimens—including the plain cement—involved submergence into lime water. This method for curing has been used for many years as a standard method of concrete/cement curing. This curing method is the key to explaining why this degradation occurred at 28 days, as discussed in the following paragraphs.

A possible explanation for the degradation of most of the nanocomposites at 28 days can be derived based on a chemical point of view. According to Mindess and Young [106], the main hydrate components in cement before hydration are the following: tricalcium sillicate (C_3S; $3CaO.SiO_2$), which typically forms about 55% of the cement weight and is responsible for the early strength of the cement paste hydrate and its continuation at a later stage; and dicalcium silicate (C_2S; $2CaO.SiO_2$), which typically forms about 25% of cement weight and contributes to the strength at a later stage. These two components react with water (H_2O) and form the C-S-H, which is a fine amorphous in structure that makes 50% to 65% of the volume of the hydrated cement paste and is mainly responsible for the strength of the cement paste. Another product of the hydration of the C_3S and the C_2S is calcium hydroxide (CH; $Ca[OH]_2$).

Calcium hydroxide in cement chemistry notations is typically a crystalline structure that contributes indirectly to reserving the strength of the cement paste hydrate by reducing the porosity of the matrix and filling the capillary pores within the cement paste matrix. An SEM image of the C-S-H and the CH within the cement paste matrix is shown in Fig. 43.

The author believed that leaching of calcium hydroxide from the cement paste submerged into the lime water would increase the porosity (capillary voids) of the matrix and hence degrade the mechanical properties of the cement paste. Carde et al. [107] showed experimentally that the compressive strength of the plain cement paste of micro-cylinders (diameters of 10 mm to 30 mm) degraded significantly due to the leaching process of calcium hydroxide. The degradation in the compressive strength for a 10 mm diameter specimen, which is larger than the

specimens in the current study, could reach 50% [107]. It has been proposed that leaching of $Ca(OH)_2$ from the external layers (leaching zone) of the plain cement paste specimens and the loss of calcium ion content due to the progressive decalcification of the C-S-H plays a major role in the degradation of the mechanical properties of cement paste [108].

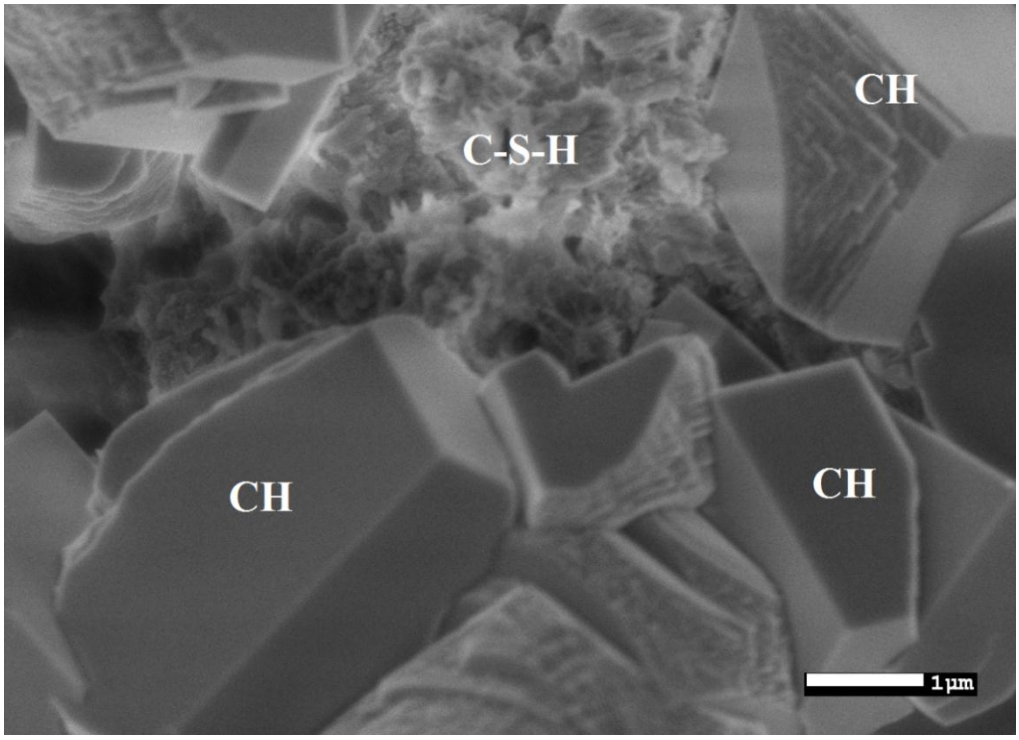

Fig. 43. SEM image showing the C-S-H and the crystalized CH of the cement paste.

Although the leaching kinetics are usually slow, due to the special case in this study of testing a very small specimen size (6.5 mm × 6.5 mm cross-section) with a large surface area/volume ratio, the leaching process was expedited. The loss of the calcium hydroxide creates macro-voids since the size of the $Ca(OH)_2$ crystals is close to the size of the capillary porosity, thereby effectively increasing the overall matrix porosity, which then causes degradation in the mechanical properties, especially for small-sized specimens. In addition, a decrease in the C/S ratio in the C-S-H due to the progressive decalcification process of the C-S-H increases the micro-voids and the porosity of the material, causing deterioration in the mechanical properties [109-111].

Calcium hydroxide is a layered structure; the calcium atoms are octahedral, the oxygen atoms are tetrahedral, and the unit cell is hexagonal. Ideally, the CH forms hexagonal plates, but the morphology of the crystallization of the CH could vary based on the admixtures in the cement paste mix. Some studies have suggested that there is amorphous CH in the calcium silicate pastes, but there is no convincing evidence that this is true, at least experimentally [112]. In cement pastes, TEM images have shown small portions of the CH as cryptocrystalline tightly bound with the C-S-H [113, 114]. Methods used to determine the CH in hydrated cement paste include quantitative X-ray diffraction analysis (QXDA), thermal gravimetric analysis (TG), DTG, semi-isothermal DTG, thermal evolved gas analysis, DTA, differential scanning calorimetry (DSC), IR spectroscopy, image analysis of back-scattered electron images, and other chemical extraction methods [112]. The dissolution of CH in water is exothermic (ΔH = -13.8 kJ/mol at 25°C) [115], so with the increase of the temperature, the solubility decreases. The solubility at 25°C is 1.13 g CaO/l [116].

During the dissolution of the C_3S in cement pastes and the growth of the C-S-H, the concentrations of the Ca^{2+} and OH^- in the solution increase steadily until they reach the saturation level, and then the CH precipitation starts in significant amounts, resulting in a drop in the concentrations of Ca^{2+} and OH^-. The smaller grains of C_3S, generally, react completely by a dissolution and precipitation process during the acceleratory stage [112].

Crumbie et al. [117] tested concrete specimens with a w/c ratio of 0.4 and 0.6. The specimens were cured in a saturated CH solution after 24 hr of casting. The SEM back-scattered images and the methanol-exchange porosity testing confirmed that the porosity and the permeability increased near the surface. Also, the authors reported that the surface region was depleted in CH content and leaching of the CH occurred even though the specimens were immersed in a saturated CH solution. When considering the leaching process, the attack or dissolution of CH and other components depends on the type and geometry of concrete, rate of water flow, temperature, and concentration and types of solutes in the water. A solution of CO_2 (CO_2 per unit volume of the solution) can dissolve $CaCO_3$ or CH from the solid cement paste and free the calcium ions, Ca^{2+}. Adenot and co-workers [108, 118] reported that the CH was the first to dissolve from the surface, followed by the monosulfate and the ettringite, and then the C-S-H was progressively attacked through decalcification.

In order to investigate the leaching effects due to lime water curing on the mechanical properties of cement paste, the author fabricated a similar batch to the plain cement paste tested before. The new plain cement paste batch had the same size, geometry, procedure, and components as the previous one but was cured in a moisture room (closed room with constant humidity of 95% at a temperature of 23^{o}C). The comparison results showed that higher strength, ductility, and toughness were obtained for the moisture curing approach. Fig. 44 through Fig. 47 show the improvements in the mechanical properties, which reached 50% to 60% or more for the moisture room curing compared to the lime water curing results. These results match the experimental results reported by Carde et al. [107] for a similar cross-section area size.

Furthermore, the plain cement paste batches with superplasticizer showed significantly lower mechanical properties compared to the plain cement paste batches without any superplasticizer. This finding could be due to the excess amount of water available for the cement hydration due to the existence of the water-reducing agent (superplasticizer). Simard et al. [119] tested different batches of cement paste with a fixed water/cement ratio (w/c ratio = 0.35), and they used two different commercial superplasticizers (Na-PNS and Ca-PNS, both poly-B-naphthalene sulfonates [PNS]) at different concentrations. Their results showed that there were variations in the heat flux of the hydration and retardation in the hydration process with the increase in the concentration of the superplasticizers. The compression tests showed degradations in the strength of all cement paste batches with an increase in the concentration of the superplasticizers. This decrease in strength was also a function of cement type (chemistry). The degradation in the compressive strength varied from 20% to 100% depending on the type and concentrations of the cement and the superplasticizers. The authors also reported that retardation in hydration was greater for cement types of low C_3A content. However, more investigations on curing methods and superplasticizer effects on the mechanical properties of cement paste need to be performed in the future.

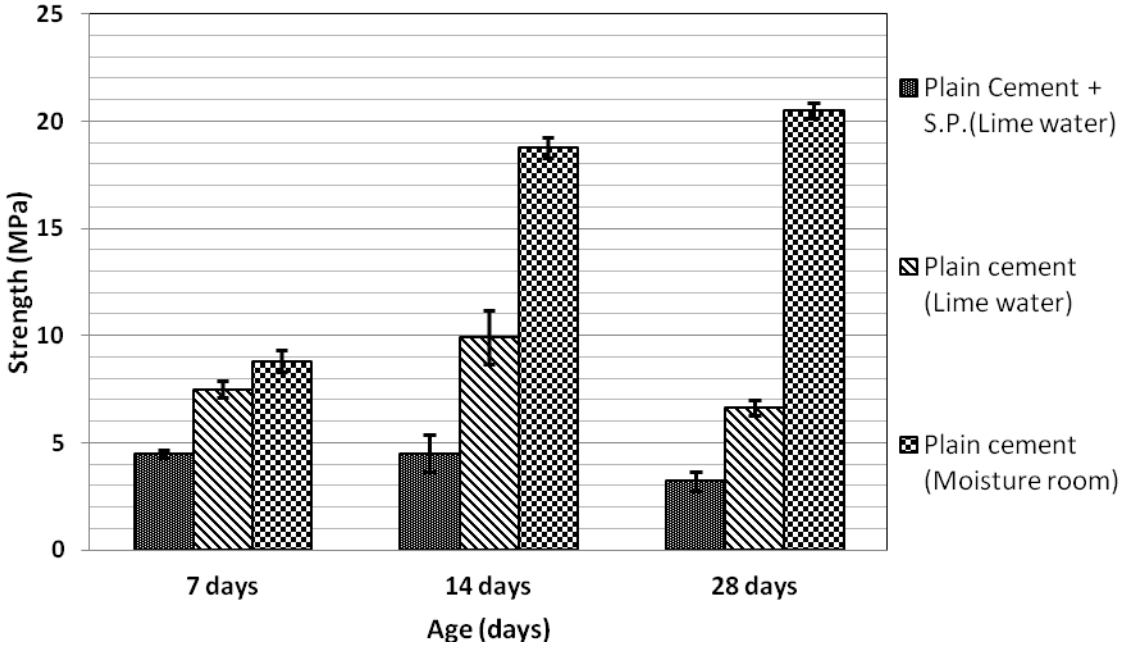

Fig. 44. Average flexural strength results for different plain cement specimens with the standard error of the mean.

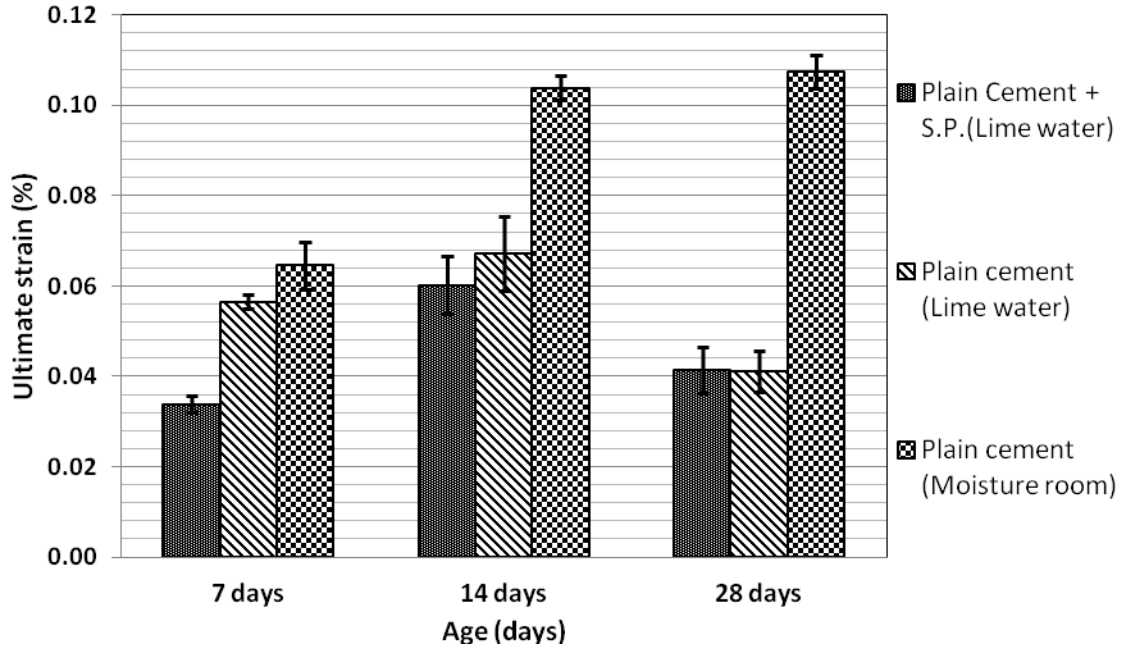

Fig. 45. Average ultimate strain results for different plain cement specimens with the standard error of the mean.

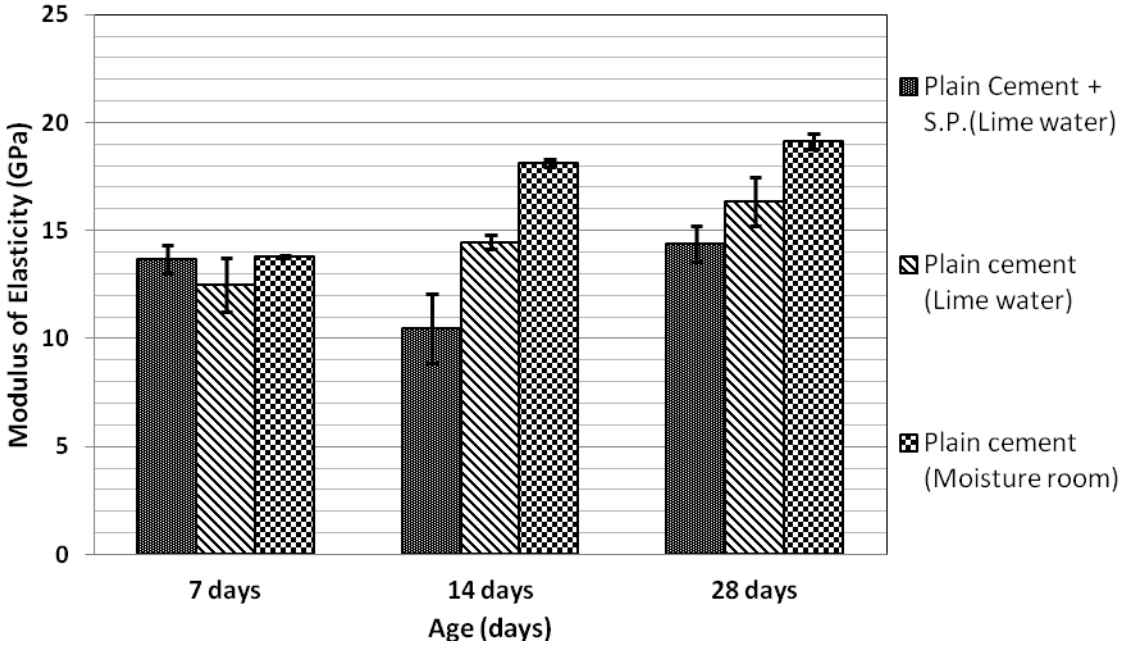

Fig. 46. Average modulus of elasticity results for different plain cement specimens with the standard error of the mean.

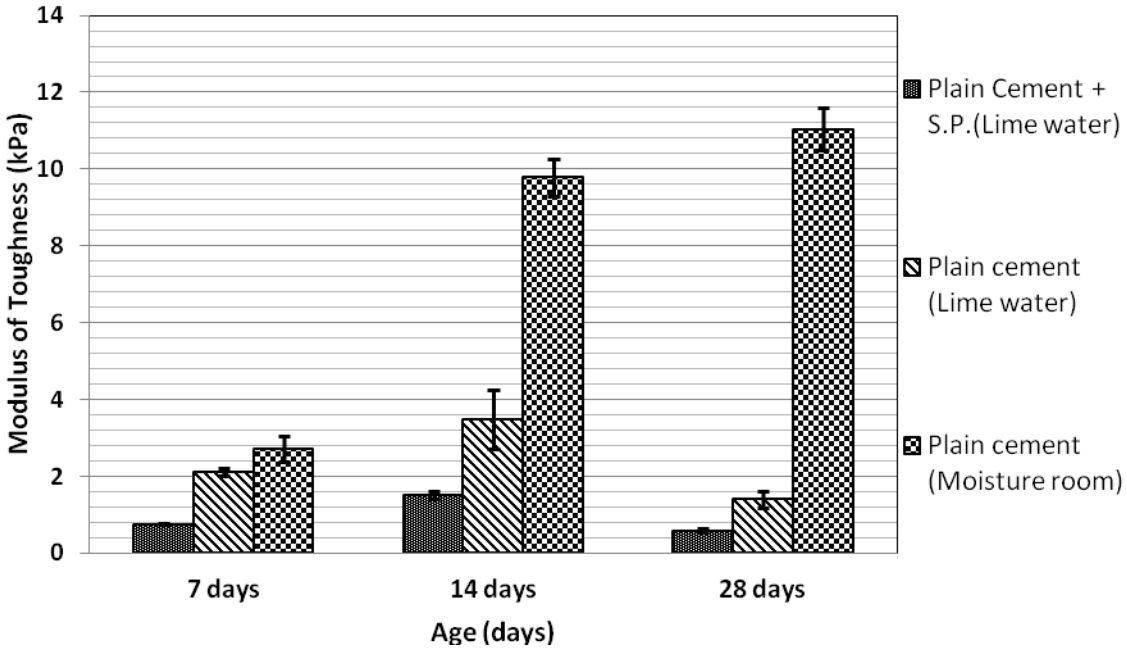

Fig. 47. Average modulus of toughness results for different plain cement specimens with the standard error of the mean.

The reliability of the results obtained for all 10 batches of this study is preserved. Since all 10 batches were cured for the same time in the same lime water solution, the author believes that they all had the same effects from lime water curing. Hence, the comparison between all batches is valid, at least qualitatively. However, based on this plain cement study, the author believes that if a different curing method were adopted (like moisture curing), the results would show improvements in the mechanical properties of the nanocomposite specimens due to the reduction in leaching, but the relative behavior and trend of all batches would be the same. The curing method effects need additional investigation and will be studied in a future work.

4.5 SEM and TEM Microstructural Imaging

In order to investigate the microstructure of the MWCNTs/cement composites, SEM images were taken for the fracture surface of the nanocomposites. A very small portion cut from the fracture surface were mounted on an SEM holder and coated with a very thin layer (3-4 nm) of platinum/palladium to enhance the image quality by improving the charge-discharge on the top of the sample under the electron beam of the SEM. A JEOL JSM-7500F machine, an ultra-high resolution field emission scanning electron microscope (FE-SEM), was used in order to capture the MWCNTs within the cement paste. Finding the CNTs within the cement paste is challenging compared to capturing carbon nanofibers or microfibers. Two main categories that the author believed would have major effects on the mechanical properties of the CNT nanocomposites were taken into consideration: CNT crack bridging (pullout action) and dispersion of CNTs within the matrix.

4.5.1 CNT Pullout and Crack Bridging

As seen in Fig. 48 and Fig. 49, the MWCNTs effectively bridged micro-cracks within the cement paste matrix. Clear evidence that many CNTs stretched across the micro-cracks is shown in the figures. CNT breakage can also be seen for many of the CNTs bridging the micro-crack. This implies a good bonding between the CNT surfaces and the surrounding cement paste. However, it was difficult to capture a clear pullout image and the corresponding fiber hole in the matrix.

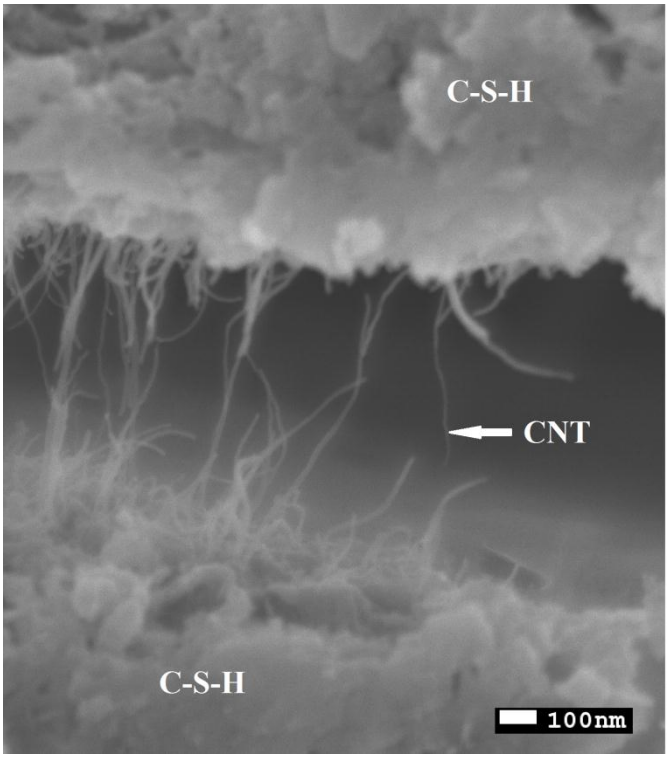

Fig. 48. SEM image showing the micro-crack bridging and breakage of the MWCNTs within the cement paste.

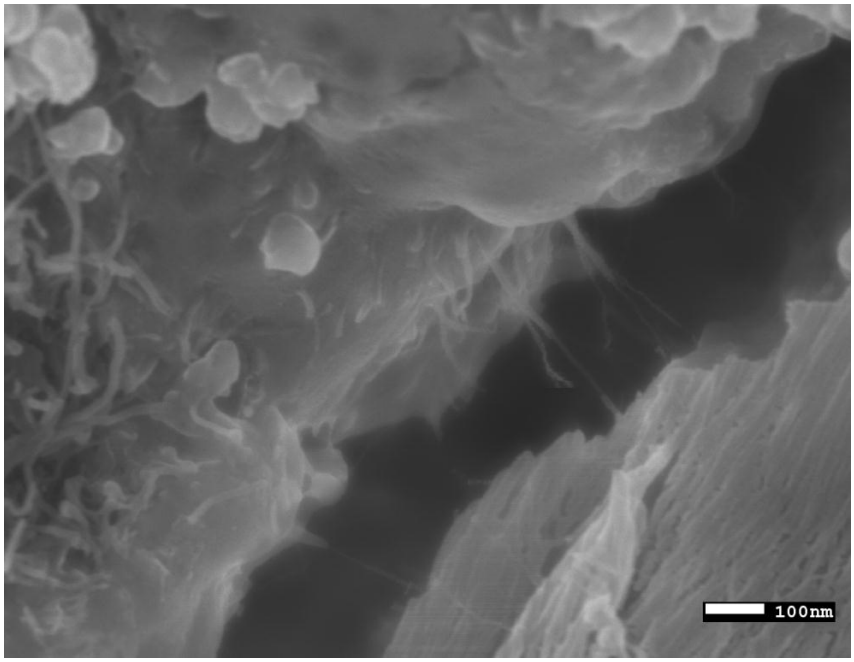

Fig. 49. SEM image showing a micro-crack bridging by a few MWCNTs within the cement paste.

The breakage seen in the images indicates very high stresses applied to the CNTs. Since the theoretical tensile strength of CNTs is very high, more CNTs are needed in order to carry the stresses. This could imply that good dispersion is the real key to improving the mechanical properties of cement nanocomposites rather than the bonding between the CNTs and the matrix, at least in cement paste, as breakage, not pullout, is seen in the images. However, the effective tensile strength of CNTs is affected by the amount of defects in the atomic structure of the CNT walls, and the increase in the defects will decrease the strength and make the CNTs curve and bundle. Still, Musso et al. and Tyson et al. [62, 104] concluded that even such defects may affect CNTs as individuals, but the overall strength of the composite can be increased with good dispersion.

4.5.2 Dispersion and Agglomeration

In the previous subsection discussion, it was proposed that dispersion of CNTs within the cement paste matrix could be more important and critical than bonding since breakage of the CNTs occurred before the pullout action. This could imply that, at least in this study, sufficient bonding was obtained between the CNTs and the surrounding cement paste.

As mentioned before, good dispersion of the CNTs within the aqueous solution does not guarantee good dispersion of the CNTs within the cement paste. As seen in Fig. 50, a large number of MWCNTs agglomerated and bundled within a very small area on the fracture surface of the cement nanocomposite. Fig. 51 shows a cryo-TEM image of MWCNTs within a thin strip of cement paste.

Based on these SEM and TEM observations of the fractured surface, two main reasons could explain the poor dispersion obtained. The first reason is that the sonication (dispersion) of the CNTs in the mixing water and/or the mixing of the CNT solution with cement powder was not very effective, and more enhancements are needed in that area to improve the current mixing and dispersing techniques or to create new dispersing techniques.

The second reason that could explain the poor dispersion involves the cement grain size. It is well known that the cement grain diameter is greater than the size of CNTs by hundreds of times. When mixing a well-dispersed CNT solution with the cement powder, the CNTs will be in the water surrounding the cement grains. When the cement paste hydrates and hardens, the CNTs will be at the original location outside the original perimeter of the cement grains. Hence,

locations with agglomerations of CNTs, and locations without any presence of CNTs (the original cement grain areas), will be formed. In this study, during the searching process for the CNTs on the fracture surface using the SEM, it was clearly noticed that at the nano scale, large areas were empty of CNTs, while some limited locations contained CNTs. This second reason could be the most important element to obtaining good dispersion [49].

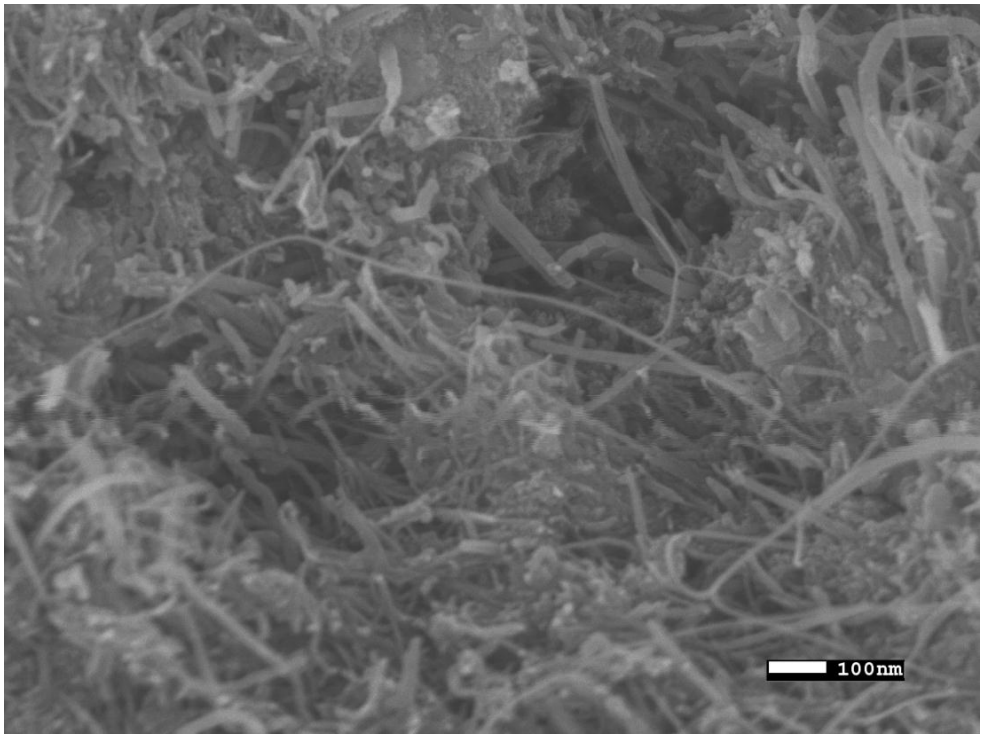

Fig. 50. SEM image of MWCNT agglomerations within a small area of cement paste.

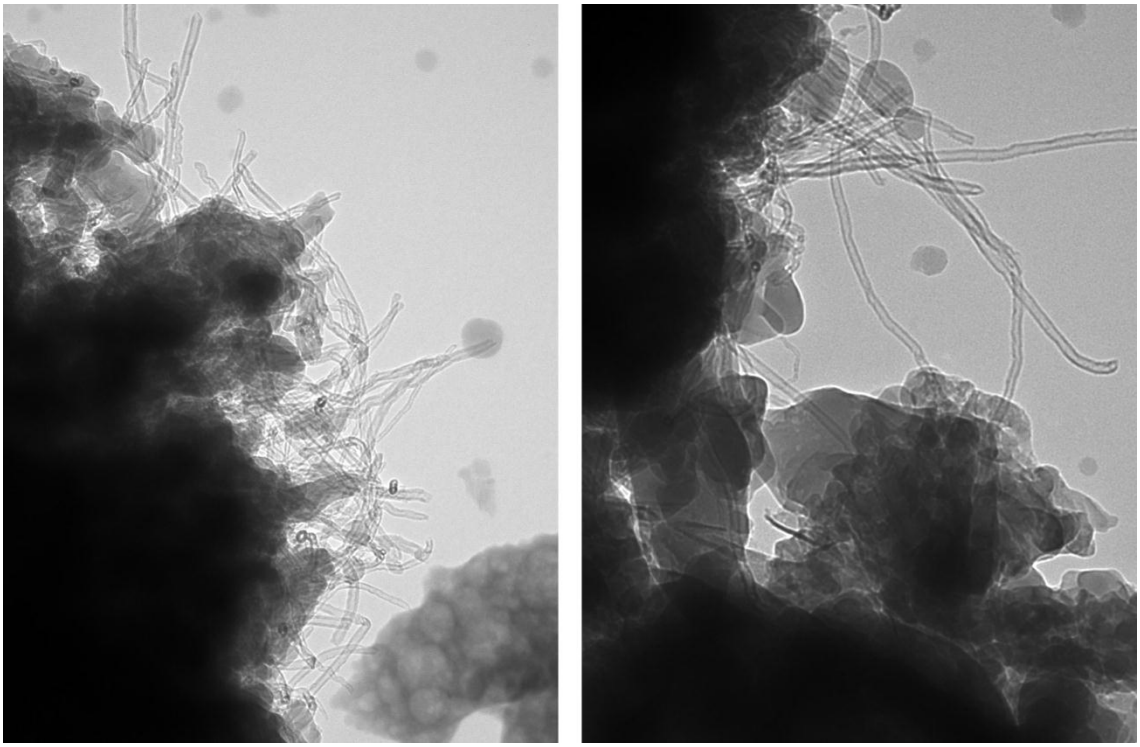

Fig. 51. A cryo-TEM image of MWCNTs within cement paste (picture courtesy of Bryan M. Tyson).

As mentioned in the previous section, the excessive formation of the expansive ettringite needles caused micro-cracks and damage inside the cement paste matrix, resulting in degradation of the mechanical properties of the material. Fig. 52 includes an SEM image showing a huge formation of ettringite needles within the C-S-H of the cement paste. The figure shows that air voids (spaces) existed within and around the ettringite formation within the hydrated cement paste.

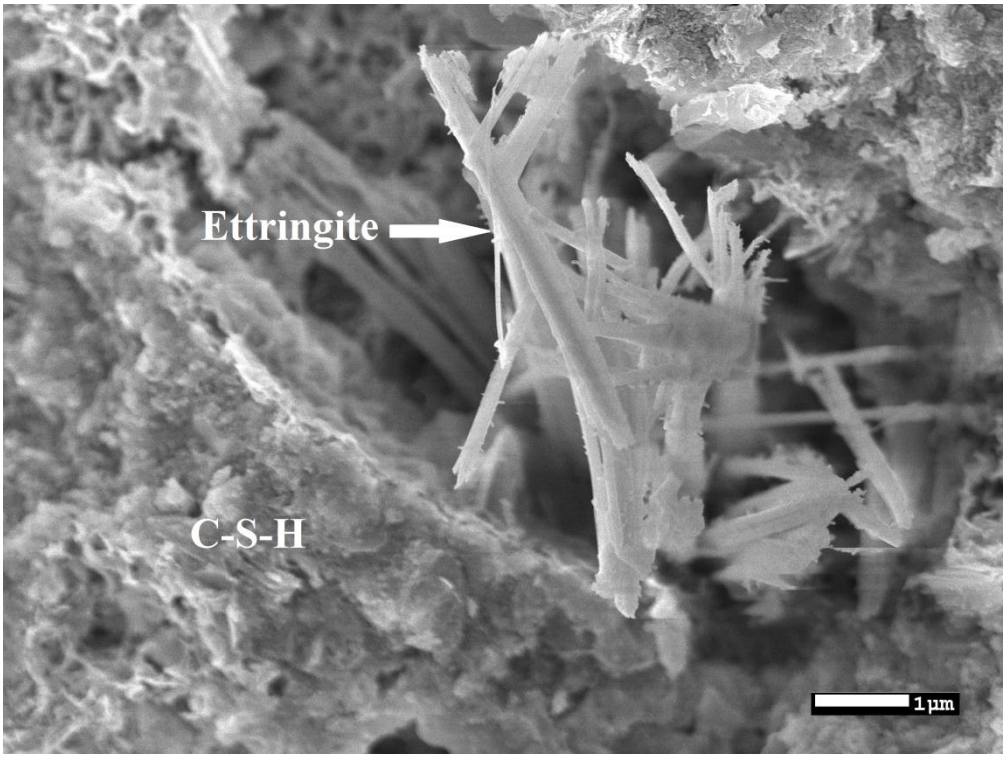

Fig. 52. SEM image showing a huge formation of ettringite needles within the C-S-H of the cement paste (notice the air void [space] within and surrounding the ettringite formation).

5. CONCLUSIONS AND FUTURE WORK

5.1 Conclusion

In this study, the effects of the aspect ratio of the functionalized and non-functionalized multi-walled carbon nanotubes on the mechanical properties of cement paste were investigated. Four different types of MWCNTs were used as nano reinforcements for the cement paste composite: two aspect ratio MWCNTs and two functional groups (COOH and OH) of the MWCNTs. Ten different batches of cement composites with different MWCNTs types and concentrations were fabricated and tested. The mechanical properties of the MWCNTs/cement paste composites were tested by a custom-made three-point flexural test apparatus. The microstructural characteristics of the MWCNTs/cement composites were investigated by the use of SEM and TEM machines images.

The first step in this work was to disperse the CNTs within water with a surfactant. Then this solution was sonicated using an ultrasonic wave mixer. It has been mentioned that a proper chemical surfactant has to be compatible with cement. Excessive amounts of a surfactant will enhance the dispersivity of CNTs and reduce the amount of ultrasonication power and time but will have negative effects on the cement paste hydration process. Less surfactant means more energy (sonication) needed for well dispersion, but that will cause breakage and dissolving of the CNTs. Thus, an optimum level of both surfactant and ultrasonication needed to be achieved.

Short MWCNTs were acid treated (functionalized) using a combination of sulfuric and nitric acids. The obtained functionalized MWCNTs had the functional group COOH. The XPS testing showed an increase in the oxygen content of 10 times more after the functionalization. The CNT functionalization process was very important in order to improve the dispersion and enhance the bonding between the CNTs and the surrounding cement paste matrix. Providing the specific type of functional group that would bond with the matrix and optimizing the level of functionalization was crucial and involved providing sufficient side functional groups without excessively damaging the CNTs.

To investigate the mechanical properties of the MWCNTs/cement composites, 10 different batches were made by sonicating the MWCNTs with the water and the surfactant and then mixing this solution with cement powder using a water/cement ratio of 0.4. The specimens

were cast into a small acrylic mold and were tested under three-point flexural testing at 7, 14, and 28 days from the casting day. Four different mechanical properties were measured: flexural strength, ultimate strain (ductility), modulus of elasticity, and modulus of toughness.

Most of the nanocomposites showed multi-peak behavior in the stress-strain diagrams. After the first crack, the material softened or yielded in some cases and sometimes showed a gradual increase in the strength to become higher than the first-crack strength. This behavior clearly indicated CNT pullout action, which increased the composite ductility (strain capacity) and toughness.

The mechanical testing results showed that for flexural strength at 28 days, almost all of the MWCNT composites increased the flexural strength of the cement nanocomposites. At 28 days, the long MWCNTs had increased the flexural strength more than the short MWCNTs, although the short MWCNTs improved the flexural strength more at 7 days. In addition, at 7, 14, and 28 days, the ultimate strain (ductility) of the short MWCNT nanocomposites was more than the ultimate strain of the long MWCNT nanocomposites. This could be because a better level of dispersion had been achieved in the short MWCNTs than in the long ones.

The short 0.2% MWCNT showed a significant increase in flexural strength, which specifically increased by 269% compared to the plain cement sample. The long 0.1% MWCNT also increased in flexural strength by 65%. The long 0.04% MWCNT (OH) showed an improvement of 83% in flexural strength at 28 days compared to the plain cement sample. The highest ductility (strain capacity) at 28 days was for the short 0.1% MWCNT and short 0.2% MWCNT, with an improvement of 86% and 81%, respectively. Also, at 28 days, the short 0.2% MWCNT (COOH) and the long 0.1% MWCNT (OH) ductility increased by 36% and 31%, respectively.

A general degradation in strength and toughness was noticed for all specimens at 28 days. The author believes that leaching of calcium hydroxide from the cement paste submerged into the lime water increased the porosity (capillary voids) of the matrix and hence degraded the mechanical properties.

SEM images implied that the uniformity of the distribution of the MWCNTs within the aqueous solution did not guarantee a uniform distribution of the nanofilaments within the cement paste composites. Agglomerations and a plain cement area without the CNTs were noticed by the

SEM. However, the images showed clear evidence that many of the CNTs were stretching across the micro-cracks. CNT breakage was also seen for many of the CNTs bridging the micro-crack. This implied good bonding between the CNT surfaces and the surrounding cement paste.

5.2 Limitations

There are many limitations associated with the experimental work of this research. The first limitation involves the CNT dispersion measurement and optimization. The evaluation of the dispersion of the CNTs within the aqueous solution was difficult and not accurate since it depended on the visual evaluation, including the TEM images, which covered a limited area that might not be representative. It was even more difficult and complicated to measure the dispersion of the CNTs within the cement paste composite, as the SEM images only covered a limited area and depth on the distribution of the CNTs within the cement paste volume. The final length of the CNTs after ultrasonication was not measured to verify the breakage amount of the CNTs due to the ultrasonication process. This could have effectively changed the actual aspect ratio of the CNTs assumed before the ultrasonication.

Another important limitation regarding the testing involves the size of the specimens (beams). The small cross-section area of the specimens made them very sensitive to any micro defects, like air voids or bubbles. These micro defects greatly affected the strength and mechanical behavior of the composite. Also, the data collection for the behavior after the first crack was limited and insensitive since the first crack usually fractured the specimen and ended the measurement. If larger cross-section beams were tested, the yielding behavior or the crack propagation observations would be more accurate. As for the nanocomposite behavior, the data capturing of the pullout behavior after the first crack was important to understand the micro-crack bridging mechanism.

Finally, the three-point bending test has a limitation of a peak maximum bending moment at mid-span, as the location of the first crack might not be at mid-span. Introducing a notch (seam) at mid-span for this size of specimens would make it more difficult to capture any ductility, and the failure would be very brittle. The four-point bending test has the advantage of a constant bending moment over the mid-part of the beam, and that could reduce the errors.

5.3 Future Work

More investigations are needed on the optimization of the dispersion of CNTs within the aqueous solution by examining the optimization of the amount of the surfactant needed, the concentration of the CNT/surfactant ratio and the CNT/water ratio, and the ultrasonication power and duration needed to maximize dispersion without damaging the CNTs.

More examination is also needed on the optimization and quantification of the dispersion of CNTs within a cement paste composite. Measuring dispersion and distribution of these nanofilaments is needed in order to optimize the mixing techniques and effectively utilize the CNTs within the cement paste matrix.

Further investigations are needed on the effects of the curing methods on the hydration process, porosity, and chemistry of the cement paste composites, especially the curing in lime water, in order to support and verify the leaching of the $Ca(OH)_2$ hypothesis. The specimens' geometry and size along with the saturation level of the lime in the curing water will cause leaching, which significantly affects the mechanical properties of the cement paste composites.

In addition, testing a larger beam size, using a four-point bending testing, will provide more details about the post first-crack behavior.

Finally, performing finite element modeling for the CNTs/cement composites is needed to verify and understand the mechanism of crack bridging and strengthening of the matrix caused by the existence of CNTs.

REFERENCES

[1] Altoubat S, Yazdanbakhsh A, Rieder K-A. Shear behavior of macro-synthetic fiber-reinforced concrete beams without stirrups. ACI Mater J. 2009;106(4):381-9.

[2] Fischer G, Li VC. Effect of fiber reinforcement on the response of structural members. Eng Fract Mech. 2007;74(1-2):258-72.

[3] Li VC, Maalej M. Toughening in cement based composites. Part II: Fiber reinforced cementitious composites. Cem Concr Compos. 1996;18(4):239-49.

[4] Mangat PS, Motamedi-Azari M, Shakor Ramat BB. Steel fibre-cement matrix interfacial bond characteristics under flexure. Int J Cem Compos Lightweight Concrete. 1984;6(1):29-37.

[5] Ostertag CP, Yi CK, Vondran G. Tensile strength enhancement in interground fiber cement composites. Cem Concr Compos. 2001;23(4-5):419-25.

[6] Savastano JH, Warden PG, Coutts RSP. Microstructure and mechanical properties of waste fibre-cement composites. Cem Concr Compos. 2005;27(5):583-92.

[7] Wang C, Li K-Z, Li H-J, Jiao G-S, Lu J, Hou D-S. Effect of carbon fiber dispersion on the mechanical properties of carbon fiber-reinforced cement-based composites. Mater Sci Eng A. 2008;487(1-2):52-7.

[8] Demczyk BG. Direct mechanical measurement of the tensile strength and elastic modulus of multiwalled carbon nanotubes. Mater Sci Eng A Struct Mater Prop Microstruct Process. 2002;334(1):173-8.

[9] Collins PG, Avouris P. Nanotubes for electronics. Scientific American. 2000(December 2000):67-9.

[10] Coleman JN, Khan U, Blau WJ, Gun'ko YK. Small but strong: A review of the mechanical properties of carbon nanotube-polymer composites. Carbon. 2006;44(9):1624-52.

[11] Marrs B, Andrews R, Pienkowski D. Multiwall carbon nanotubes enhance the fatigue performance of physiologically maintained methyl methacrylate-styrene copolymer. Carbon. 2007;45(10):2098-104.

[12] Wang JG, Fang ZP, Gu AJ, Xu LH, Liu F. Effect of amino-functionalization of multi-walled carbon nanotubes on the dispersion with epoxy resin matrix. J Appl Polym Sci. 2006;100(1):97-104.

[13] Bacsa RR, Laurent C, Peigney A, Bacsa WS, Vaugien T, Rousset A. High specific surface area carbon nanotubes from catalytic chemical vapor deposition process. Chem Phys Lett. 2000;323(5-6):566-71.

[14] Radushkevich LV, Lukyanovich VM. The structure of carbon produced by thermal decomposition of carbon monoxide on an iron contact (Russian). ЖФХ. 1952;26(1):88-95. http://www.nanometer.ru/2007/04/06/nanotubes.html#

[15] Iijima S. Helical microtubules of graphitic carbon. Nature. 1991;354(6348):56-8.

[16] Graphite. 2011; http://mrsec.wisc.edu/Edetc/nanoquest/carbon/index.html

[17] Hedberg JA. Schematic image of graphene sheet structure. 2011; http://www.jameshedberg.com/scienceGraphics.php?sort=graphene&id=graphene-wavey-lensBlur

[18] Schematic image of fullerenes (buckyballs) structure made of 60 carbon atoms. 2011; http://mrsec.wisc.edu/Edetc/nanoquest/carbon/index.html

[19] Single-walled carbon nanotube. 2011; http://www.istockphoto.com/stock-photo-10936011-single-walled-carbon-nanotube.php

[20] Multi-walled carbon nanotube. 2011; http://www.topnews.in/law/1-ounce-new-frozen-smoke-can-carpet-3-football-fields-246298

[21] Schematic image of three examples of carbon nanotubes structural orientaions. 2011; http://coecs.ou.edu/Brian.P.Grady/images/nanotube.jpg

[22] Mamalis AG, Vogtländer LOG, Markopoulos A. Nanotechnology and nanostructured materials: Trends in carbon nanotubes. Precis Eng. 2004;28(1):16-30.

[23] Yakobson BI, Smalley RE. Fullerene nanotubes: C-1000000 and beyond. Am Scientist. 1997;85(4):324-37.

[24] Thess A, Lee R, Nikolaev P, Dai HJ, Petit P, Robert J, et al. Crystalline ropes of metallic carbon nanotubes. Science. 1996;273(5274):483-7.

[25] Yu MF, Lourie O, Dyer MJ, Moloni K, Kelly TF, Ruoff RS. Strength and breaking mechanism of multiwalled carbon nanotubes under tensile load. Science. 2000;287(5453):637-40.

[26] Wong EW, Sheehan PE, Lieber CM. Nanobeam mechanics: Elasticity, strength, and toughness of nanorods and nanotubes. Science. 1997;277(5334):1971-5.

[27] Hata K. From highly efficient impurity-free CNT synthesis to DWNT forests, CNT solids, and super-capacitors In: Proceedings of SPIE—The International Society for Optical Engineering. Bellingham, WA, ETATS-UNIS; 2007. p. 64791L.1-L.12.

[28] Qian D, Dickey EC, Andrews R, Rantell T. Load transfer and deformation mechanisms in carbon nanotube-polystyrene composites. Appl Phys Lett. 2000;76(20):2868-70.

[29] Park SH, Bandaru PR. Improved mechanical properties of carbon nanotube/polymer composites through the use of carboxyl-epoxide functional group linkages. Polymer. 2010;51(22):5071-7.

[30] Xu CL, Wei BQ, Ma RZ, Liang J, Ma XK, Wu DH. Fabrication of aluminum-carbon nanotube composites and their electrical properties. Carbon. 1999;37(5):855-8.

[31] Dong SR, Tu JP, Zhang XB. An investigation of the sliding wear behavior of Cu-matrix composite reinforced by carbon nanotubes. Mater Sci Eng, A. 2001;313(1-2):83-7.

[32] Flahaut E, Peigney A, Laurent C, Marliere C, Chastel F, Rousset A. Carbon nanotube-metal-oxide nanocomposites: Microstructure, electrical conductivity and mechanical properties. Acta Mater. 2000;48(14):3803-12.

[33] Deng CF, Wang DZ, Zhang XX, Li AB. Processing and properties of carbon nanotubes reinforced aluminum composites. Mater Sci Eng A. 2007;444(1-2):138-45.

[34] Esawi AMK, Morsi K, Sayed A, Taher M, Lanka S. The influence of carbon nanotube (CNT) morphology and diameter on the processing and properties of CNT-reinforced aluminium composites. Compos Part A: Appl Sci Manuf. 2010;42(3):234-43.

[35] Peigney A, Laurent C, Flahaut E, Rousset A. Carbon nanotubes in novel ceramic matrix nanocomposites. Ceram Int. 2000;26(6):677-83.

[36] Ma RZ, Wu J, Wei BQ, Liang J, Wu DH. Processing and properties of carbon nanotubes–nano-SiC ceramic. J Mater Sci. 1998;33(21):5243-6.

[37] Peigney A, Flahaut E, Laurent C, Chastel F, Rousset A. Aligned carbon nanotubes in ceramic-matrix nanocomposites prepared by high-temperature extrusion. Chem Phys Lett. 2002;352(1-2):20-5.

[38] Balázsi, Kónya Z, Wéber F, Biró LP, Arató P. Preparation and characterization of carbon nanotube reinforced silicon nitride composites. Mater Sci Eng C. 2003;23(6-8):1133-7.

[39] Boo WJ, Sun LY, Liu J, Moghbelli E, Clearfield A, Sue HJ, et al. Effect of nanoplatelet dispersion on mechanical behavior of polymer nanocomposites. J Polym Sci Pt B-Polym Phys. 2007;45(12):1459-69.

[40] Hussain M, Oku Y, Nakahira A, Niihara K. Effects of wet ball-milling on particle dispersion and mechanical properties of particulate epoxy composites. Mater Lett. 1996;26(3):177-84.

[41] Hamming LM, Qiao R, Messersmith PB, Catherine Brinson L. Effects of dispersion and interfacial modification on the macroscale properties of TiO_2 polymer-matrix nanocomposites. Compos Sci Technol. 2009;69(11-12):1880-6.

[42] Pu ZC, Mark JE, Jethmalani JM, Ford WT. Effects of dispersion and aggregation of silica in the reinforcement of poly(methyl acrylate) elastomers. Chem Mat. 1997;9(11):2442-7.

[43] Stoeffler K, Lafleur PG, Denault J. The effect of clay dispersion on the properties of LLDPE/LLDPE-g-MAH/Montmorillonite nanocomposites. Polym Eng Sci. 2008; 48(12):2459-73.

[44] Prasad VVB, Bhat BVR, Mahajan YR, Ramakrishnan P. Structure–property correlation in discontinuously reinforced aluminium matrix composites as a function of relative particle size ratio. Mater Sci Eng A. 2002;337(1/2):179-86.

[45] Slipenyuk A, Kuprin V, Milman Y, Spowart JE, Miracle DB. The effect of matrix to reinforcement particle size ratio (PSR) on the microstructure and mechanical properties of a P/M processed AlCuMn/SiCp MMC. Mater Sci Eng, A. 2004;381(1-2):165-70.

[46] Akkaya Y, Shah SP, Ankenman B. Effect of fiber dispersion on multiple cracking of cement composites. J Eng Mech-ASCE. 2001;127(4):311-6.

[47] Akkaya Y, Picka J, Shah SP. Spatial distribution of aligned short fibers in cement composites. J Mater Civ Eng. 2000;12(3):272-9.

[48] Rapoport JR, Shah SR. Cast-in-place cellulose fiber-reinforced cement paste, mortar, and concrete. ACI Mater J. 2005;102(5):299-306.

[49] Yazdanbakhsh A, Grasley Z, Tyson B, Abu Al-Rub R. Carbon nanofibers and nanotubes in cementitious materials: Some issues on dispersion and interfacial bond. ACI Special Publication. 2009;267:21-34.

[50] Yazdanbakhsh A, Grasley Z, Tyson B, Abu Al-Rub RK. Dispersion quantification of inclusions in composites. Compos Part A: Appl Sci Manuf. 2011;42(1):75-83.

[51] Makar JM, Beaudoin JJ. Carbon nanotubes and their application in the construction industry. In: 1st International Symposium on Nanotechnology in Construction. Paisley, Scotland; 2003. p. 331-41.

[52] Cwirzen A, Habermehl-Cwirzen K, Nasibulina LI, Shandakov SD, Nasibulin AG, Kauppinen EI, et al. CHH cement composite. Berlin: Springer-Verlag Berlin; 2009.

[53] Makar JM, Margeson JC, Luh J. Carbon nanotube/cement composite—early results and potential applications. In: 3rd International Conference on Construction Materials: Performance, Innovation and Structural Implications. Vancouver, BC; 2005. p. 1-10.

[54] Li GY, Wang PM, Zhao XH. Mechanical behavior and microstructure of cement composites incorporating surface-treated multi-walled carbon nanotubes. Carbon. 2005;43(6):1239-45.

[55] Li GY, Wang PM, Zhao X. Pressure-sensitive properties and microstructure of carbon nanotube reinforced cement composites. Cem Concr Compos. 2007;29(5):377-82.

[56] Cwirzen A, Habermehl-Cwirzen K, Penttala V. Surface decoration of carbon nanotubes and mechanical properties of cement/carbon nanotube composites. Adv Cem Res. 2008;20(2):65-73.

[57] Nasibulin AG, Shandakov SD, Nasibulina LI, Cwirzen A, Mudimela PR, Habermehl-Cwirzen K, et al. A novel cement-based hybrid material. New J Phys. 2009;11:1-11.

[58] Shah SP, Konsta-Gdoutos MS, Metaxa ZS. Highly-dispersed carbon nanotubes—reinforced cement-based materials. Publication USPA US 2009/0229494 A1, 2009.

[59] Konsta-Gdoutos MS, Metaxa ZS, Shah SP. Multi-scale mechanical and fracture characteristics and early-age strain capacity of high performance carbon nanotube/cement nanocomposites. Cem Concr Compos. 2009;32(2):110-5.

[60] Konsta-Gdoutos MS, Metaxa ZS, Shah SP. Highly dispersed carbon nanotube reinforced cement based materials. Cem Concr Res. 2010;40(7):1052-9.

[61] Abu Al-Rub RK, Tyson BM, Yazdanbakhsh A, Grasley Z. Mechanical properties of nanocomposite cement incorporating surface-treated and untreated carbon nanotubes and carbon nanofibers. J Nanomech Micromechan-ASCE. 2011;(in press).

[62] Tyson BM, Al-Rub RKA, Yazdanbakhsh A, Grasley Z. Carbon nanotubes and carbon nanofibers for enhancing the mechanical properties of nanocomposite cementitious materials. J Mater Civ Eng—ASCE. 2011;23(7):1028-35.

[63] Luo JL, Duan ZD, Zhao TJ, Li QY. Effect of multi-wall carbon nanotube on fracture mechanical property of cement-based composite. Adv Mater Res. 2011;Advances in Composites(146-147):581-4.

[64] Luo JL, Duan ZD, Zhao TJ, Li QY. Cement-based composite with carbon nanotubes reinforcement tailored for structural damping. Adv Mater Res. 2011;Advances in Composites(150-151):526-9.

[65] Hunashyal AM, Lohitha SJ, Quadri SS, Banapurmath NR. Experimental investigation of the effect of carbon nanotubes and carbon fibres on the behaviour of plain cement composite beams. IES J Part A: Civil Struct Eng. 2011;4(1):29-36.

[66] Vibra-cell liquid processing. 2011; http://www.sonics.biz/lp-vibra.htm

[67] Moore VC, Strano MS, Haroz EH, Hauge RH, Smalley RE, Schmidt J, et al. Individually suspended single-walled carbon nanotubes in various surfactants. Nano Lett. 2003;3(10):1379-82.

[68] Chen W, Auad ML, Williams RJJ, Nutt SR. Improving the dispersion and flexural strength of multiwalled carbon nanotubes-stiff epoxy composites through β-hydroxyester surface functionalization coupled with the anionic homopolymerization of the epoxy matrix. Eur Polym J. 2006;42(10):2765-72.

[69] Kim JA, Seong DG, Kang TJ, Youn JR. Effects of surface modification on rheological and mechanical properties of cnt/epoxy composites. Carbon. 2006;44(10):1898-905.

[70] Li SQ, Wang F, Wang Y, Wang JW, Ma J, Xiao J. Effect of acid and teta modification on mechanical properties of MWCNTs/epoxy composites. J Mater Sci. 2008;43(8):2653-8.

[71] Xie X-L, Mai Y-W, Zhou X-P. Dispersion and alignment of carbon nanotubes in polymer matrix: A review. Mater Sci Eng R. 2005;49(4):89-112.

[72] Zhang HW, Wang JB, Guo X. Predicting the elastic properties of single-walled carbon nanotubes. J Mech Phys Solids. 2005;53(9):1929-50.

[73] Bandyopadhyaya R, Nativ-Roth E, Regev O, Yerushalmi-Rozen R. Stabilization of individual carbon nanotubes in aqueous solutions. Nano Lett. 2001;2(1):25-8.

[74] Islam MF, Rojas E, Bergey DM, Johnson AT, Yodh AG. High weight fraction surfactant solubilization of single-wall carbon nanotubes in water. Nano Lett. 2003;3(2):269-73.

[75] Kuznetsova A, Popova I, Yates JT, Bronikowski MJ, Huffman CB, Liu J, et al. Oxygen-containing functional groups on single-wall carbon nanotubes: Nexafs and vibrational spectroscopic studies. J Am Chem Soc. 2001;123(43):10699-704.

[76] Lee Y-J, Kim H-H, Hatori H. Effects of substitutional b on oxidation of carbon nanotubes in air and oxygen plasma. Carbon. 2004;42(5-6):1053-6.

[77] Ajayan PM, Ebbesen TW, Ichihashi T, Iijima S, Tanigaki K, Hiura H. Opening carbon nanotubes with oxygen and implications for filling. Nature. 1993;362(6420):522-5.

[78] Wiltshire JG, Khlobystov AN, Li LJ, Lyapin SG, Briggs GAD, Nicholas RJ. Comparative studies on acid and thermal based selective purification of hipco produced single-walled carbon nanotubes. Chem Phys Lett. 2004;386(4-6):239-43.

[79] Simmons JM, Nichols BM, Baker SE, Marcus MS, Castellini OM, Lee CS, et al. Effect of ozone oxidation on single-walled carbon nanotubes. J Phys Chem B. 2006; 110(14):7113-8.

[80] Mawhinney DB, Naumenko V, Kuznetsova A, Yates JT, Liu J, Smalley RE. Infrared spectral evidence for the etching of carbon nanotubes: Ozone oxidation at 298 K. J Am Chem Soc. 2000;122(10):2383-4.

[81] Ago H, Kugler T, Cacialli F, Salaneck WR, Shaffer MSP, Windle AH, et al. Work functions and surface functional groups of multiwall carbon nanotubes. J Phys Chem B. 1999;103(38):8116-21.

[82] Okpalugo TIT, Papakonstantinou P, Murphy H, McLaughlin J, Brown NMD. Oxidative functionalization of carbon nanotubes in atmospheric pressure filamentary dielectric barrier discharge (APDBD). Carbon. 2005;43(14):2951-9.

[83] Hou Z, Cai B, Liu H, Xu D. Ar, O_2, CHF_3, and SF_6 plasma treatments of screen-printed carbon nanotube films for electrode applications. Carbon. 2008;46(3):405-13.

[84] Kiminobu I, et al. Enhancement of microplasma-based water-solubilization of single-walled carbon nanotubes using gas bubbling in water. Nanotechnology. 2007;18, 335602(33):1-7.

[85] Hamon MA, Hui H, Bhowmik P, Itkis HME, Haddon RC. Ester-functionalized soluble single-walled carbon nanotubes. Appl Phys A-Mater. 2002;74(3):333-8.

[86] Wong SS, Joselevich E, Woolley AT, Cheung CL, Lieber CM. Covalently functionalized nanotubes as nanometre-sized probes in chemistry and biology. (cover story). Nature. 1998;394(6688):52-5.

[87] Fu K, Huang W, Lin Y, Riddle LA, Carroll DL, Sun Y-P. Defunctionalization of functionalized carbon nanotubess. Nano Lett. 2001;1(8):439-41.

[88] Bahr JL, Tour JM. Covalent chemistry of single-wall carbon nanotubes. J Mater Chem. 2002;12(7):1952-8.

[89] Datsyuk V, Kalyva M, Papagelis K, Parthenios J, Tasis D, Siokou A, et al. Chemical oxidation of multiwalled carbon nanotubes. Carbon. 2008;46(6):833-40.

[90] Lakshminarayanan PV, Toghiani H, Pittman Jr CU. Nitric acid oxidation of vapor grown carbon nanofibers. Carbon. 2004;42(12-13):2433-42.

[91] Zhang G, Sun S, Yang D, Dodelet J-P, Sacher E. The surface analytical characterization of carbon fibers functionalized by H_2SO_4/HNO_3 treatment. Carbon. 2008;46(2):196-205.

[92] Wang Y, Iqbal Z, Mitra S. Rapidly functionalized, water-dispersed carbon nanotubes at high concentration. J Am Chem Soc. 2006;128(1):95-9.

[93] Dyke CA, Tour JM. Covalent functionalization of single-walled carbon nanotubes for materials applications. J Phys Chem A. 2004;108(51):11151-9.

[94] Hudson JL, Casavant MJ, Tour JM. Water-soluble, exfoliated, nonroping single-wall carbon nanotubes. J Am Chem Soc. 2004;126(36):11158-9.

[95] Mickelson ET, Huffman CB, Rinzler AG, Smalley RE, Hauge RH, Margrave JL. Fluorination of single-wall carbon nanotubes. Chem Phys Lett. 1998;296(1-2):188-94.

[96] Fu X, Lu W, Chung DDL. Ozone treatment of carbon fiber for reinforcing cement. Carbon. 1998;36(9):1337-45.

[97] Chen CL, Ogino A, Wang XK, Nagatsu M. Plasma treatment of multiwall carbon nanotubes for dispersion improvement in water. Appl Phys Lett. 2010;96(13):131504-6.

[98] Yazdanbakhsh A, Grasley Z, Tyson B, Abu Al-Rub RK. Distribution of carbon nanofibers and nanotubes in cementitious composites. Transp Res Record. 2010(2142):89-95.

[99] Chung DDL. Dispersion of short fibers in cement. J Mater Civ Eng. 2005;17(4):379-83.

[100] Tyson BM. Carbon nanotube and nanofiber reinforcement for improving the flexural strength and fracture toughness of Portland cement paste. Master's thesis. College Station, TX, Texas A&M University; 2010.

[101] Cheap Tubes, Inc. 2011; http://www.cheaptubesinc.com/

[102] Nanocyl, Inc. 2011; http://www.nanocyl.com

[103] Ni Labview. 2011; http://www.ni.com/labview

[104] Musso S, Tulliani J-M, Ferro G, Tagliaferro A. Influence of carbon nanotubes structure on the mechanical behavior of cement composites. Compos Sci Technol. 2009;69(11-12):1985-90.

[105] Dweck J, da Silva PFF, Buchler PM, Cartledge FK. Study by thermogravimetry of the evolution of ettringite phase during type II Portland cement hydration. J Therm Anal. 2002;69(1):179-86.

[106] Mindess S, Young JF. Concrete. Englewood Cliffs, NJ: Prentice-Hall; 1981.

[107] Carde C, François R, Torrenti J-M. Leaching of both calcium hydroxide and C-S-H from cement paste: Modeling the mechanical behavior. Cem Concr Res. 1996;26(8):1257-68.

[108] Adenot F, Buil M. Modelling of the corrosion of the cement paste by deionized water. Cem Concr Res. 1992;22(2-3):489-96.

[109] Carde C, François R. Effect of the leaching of calcium hydroxide from cement paste on mechanical and physical properties. Cem Concr Res. 1997;27(4):539-50.

[110] K. L. Scrivener JFY. Mechanisms of chemical degradation of cement-based systems. First ed: Taylor & Francis, Inc.; 1997.

[111] G.J. Verbeck RHH. Structure and physical properties of cement paste. In: Proceedings of the Fifth International Symposium on the Chemistry of Cement. Tokyo: The Cement Association of Japan; 1968. p. 1-32.

[112] Taylor HFW. Cement chemistry. 2nd ed. London: Thomas Telford Services Ltd; 1997.

[113] Groves GW. Microcrystalline calcium hydroxide in portland cement pastes of low water/cement ratio. Cem Concr Res. 1981;11(5-6):713-8.

[114] Viehland D, Li JF, Yuan LJ, Xu Z. Mesostructure of calcium silicate hydrate (C–S–H) gels in Portland cement paste: Short-range ordering, nanocrystallinity, and local compositional order. J Am Ceram Soc. 1996;79(7):1731-41.

[115] Greenberg SA, Copeland LE. The thermodynamic functions for the solution of calcium hydroxide in water. J Phys Chem. 1960;64(8):1057-9.

[116] Bassett H. Notes on the system lime–water, and on the determination of calcium. J Chem Soc. 1934;276:1270-5.

[117] Crumbie AK, Scrivener KL, Pratt PL. The relationship between the porosity and permeability of the surface layer of concrete and the ingress of aggressive ions. In: Roberts LR, Skalny JP, editors. Material Research Society Symposium Proceedings. Pittsburgh; 1989. p. 279-84.

[118] Adenot F, Richet C. Modelling of the chemical degradation of a cement paste. In: Scrivener KL, Young JF, editors. Mechanisms of Chemical Degradation of Cement-based Systems. London: E & FN Spon; 1997. p. 341-9.

[119] Simard MA, Nkinamubanzi PC, Jolicoeur C, Perraton D, Aïtcin PC. Calorimetry, rheology and compressive strength of superplasticized cement pastes. Cem Concr Res. 1993;23(4):939-50.

APPENDIX

Stress-strain diagrams for the 0.1% long MWCNT (OH)/cement composite samples:

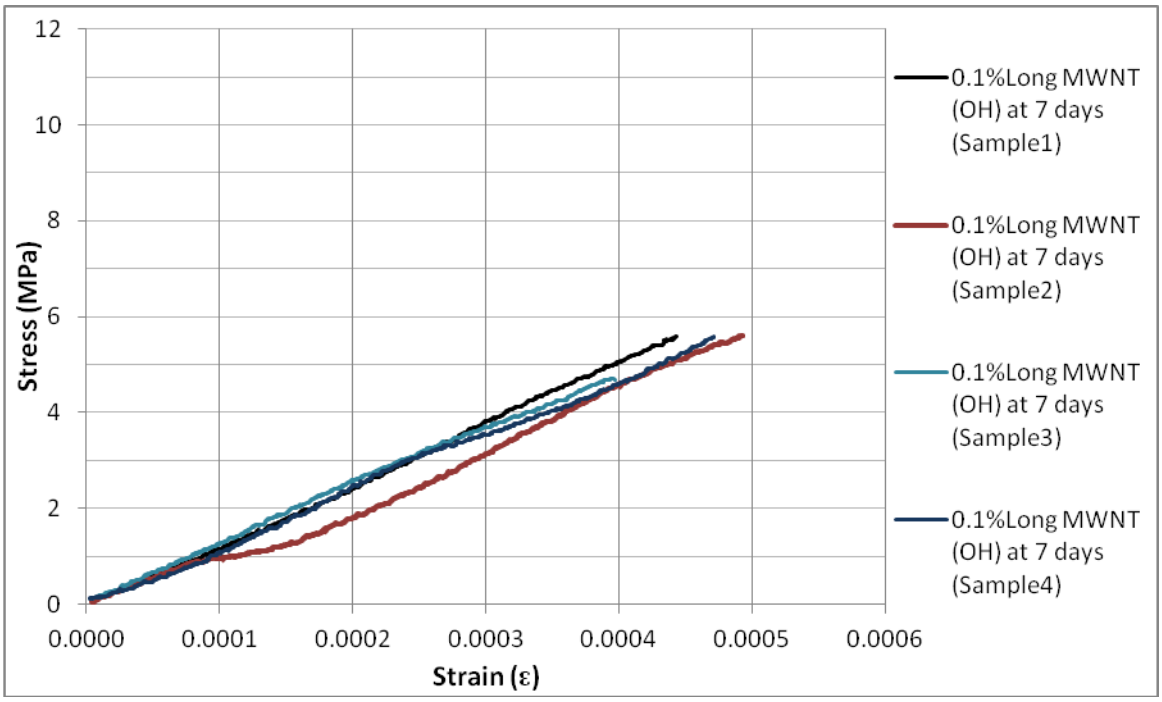

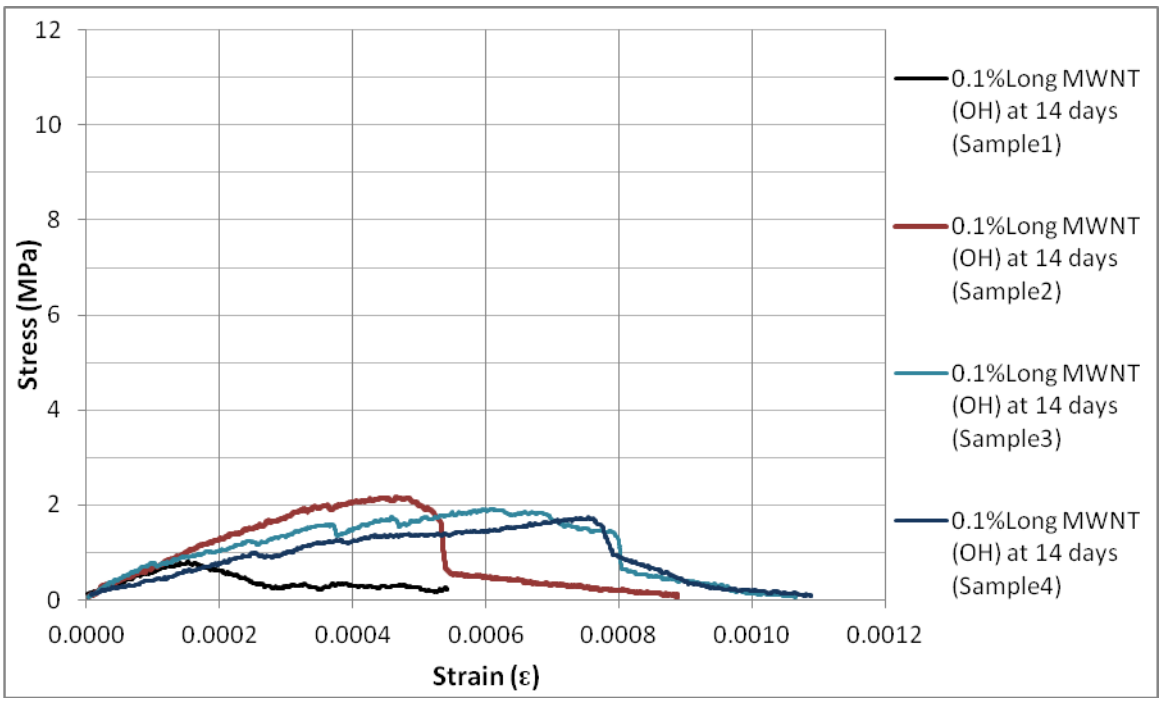

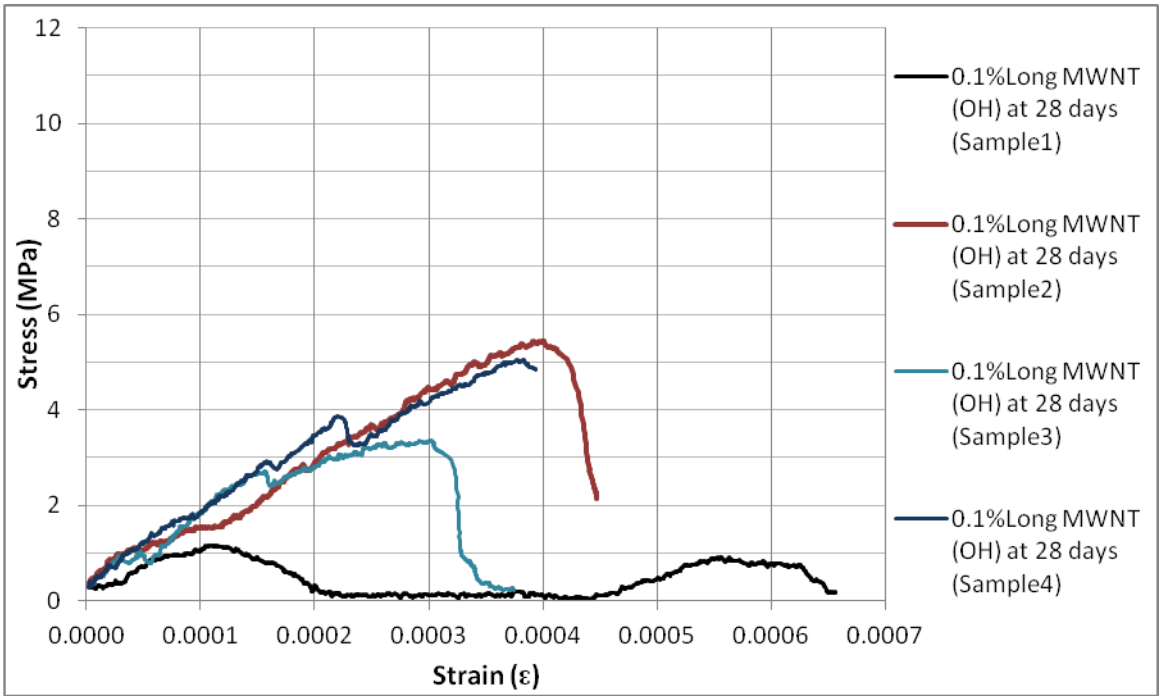
12
10
8
6
4
2
0
Stress (MPa)
0.0000
0.0001
0.0002
0.0003
0.0004
0.0005
0.0006
0.0007
Strain (ε)
0.1%Long MWNT (OH) at 28 days (Sample1)
0.1%Long MWNT (OH) at 28 days (Sample2)
0.1%Long MWNT (OH) at 28 days (Sample3)
0.1%Long MWNT (OH) at 28 days (Sample4)

Stress-strain diagrams for the 0.1% long MWCNT/cement composite samples:

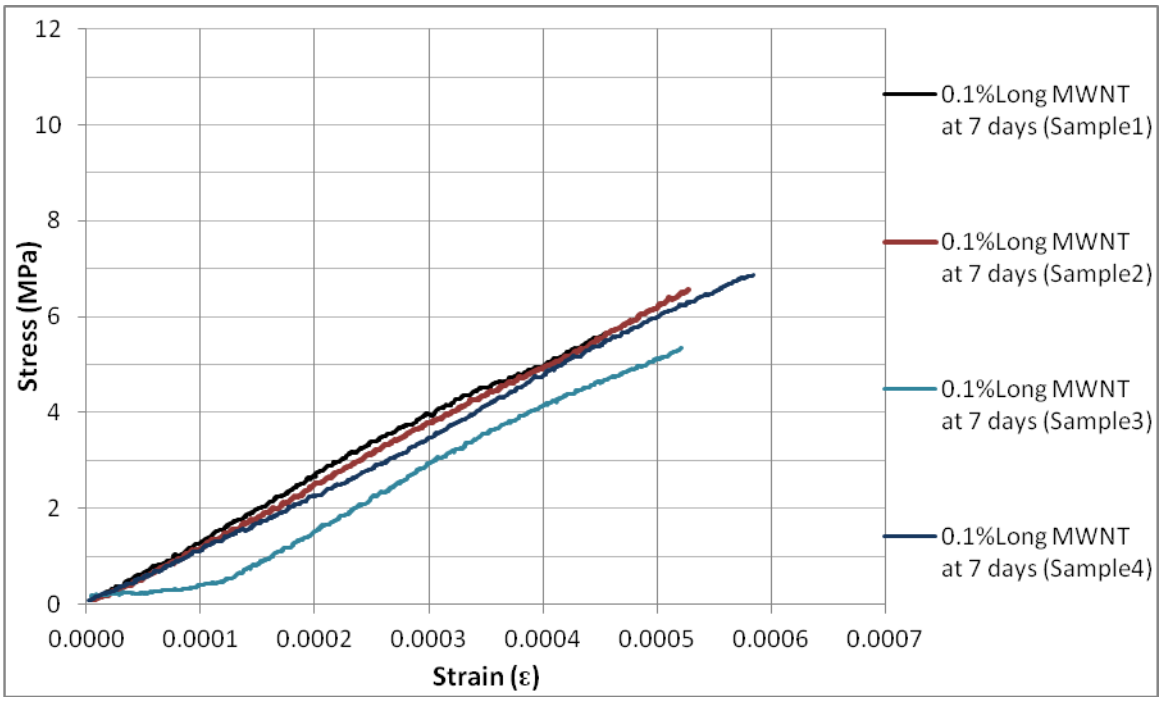

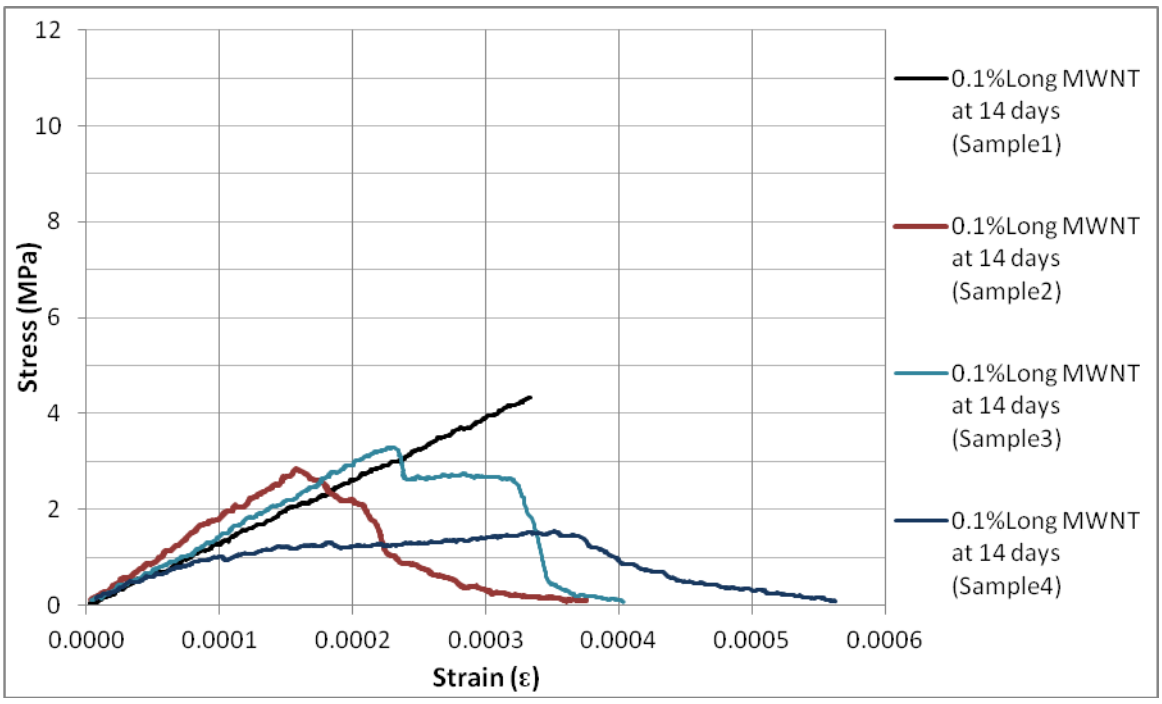

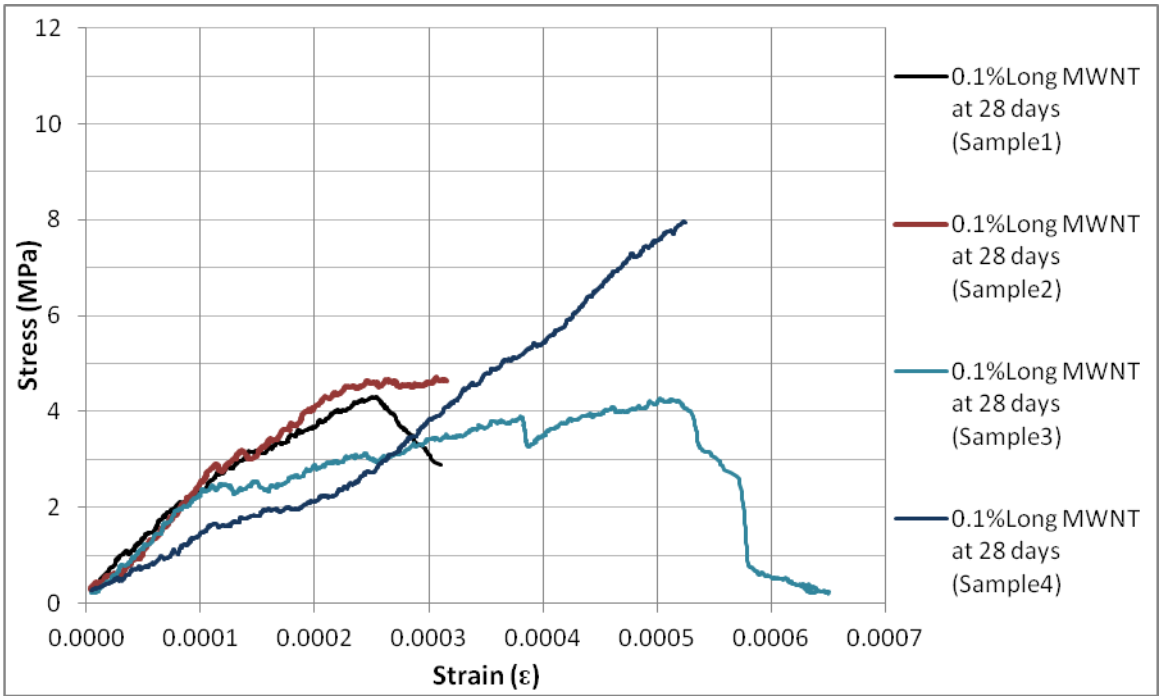
12
10
8
6
4
2
0
Stress (MPa)
0.0000
0.0001
0.0002
0.0003
0.0004
0.0005
0.0006
0.0007
Strain (ε)
0.1%Long MWNT at 28 days (Sample1)
0.1%Long MWNT at 28 days (Sample2)
0.1%Long MWNT at 28 days (Sample3)
0.1%Long MWNT at 28 days (Sample4)

Stress-strain diagrams for the 0.1% short MWCNT (COOH)/cement composite samples:

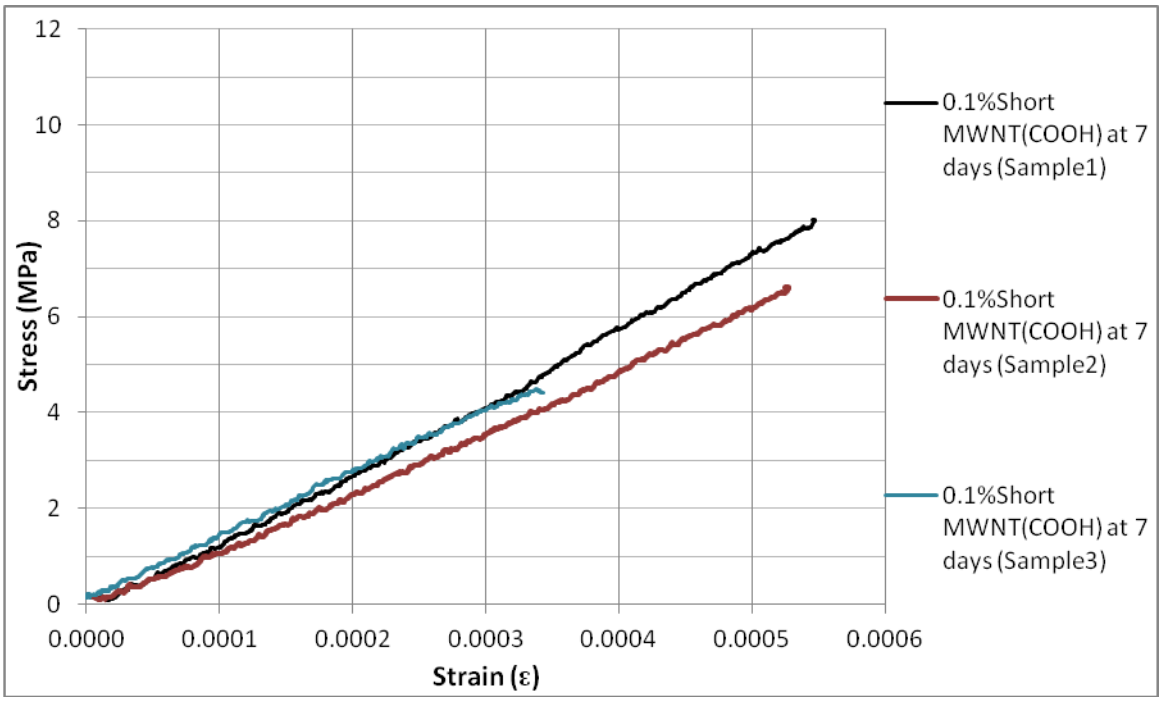

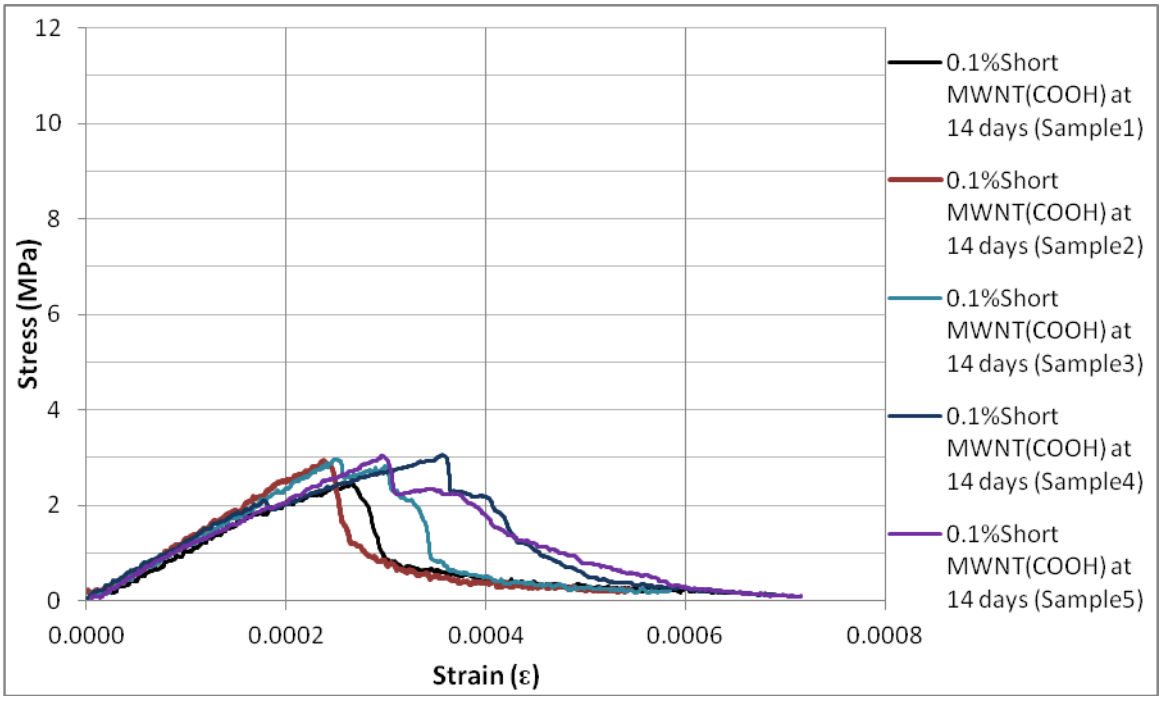

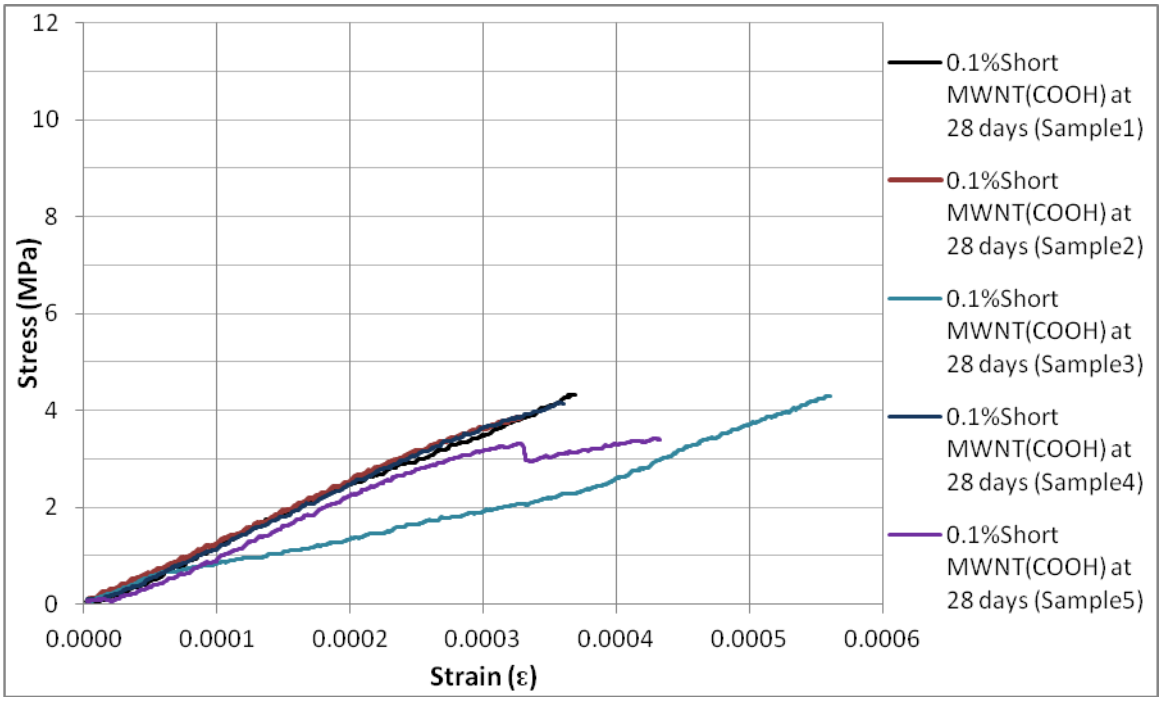
12
10
8
6
4
2
0
Stress (MPa)
0.0000
0.0001
0.0002
0.0003
0.0004
0.0005
0.0006
Strain (ε)
0.1%Short MWNT(COOH) at 28 days (Sample1)
0.1%Short MWNT(COOH) at 28 days (Sample2)
0.1%Short MWNT(COOH) at 28 days (Sample3)
0.1%Short MWNT(COOH) at 28 days (Sample4)
0.1%Short MWNT(COOH) at 28 days (Sample5)

Stress-strain diagrams for the 0.2% short MWCNT (COOH)/cement composite samples:

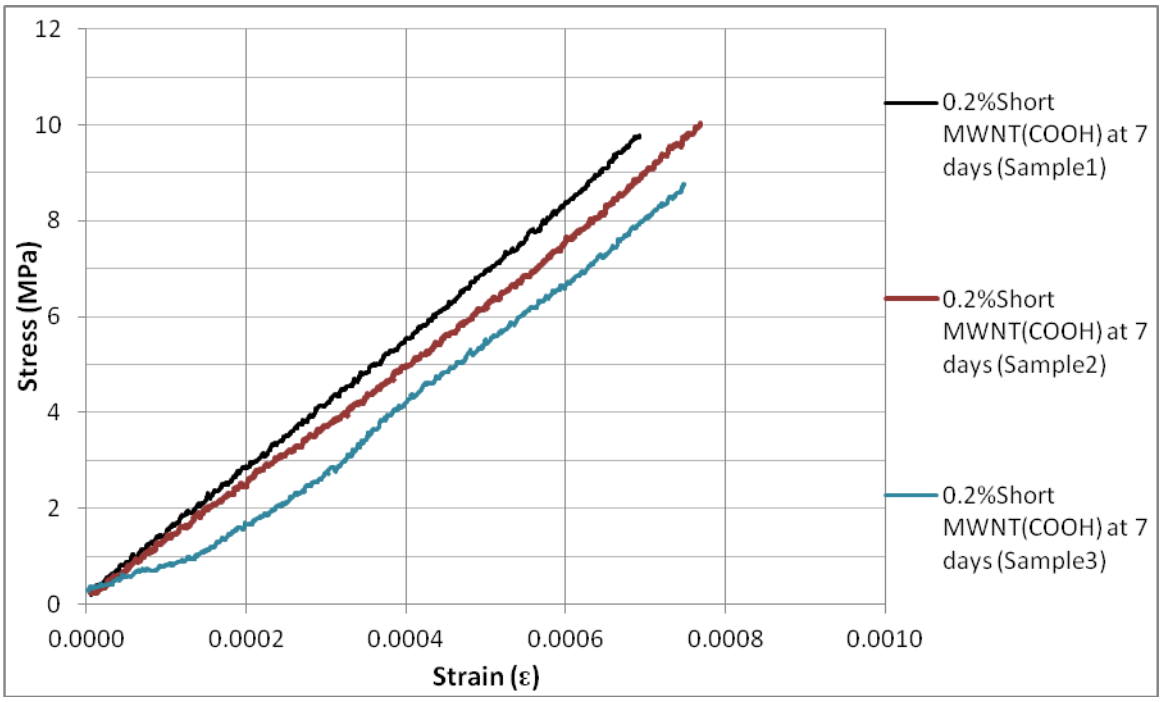

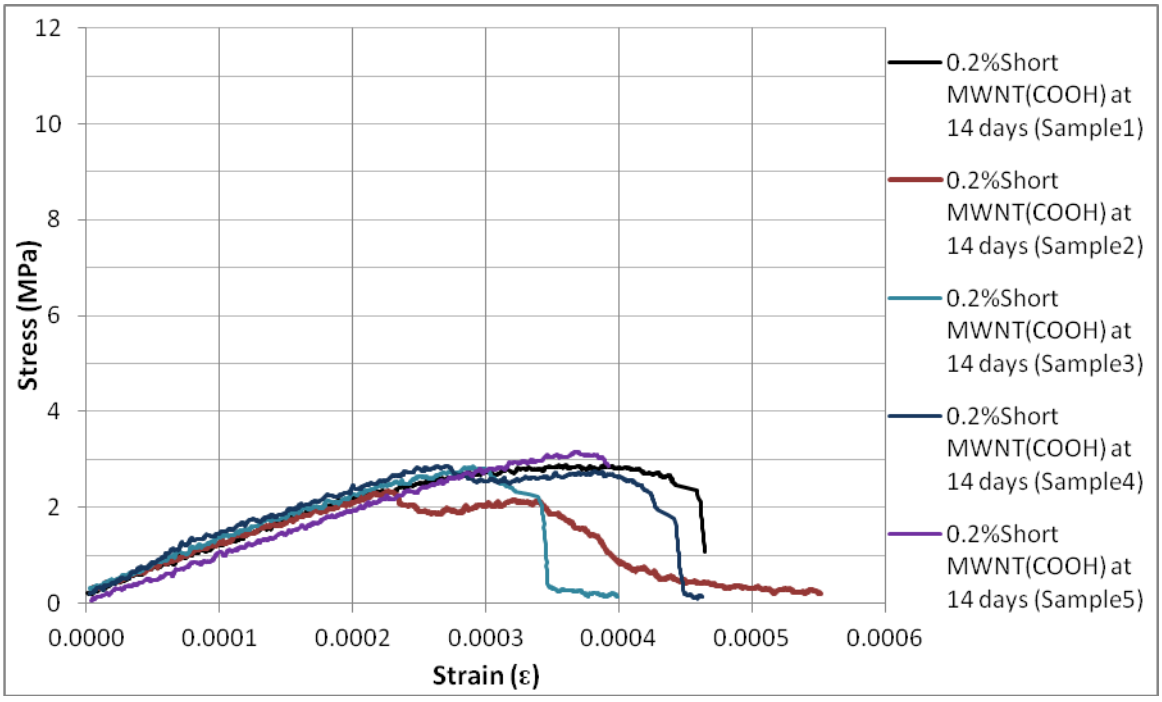

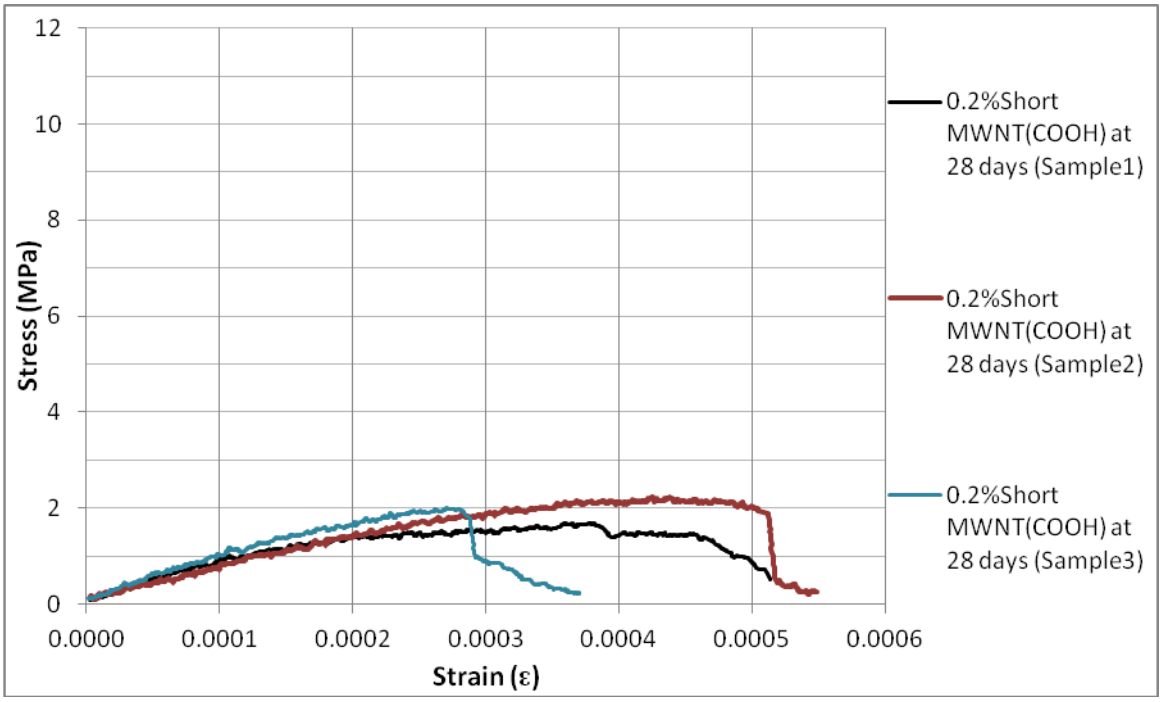
12
10
8
6
4
2
0
Stress (MPa)
0.0000
0.0001
0.0002
0.0003
0.0004
0.0005
0.0006
Strain (ε)
0.2%Short MWNT(COOH) at 28 days (Sample1)
0.2%Short MWNT(COOH) at 28 days (Sample2)
0.2%Short MWNT(COOH) at 28 days (Sample3)

Stress-strain diagrams for the 0.1% short MWCNT/cement composite samples:

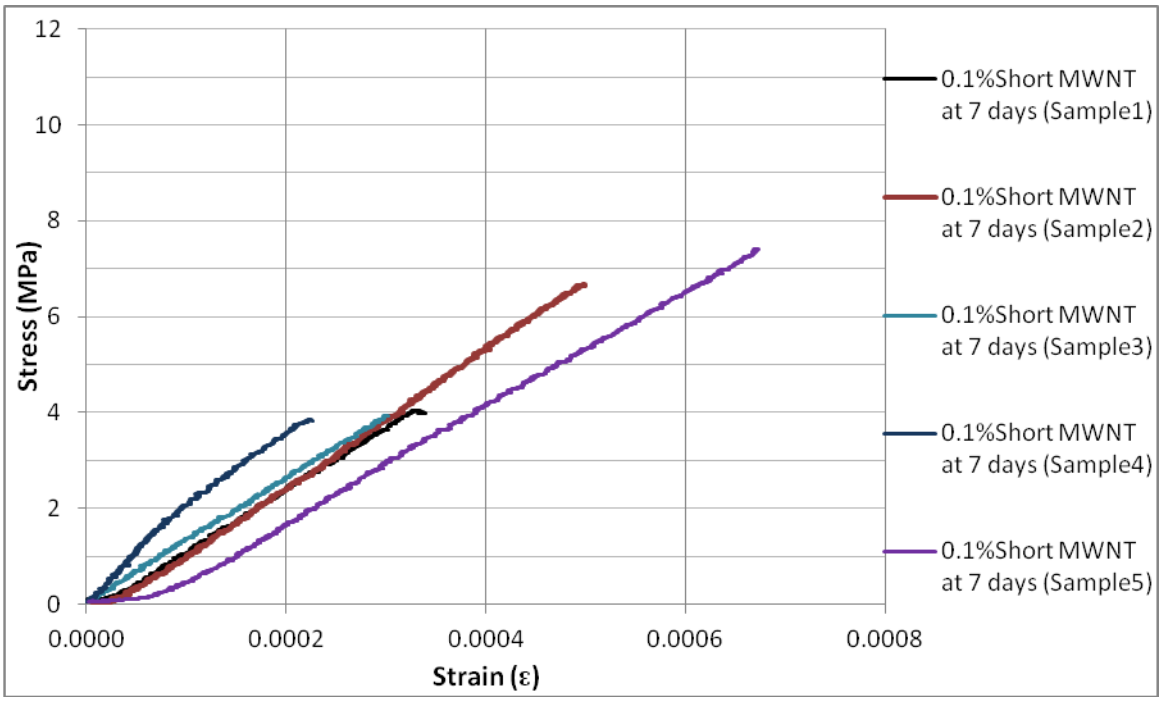

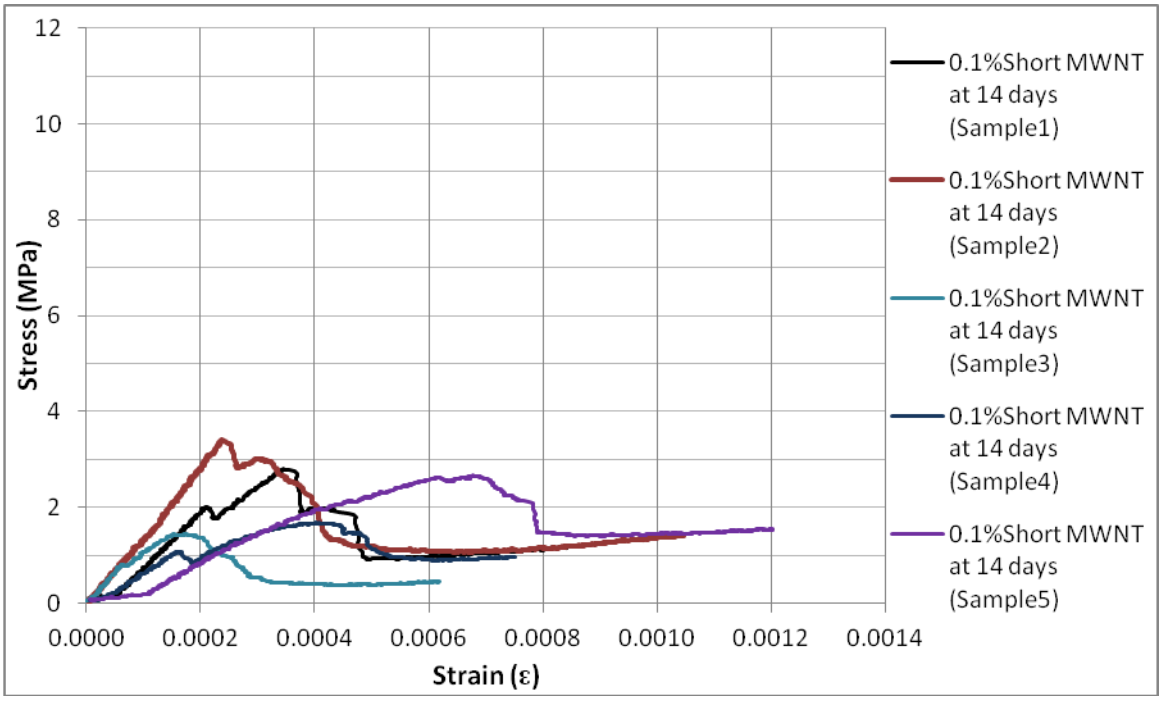

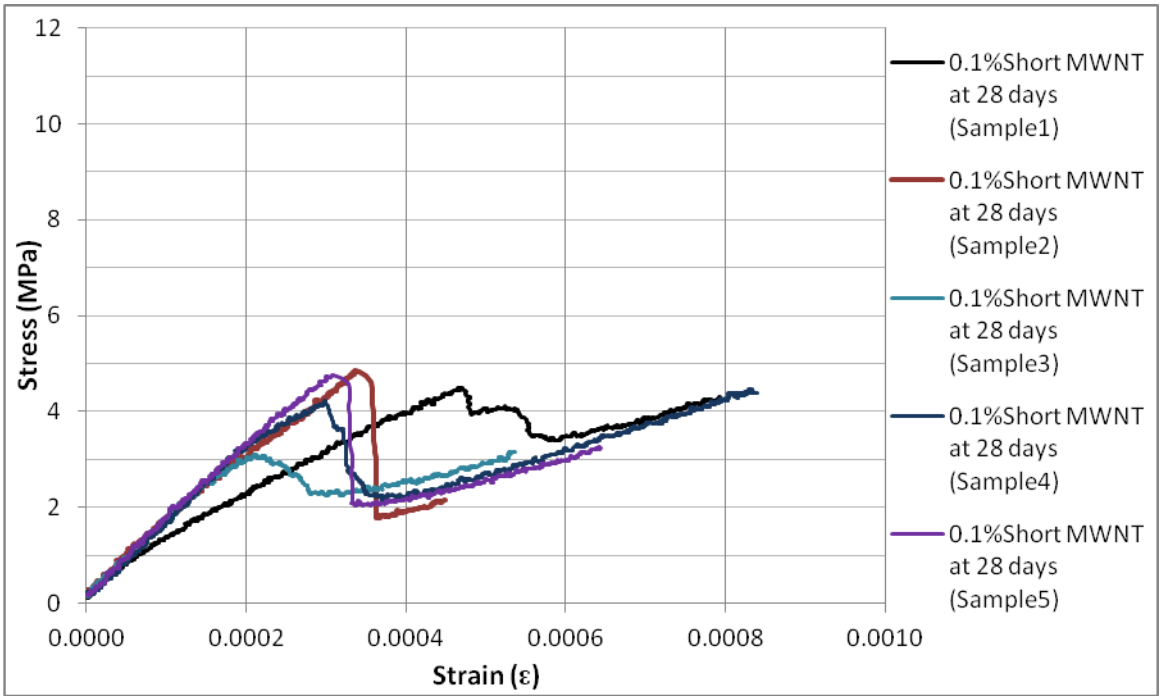
12
10
8
6
4
2
0
Stress (MPa)
0.0000
0.0002
0.0004
0.0006
0.0008
0.0010
Strain (ε)
0.1%Short MWNT at 28 days (Sample1)
0.1%Short MWNT at 28 days (Sample2)
0.1%Short MWNT at 28 days (Sample3)
0.1%Short MWNT at 28 days (Sample4)
0.1%Short MWNT at 28 days (Sample5)

Stress-strain diagrams for the 0.2% short MWCNT/cement composite samples:

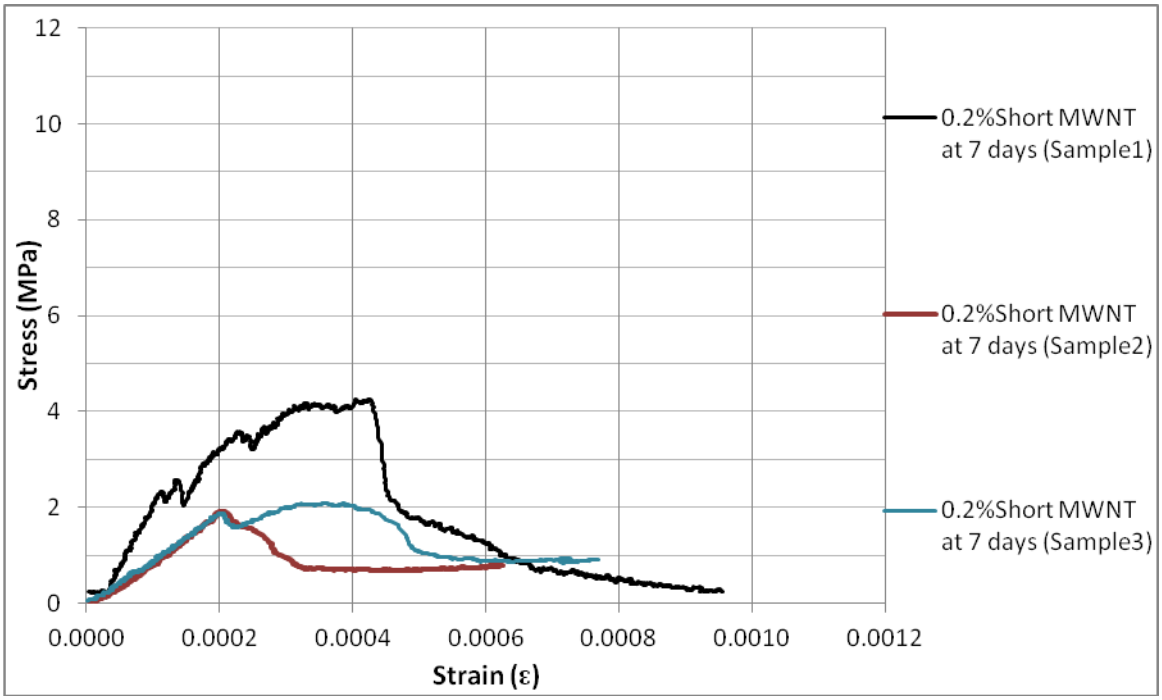

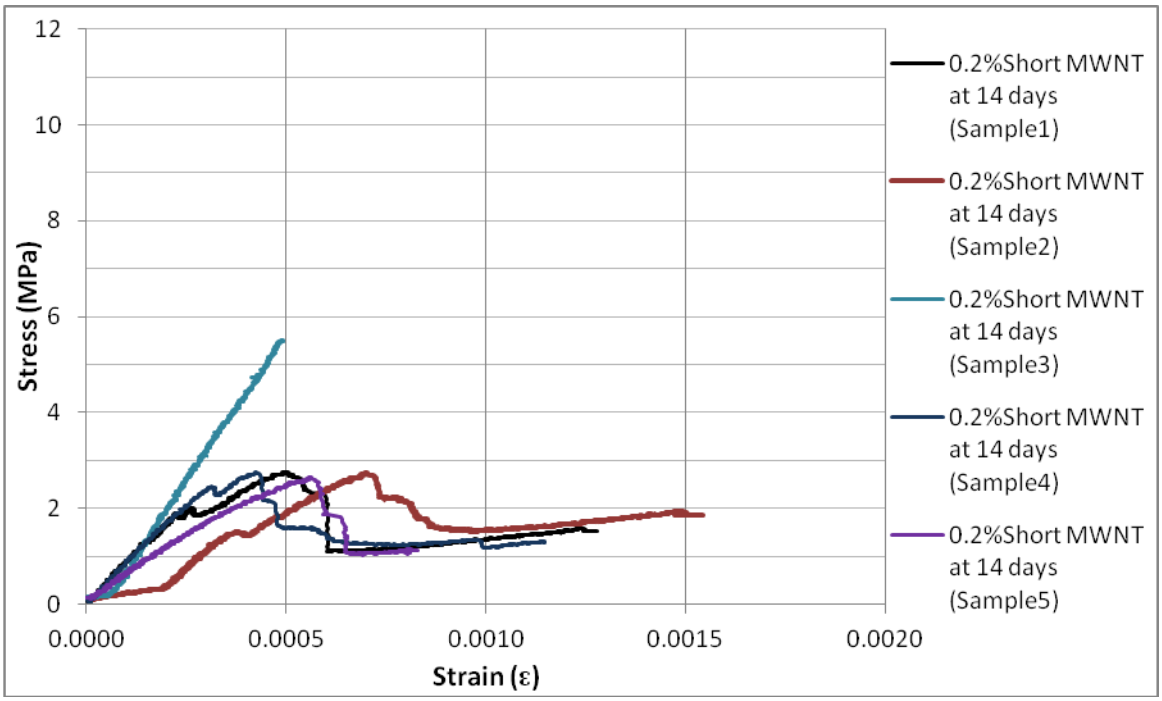

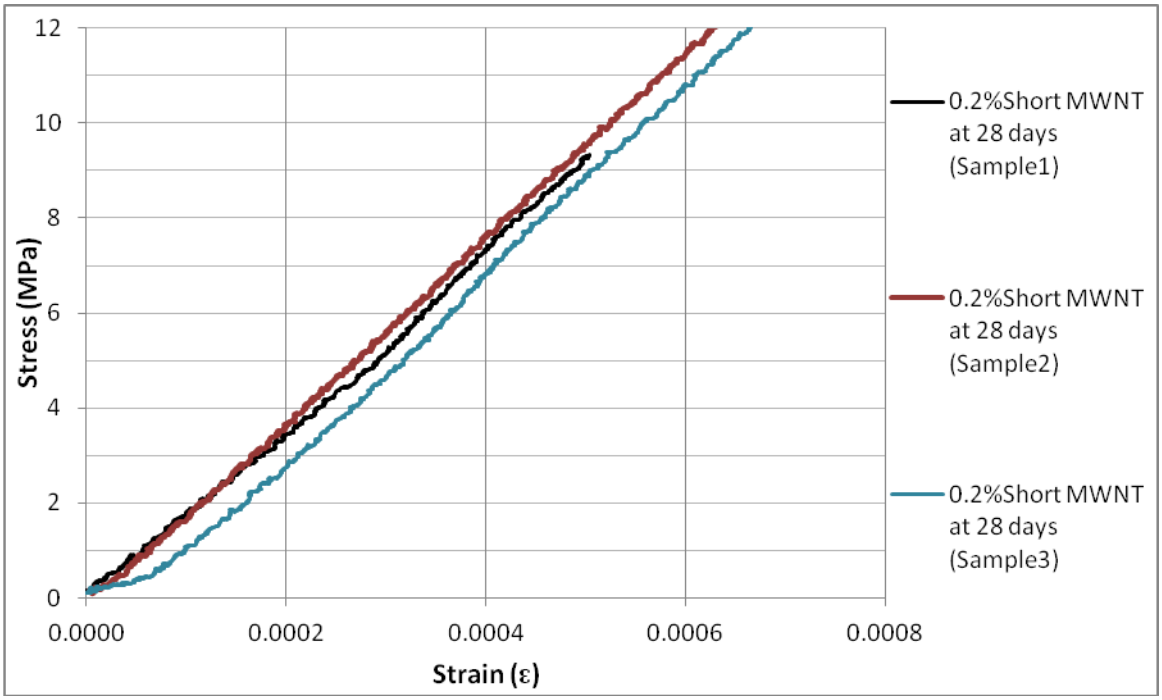
12
10
8
6
4
2
0
Stress (MPa)
0.0000
0.0002
0.0004
0.0006
0.0008
Strain (ε)
0.2%Short MWNT at 28 days (Sample1)
0.2%Short MWNT at 28 days (Sample2)
0.2%Short MWNT at 28 days (Sample3)

Stress-strain diagrams for the 0.04% short MWCNT/cement composite samples:

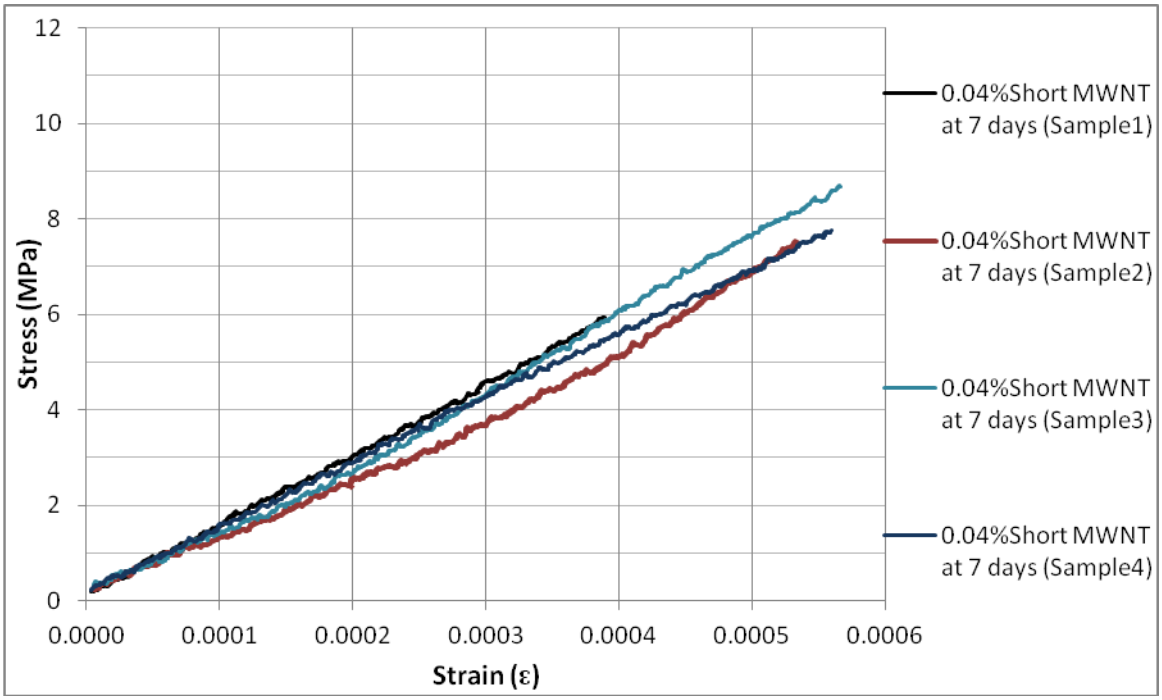

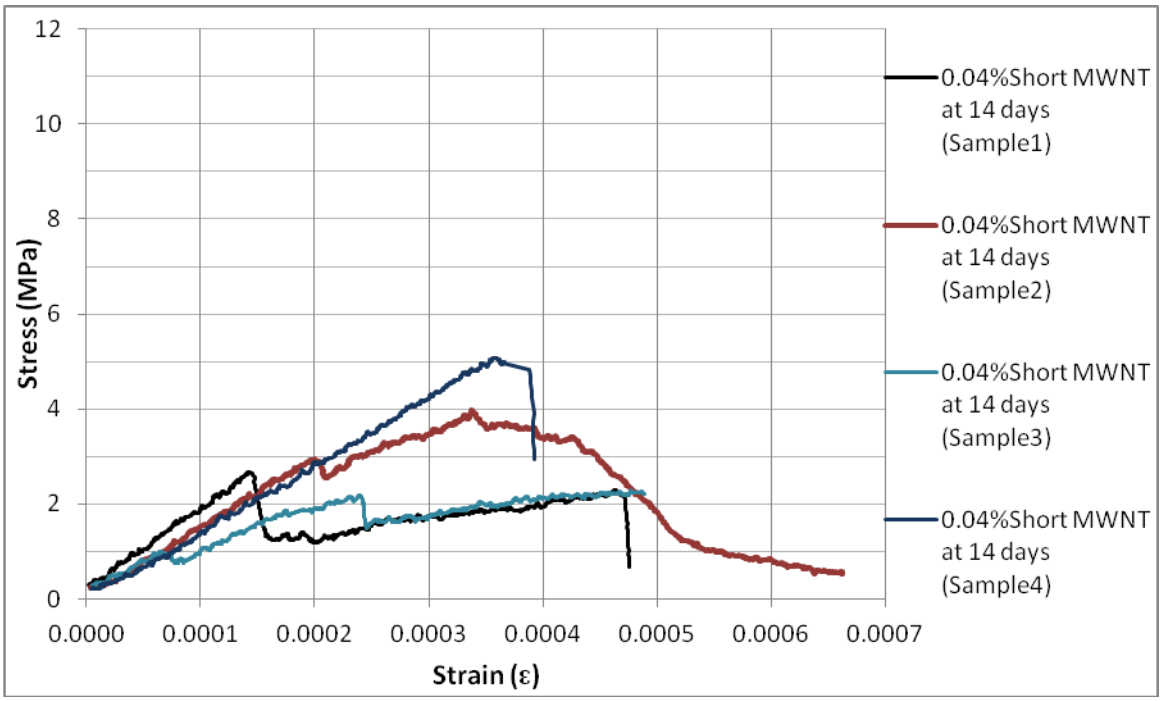

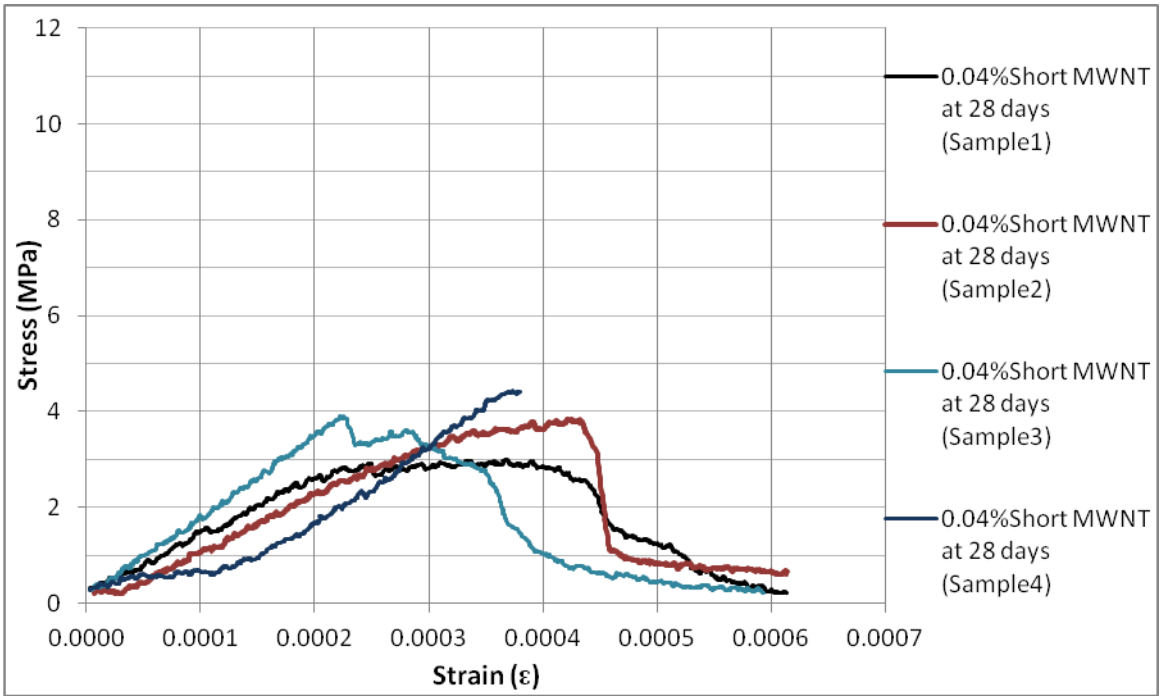
12
10
8
6
4
2
0
Stress (MPa)
0.0000
0.0001
0.0002
0.0003
0.0004
0.0005
0.0006
0.0007
Strain (ε)
0.04%Short MWNT at 28 days (Sample1)
0.04%Short MWNT at 28 days (Sample2)
0.04%Short MWNT at 28 days (Sample3)
0.04%Short MWNT at 28 days (Sample4)

Stress-strain diagrams for the 0.04% long MWCNT (OH)/cement composite samples:

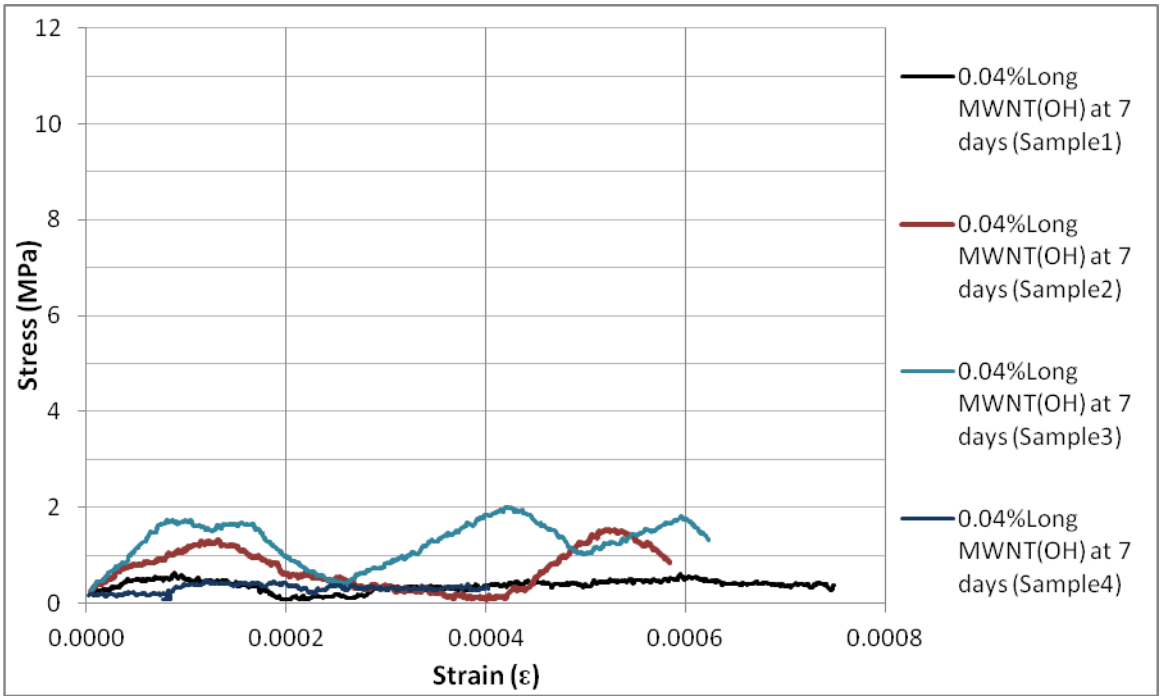

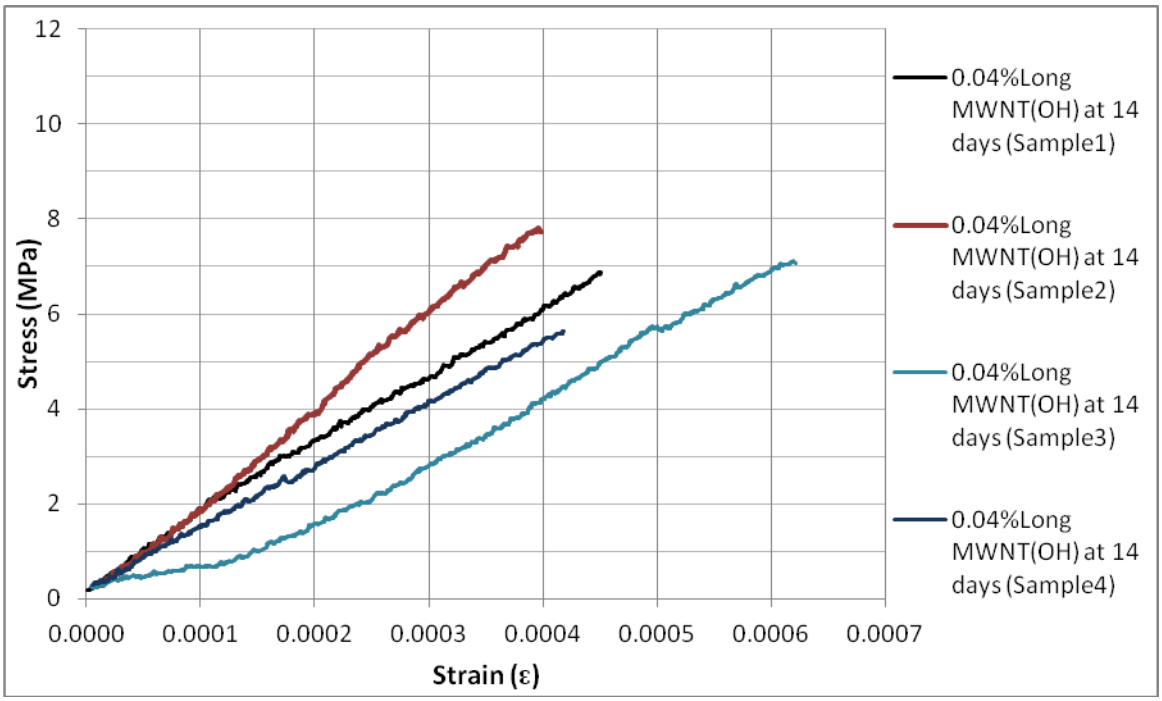

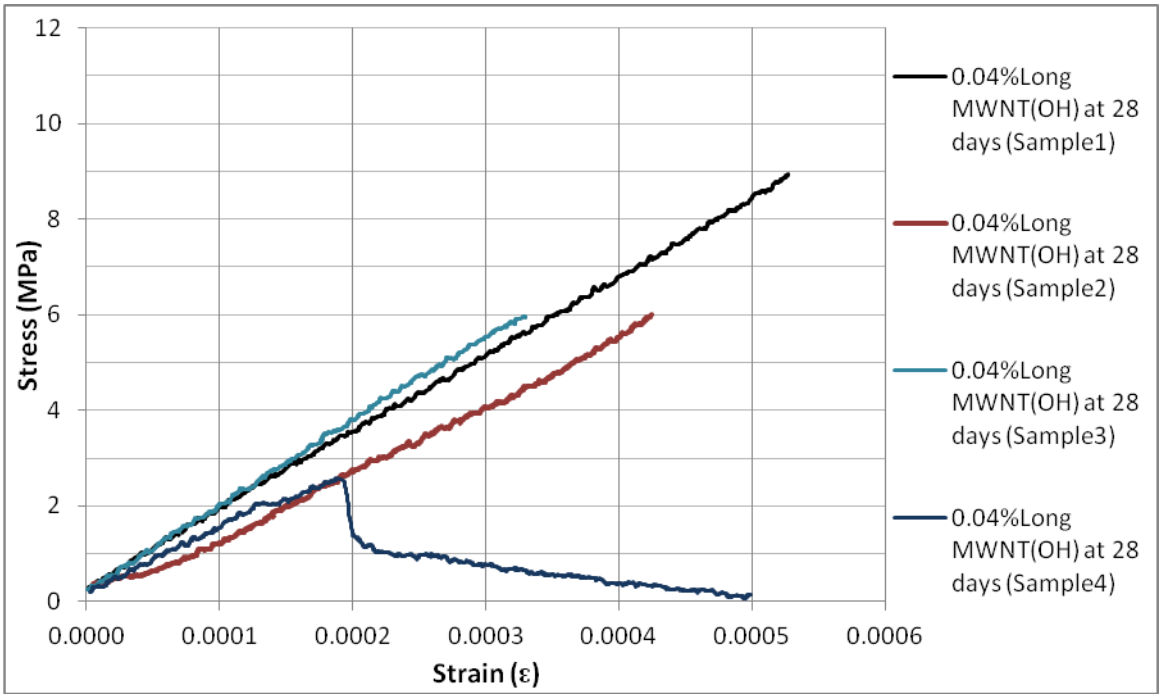
12
10
8
6
4
2
0
Stress (MPa)
0.0000
0.0001
0.0002
0.0003
0.0004
0.0005
0.0006
Strain (ε)
0.04%Long MWNT(OH) at 28 days (Sample1)
0.04%Long MWNT(OH) at 28 days (Sample2)
0.04%Long MWNT(OH) at 28 days (Sample3)
0.04%Long MWNT(OH) at 28 days (Sample4)

Stress-strain diagrams for the 0.04% long MWCNT/cement composites samples:

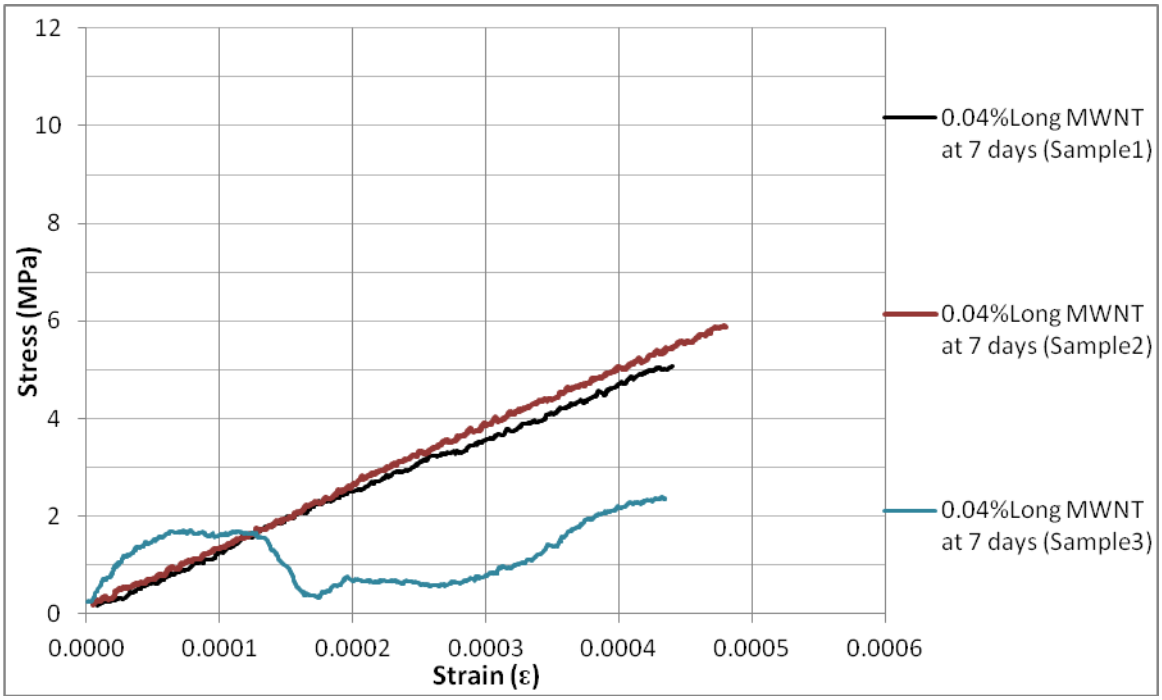

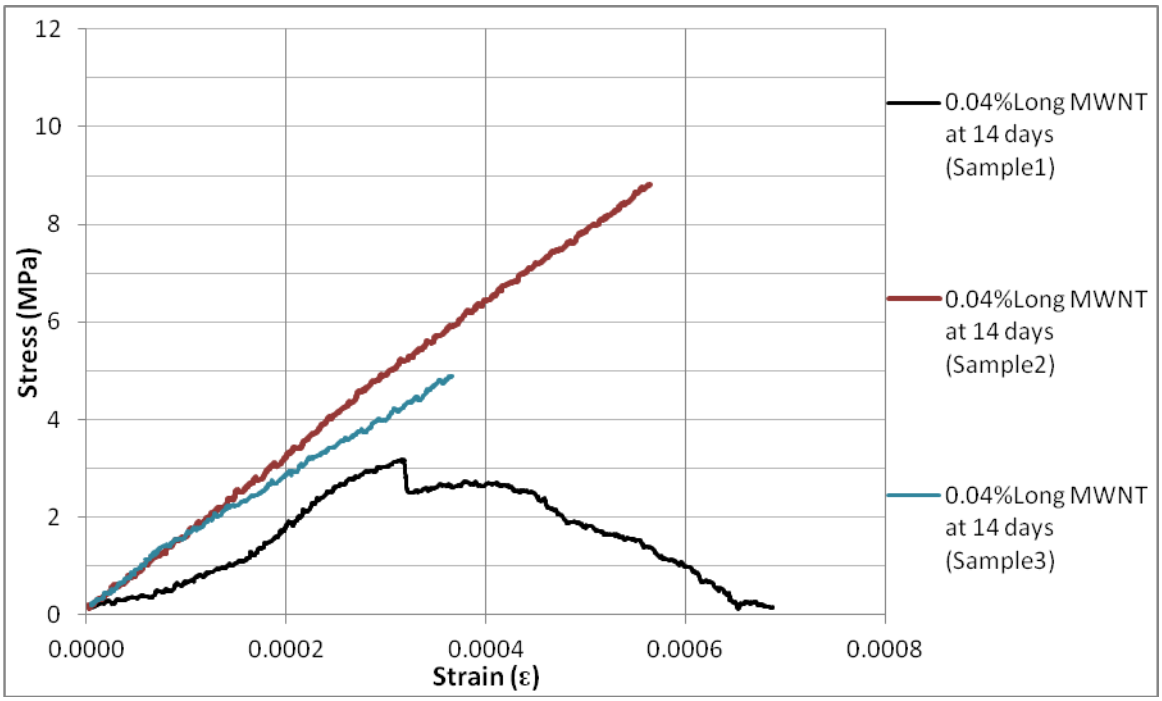

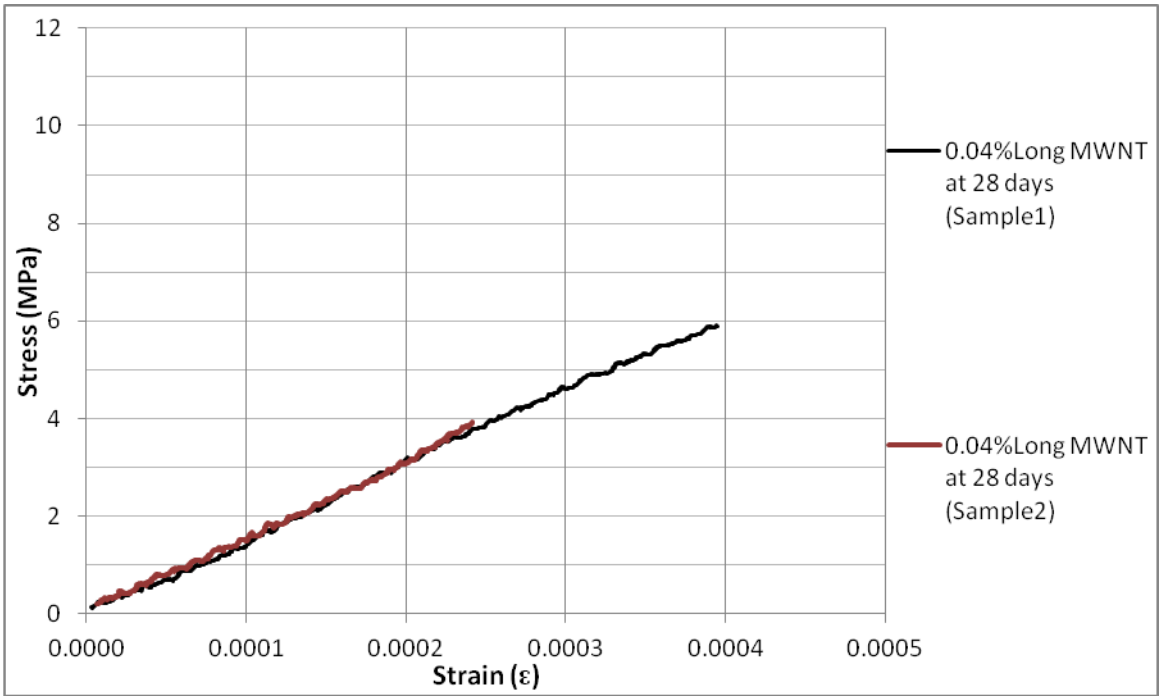
12
10
8
6
4
2
0
Stress (MPa)
0.0000
0.0001
0.0002
0.0003
0.0004
0.0005
Strain (ε)
0.04%Long MWNT at 28 days (Sample1)
0.04%Long MWNT at 28 days (Sample2)